



POLITECNICO
MILANO 1863

SCUOLA DI INGEGNERIA INDUSTRIALE
E DELL'INFORMAZIONE

Object-Oriented Dynamic Modeling and Simulation of the MSRE Primary Circuit

TESI DI LAUREA MAGISTRALE IN
NUCLEAR ENGINEERING - INGEGNERIA NUCLEARE

Author: **Mattia Barra**

Student ID: 259552

Advisor: Prof. Stefano Lorenzi

Co-advisors: Ing. Guido Carlo Masotti, Ing. Sophie Deanesi

Academic Year: 2024-2025

Abstract

The Molten Salt Reactor (MSR), which was designated as one of the six Generation IV reactor types by the Generation IV International Forum (GIF), is currently attracting significant global attention. The MSR is unique among the Gen-IV designs due to its application of liquid fuels, a feature that fundamentally eliminates the possibility of a core melting accident. Furthermore, the low operating pressure of the reactor not only translates to a lower risk of explosion and radioactive leakage but also means that the reactor vessel and components can be lightweight, thereby lowering equipment costs.

The purpose of the present thesis work is the development of an object-oriented simulation in free dynamics and its validation, through the modeling language Modelica. In addition, the exploited scenarios also refer to accident conditions, where a malfunction in the primary loop is present. The scenarios involve a primary pump failure, leading to a reduced mass flow within the circuit and involve a reactivity insertion accident, where an injection of dense, colder fluid fuel is occurring in the reactor core. To do so, as a reference, operational parameters and geometries of the Molten Salt Reactor Experiment (MSRE) were taken into account, due to the high availability of experimental data.

In these chapters, after a brief introduction to energy sustainability and an overall description of the MSRE, the single models describing the primary fuel circuit components are treated and their deployment towards successful safety scenarios.

Thanks to the work performed in this thesis, it is possible to have a solid base for further technical evaluations. For future developments, it is also worth referring to Nuclear Hybrid Energy Systems (NHES), where electrical energy and heat sources can be exploited simultaneously. On this basis, the preliminary analysis of the primary circuit done in this work, might be referred to as a starting point.

Keywords: Molten Salt Reactor Experiment, validation, transient analysis, Modelica

Abstract in lingua italiana

Il Reattore a Sali Fusi (MSR), che è stato designato come uno dei sei tipi di reattori di Quarta Generazione dal Forum Internazionale di Generazione IV (GIF), sta attualmente attirando significativa attenzione globale. L'MSR è unico tra i design Gen-IV grazie all'applicazione di combustibili liquidi, una caratteristica che elimina fundamentalmente la possibilità di un incidente di fusione del nocciolo. Inoltre, la bassa pressione operativa del reattore non solo si traduce in un minor rischio di esplosione e di fuga radioattiva, ma significa anche che il recipiente del reattore e i componenti possono essere più leggeri, riducendo così i costi dei componenti.

Lo scopo del presente lavoro di tesi è lo sviluppo di una simulazione orientata agli oggetti in dinamica libera e la sua validazione, attraverso il linguaggio di modellazione Modelica. In aggiunta, gli scenari indagati si riferiscono a condizioni incidentali, dove è presente un malfunzionamento nel circuito primario. Tali scenari coinvolgono un guasto della pompa del circuito primario, che porta ad una ridotta portata del sale combustibile all'interno del circuito, e coinvolgono un incidente di inserzione di reattività, dove un'iniezione di combustibile liquido, denso e più freddo si verifica nel nocciolo del reattore. A tal fine, come riferimento, sono stati presi in considerazione i parametri operativi e le geometrie del Molten Salt Reactor Experiment (MSRE), per via dell'elevata disponibilità di dati sperimentali. In questi capitoli, dopo una breve introduzione alla sostenibilità energetica e una descrizione generale del MSRE, vengono trattati i singoli modelli che descrivono i componenti del circuito primario del combustibile e il loro dispiegamento verso scenari di sicurezza di successo.

Grazie al lavoro eseguito in questa tesi, è possibile avere una base solida per ulteriori valutazioni tecniche. Per sviluppi futuri, è anche opportuno fare riferimento ai sistemi ibridi (NHES), dove energia elettrica e calore possono essere sfruttati simultaneamente. Su questa base, l'analisi preliminare del circuito primario fatta in questo lavoro potrebbe essere considerata come un punto di partenza.

Parole chiave: Molten Salt Reactor Experiment, validazione, analisi dei transistori, Modelica

Contents

| | |
|--------------------------------------|------------|
| Abstract | i |
| Abstract in lingua italiana | iii |
| Contents | v |
| | |
| Introduction | 1 |
| | |
| 1 State of the Art | 7 |
| 1.1 Introduction | 7 |
| 1.2 MSR technology | 9 |
| 1.2.1 Safety Advantages | 11 |
| 1.2.2 Economic Advantages | 12 |
| 1.2.3 Technical Challenges | 14 |
| 1.2.4 Ongoing Projects | 15 |
| 1.3 Aim of the Thesis | 17 |
| | |
| 2 MSRE Overview | 19 |
| 2.1 History of MSRE | 19 |
| 2.1.1 Layout | 24 |
| 2.2 Primary Circuit | 26 |
| 2.2.1 Reactor Vessel | 26 |
| 2.2.2 Fuel Pump | 29 |
| 2.2.3 Heat Exchanger | 30 |
| 2.2.4 Downcomer | 32 |
| 2.2.5 Lower Plenum | 32 |
| 2.2.6 Upper Plenum | 33 |
| 2.3 Secondary Circuit | 33 |
| 2.3.1 Radiator | 33 |

| | | |
|----------|---|-----------|
| 2.4 | Further equipment and processes | 35 |
| 2.4.1 | Materials Compatibility | 35 |
| 2.4.2 | Instrumentation and Control | 36 |
| 2.4.3 | Fuel Chemistry | 37 |
| 2.4.4 | Drain Tank Systems | 38 |
| 3 | MSRE Plant Simulator | 39 |
| 3.1 | Reactor Core | 41 |
| 3.1.1 | Fuel model | 41 |
| 3.1.2 | Graphite model | 46 |
| 3.1.3 | Neutron Kinetics | 47 |
| 3.2 | Plenums | 49 |
| 3.3 | Downcomer | 50 |
| 3.4 | Fuel Salt Legs | 50 |
| 3.5 | Fuel Circulating Pump | 51 |
| 3.6 | Primary Heat Exchanger | 51 |
| 3.6.1 | Shell side | 53 |
| 3.6.2 | Tube side | 54 |
| 4 | Results and discussion | 57 |
| 4.1 | Steady-state results | 58 |
| 4.2 | Transient behavior during normal operation | 61 |
| 4.2.1 | Dynamic response to a step reactivity insertion | 61 |
| 4.3 | Operational anomalies | 69 |
| 4.3.1 | Primary Pump Failure Accident | 69 |
| 4.3.2 | Cold slug insertion into the core | 73 |
| 5 | Conclusions and future developments | 81 |
| | Bibliography | 85 |
| A | Modelica language | 89 |
| B | Graphite | 91 |
| | List of Figures | 93 |

| | |
|-------------------------|------------|
| List of Tables | 95 |
| List of Symbols | 97 |
| Acknowledgements | 101 |

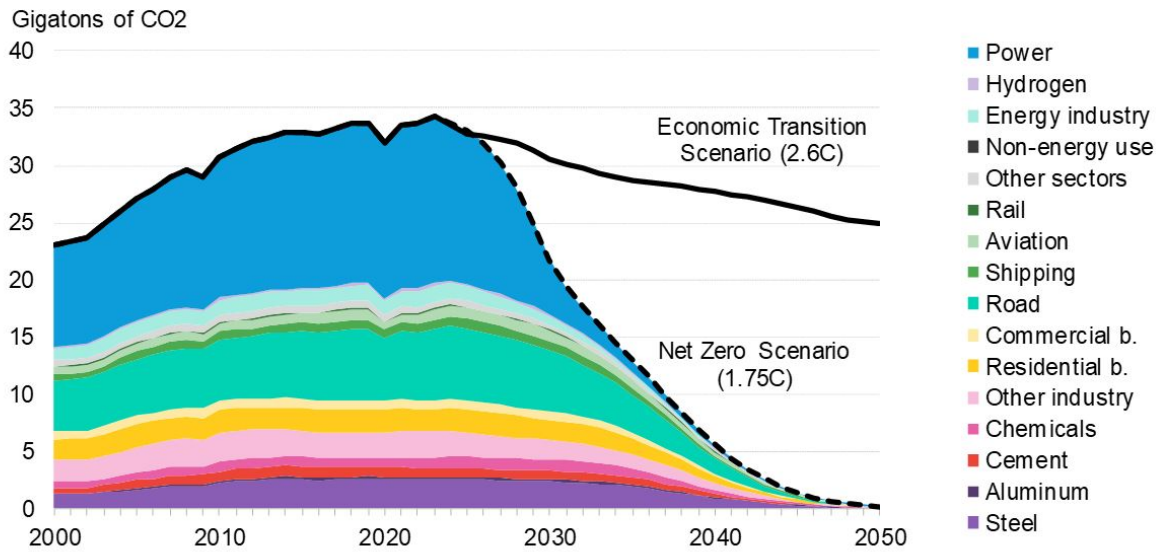
Introduction

The 21st century has clearly defined a new sight in terms of future perspective, not only because of the technological development that occurred throughout the years, but also for the awareness of limiting the emissions of greenhouse gases (GHGs). Global population in the upcoming years will certainly grow, with predictions stating that by 2050, the population will reach 9.8 billion [31]. As a consequence of that, energy demand will grow as well, leading to a further increase in GHGs emissions if we do not act now.

Throughout the years, hundreds of countries have agreed in reaching net-zero emissions goal, with flourishing examples like the European Union, aiming to achieve as the first continent, carbon neutrality by 2050 [1]. This ambitious goal is also underlined by the pathway designed to reduce carbon emissions by at least 55% by 2030 with respect to the 1990 levels [11], with a particular focus on the hydrogen value chain, aiming to reach 40 GW of electrolysis capacity installed.

Nonetheless, the Net-Zero Scenario (NZS) should also be referred to as the Economic Transition Scenario (ETS). The two scenarios are reported in the New Energy Outlook report made by Bloomberg New Energy Finance [4], dealing with the latest global energy transition outlook to 2050, focusing on the updated base-case scenario and the economic, policy, and geopolitical dynamics influencing energy. As Figure 1 depicts, most experts expect an insufficient reduction in CO₂ emissions, as they outline different potential pathways for energy-related CO₂ emissions by 2050. The above outcome serves as a visual warning related to the gap existing between current market-driven trends and the ambitious goal of a Net-Zero Scenario, widely exceeding the main target of the Paris Agreement.

To prevent dangerous climate change, heavy investments must occur in the energy sector, in which annual energy sector investments, which averaged USD 2.3 trillion globally in recent years, jump to USD 5 trillion by 2030 in the Net-Zero Scenario. The NZS taps into all the opportunities to decarbonize the energy sector, across all fuels and all technologies, still having some uncertainties. Following the NZS, energy efficiency, solar energy and wind provide half of the emission savings in the next decade, as well as carbon capture and storage (CCUS) and hydrogen deployment.



Source: BloombergNEF. Note: b. is buildings

Figure 1: Economic Transition Scenario [4]

In particular, carbon capture and storage is becoming widely adopted in industrial processes where multiple CO₂ sources are available, typically referred as post-combustion CO₂ capture. Typically, when multiple carbon sources are present, a gathering, transmission and distribution network is needed, and it is called a hub. Each hub has its own standards for CO₂ purity, acceptable impurities, pressure and temperature; currently operating hubs are almost located in the US, with some projects ongoing in Europe and Canada.

As of now, efforts are needed to develop a transport network capable of handling the projected 2030 volumes of CO₂ of 50 million tonnes per year, and 450 million tonnes by 2050, as depicted in Figure 2. Such transport network will be fundamental in terms of delivering captured CO₂ directly to some permanent storage sites, which can be underground facilities where gaseous CO₂ is injected into existing saline aquifers.

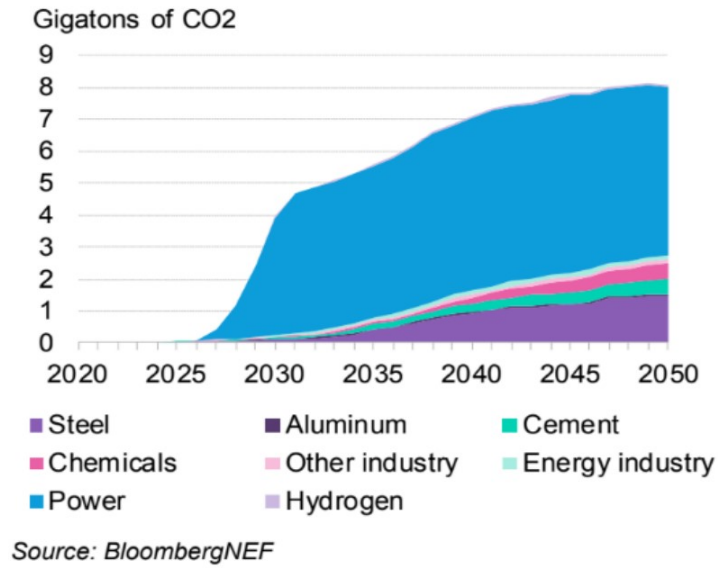


Figure 2: CO₂ captured [4]

Many deployments of CO₂ re-use have been analyzed in recent years, with CO₂ re-use to carbonate materials, CO₂ re-use to chemicals, CO₂ re-use to fuels and CO₂ re-use to polymers and bioplastics. As aforementioned, hydrogen coming from renewable power sources, known as green hydrogen, might play a fundamental role in terms of energy vectors. This compound has been carefully reviewed because of its widespread use.

Likely, the first areas of commercial applications would be in the hard to abate sectors and in electric power production and storage. A detailed description may be found in Figure 3.

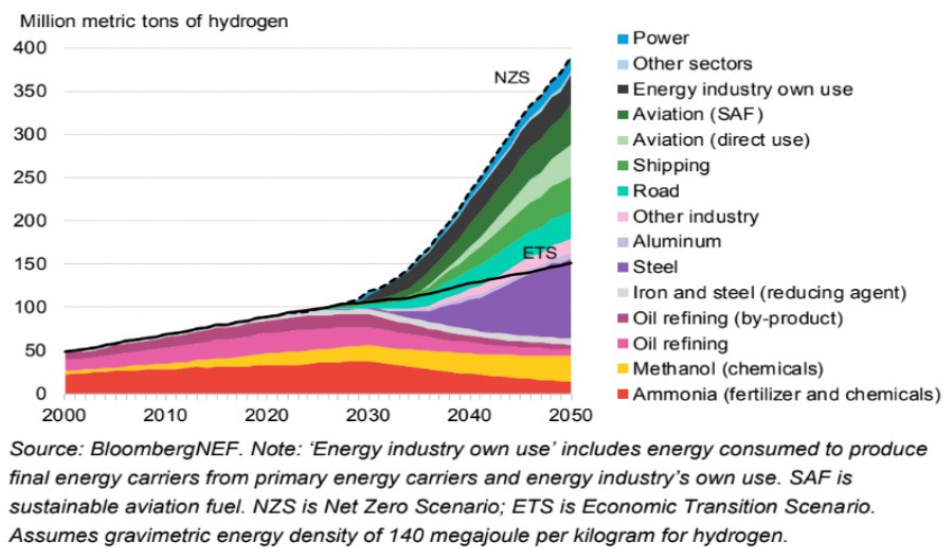


Figure 3: H₂ in NZS and in ETS [4]

As Figure 4 shows, energy resources such as wind, solar, geothermal, bioenergy and nuclear are meant to replace fossil fuel power plants over time in the generation of electricity and heat.

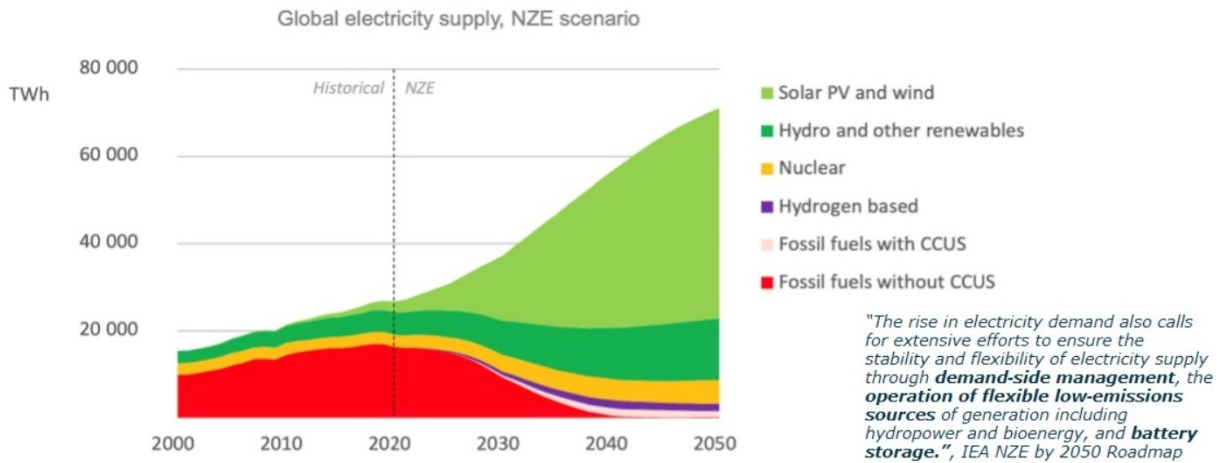


Figure 4: Low emission sources of electricity [19]

Notably, nuclear energy may be found among carbon-free power sources, and its strength may rely on its capability of working in base load scenarios, leading to a perfect integration with intermittent renewable energy sources.

By performing a Life Cycle Analysis (LCA), different energy sources may be compared with nuclear energy in terms of CO₂ emissions. Not surprisingly, among the many studies conducted by government agencies and International research institutions, nuclear power shows its powerful capacity not only to be a high energy density power source, but also one of the cleanest sources available on Earth.

An insight towards equivalent emissions of CO₂ per source of electricity is shown in Table 1.

It is clearly visible from Table 1, how sources are expressed in terms of a CO₂ emission range, mainly depending on the geographical location and on the methodology used to perform a Life Cycle Assessment. And so nuclear, being a carbon-free source, has been considered in the production of renewable hydrogen, by exploiting its electrical energy output (and heat if needed) and coupling it with an electrolysis stack; this takes the name of pink hydrogen.

| Energy Source | Emission CO _{2eq} /kWh |
|------------------------------|---------------------------------|
| Nuclear | 5 – 11 |
| Onshore Wind | 7.8 – 16 |
| Hydroelectric | 70 |
| PV | 8 – 83 |
| Biomass | 8.5 – 130 |
| Natural Gas (Combined Cycle) | 400 – 550 |
| Coal | 800 – 1200 |
| Offshore Wind | 12 – 23 |

Table 1: Energy source emissions [32]

To conclude, nuclear energy has always been widely discussed, mainly because few people have really understood its meaningfulness, but with the climate change we are living in, things have started to change. This is why, in recent years, bureaucrats and politicians have begun to take into consideration the benefits of nuclear energy and its possible integration with renewables.

The development of new technologies in the field of nuclear energy, might have a role in fighting climate change. As an example, recent nuclear reactor technologies may face this challenge from a wider perspective, having a greater capability to be integrated within other energetic and industrial systems, thus improving their efficiency. In line with this goal, this work assesses the flexibility of new nuclear technologies. Therefore, the present work focuses on the development of an object-oriented model to describe the dynamic behavior of a new generation reactor, and its subsequent validation and assessment of operational flexibility.

1 | State of the Art

1.1. Introduction

Advanced reactors might play a crucial role in the decarbonization scenario, not only by providing electrical energy but also by enabling the exploitation of high-temperature heat sources. These reactors hold peculiar features, offering improvements and more opportunities concerning flexible operation [24]. The term ‘advanced’ refers to the upgrades with respect to their predecessors, i.e. conventional nuclear power plants in operation. The next generation of nuclear power reactors aims to use fuel more efficiently, reduce waste production, be economically competitive and meet tight standards of safety and proliferation resistance [24].

With these goals in mind, experts stated the six concepts of advanced reactors, which are: Lead-cooled Fast Reactor (LFR), Sodium-cooled Fast Reactor (SFR), Gas-cooled Fast Reactor (GCR), Supercritical Water-cooled Reactor (SCWR), Very-High-Temperature Reactor (VHTR) and Molten Salt Reactor (MSR).

Their designs feature thermal and fast neutron spectra, closed and open fuel cycles, and span over a wide range of reactor sizes. These advanced reactors, also known as Generation IV systems, aim at performance improvement, considering new applications for nuclear energy and sustainable approaches to the management of nuclear materials.

Among them, high temperature systems offer the possibility of efficient process-heat application and hydrogen production. In particular, the pink hydrogen market is expected to grow quite fast in the upcoming years, as depicted in Figure 1.1, showing a noticeable increase in the production of hydrogen using nuclear energy as its power source.

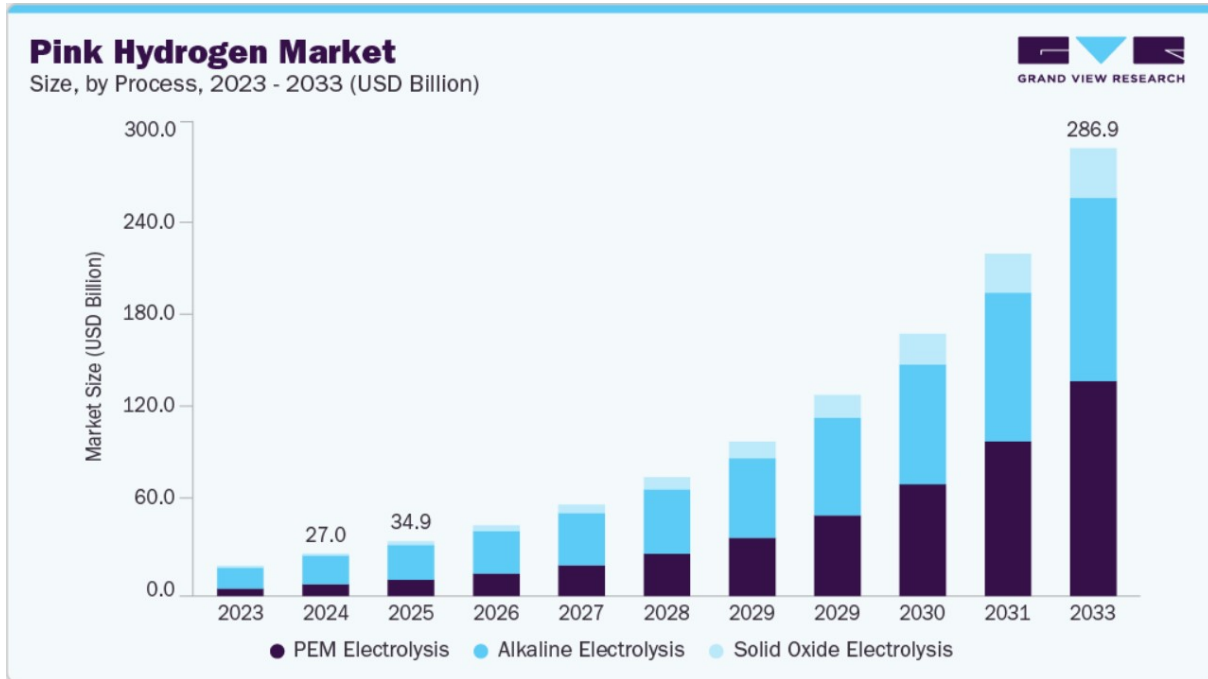


Figure 1.1: Pink Hydrogen Market [14]

Primarily, to enhance sustainability, the adoption of a closed fuel cycle might be employed, focusing on the reprocessing and recycling of uranium, plutonium and minor actinides in fast reactors, present in the spent nuclear fuel. These steps allow us to obtain a notable reduction in waste generation and uranium resource requirements.

In Table 1.1, an overview of Generation IV systems may be found.

| No. | System | Neutron spectrum | Coolant | Outlet T (°C) | Fuel cycle | Size (MW _{el}) |
|-----|--------|------------------|----------------------------|---------------|-------------|--------------------------|
| 1 | VHTR | Thermal | Helium | 900–1000 | Open | 250–300 |
| 2 | GFR | Fast | Helium | 850 | Closed | 1200 |
| 3 | SFR | Fast | Sodium | 500–550 | Closed | 50–150 |
| | | | | | | 300–1500 |
| 4 | LFR | Fast | Lead | 480–570 | Closed | 20–180 |
| | | | | | | 300–1200 |
| | | | | | | 600–1000 |
| 5 | MSR | Thermal/Fast | Chloride or fluoride salts | 700–800 | Closed | 300–1000 |
| 6 | SCWR | Thermal/Fast | Water | 510–625 | Open/Closed | 300–700 |
| | | | | | | 1000–1500 |

Table 1.1: Overview of Gen-IV systems [24]

1.2. MSR technology

In the light of foregoing, Nuclear Power Plants might be based on different technologies. One of the most cited in this work is the one dealing with molten salts.

Molten salt reactors have been investigated since the 1950s [25], opening quite important research areas, both based on the chemical behavior of molten salts and nuclear reactor design. The key feature of such technology can be found in the dual behavior of the molten salt mixture, acting both as a fuel and a coolant. They are also referred to as Homogeneous Reactors.

Molten salt reactors, as stated before, took part in the GIF in 2001, being one of the six more prominent advanced reactors, see Figure 1.2. From the cited picture, a reactor vessel is implemented as a structural containment of the reactor core. In addition, the fuel pump as well as the heat exchanger are depicted, with the latter having the role to overheat some steam in order to supply it to a turbine train, where it is mechanically coupled with an electric generator, hence producing electricity. Furthermore, heat extracted from the reactor, may be employed for non-electrical applications, such as district heating or heat supply for electrolyzers.

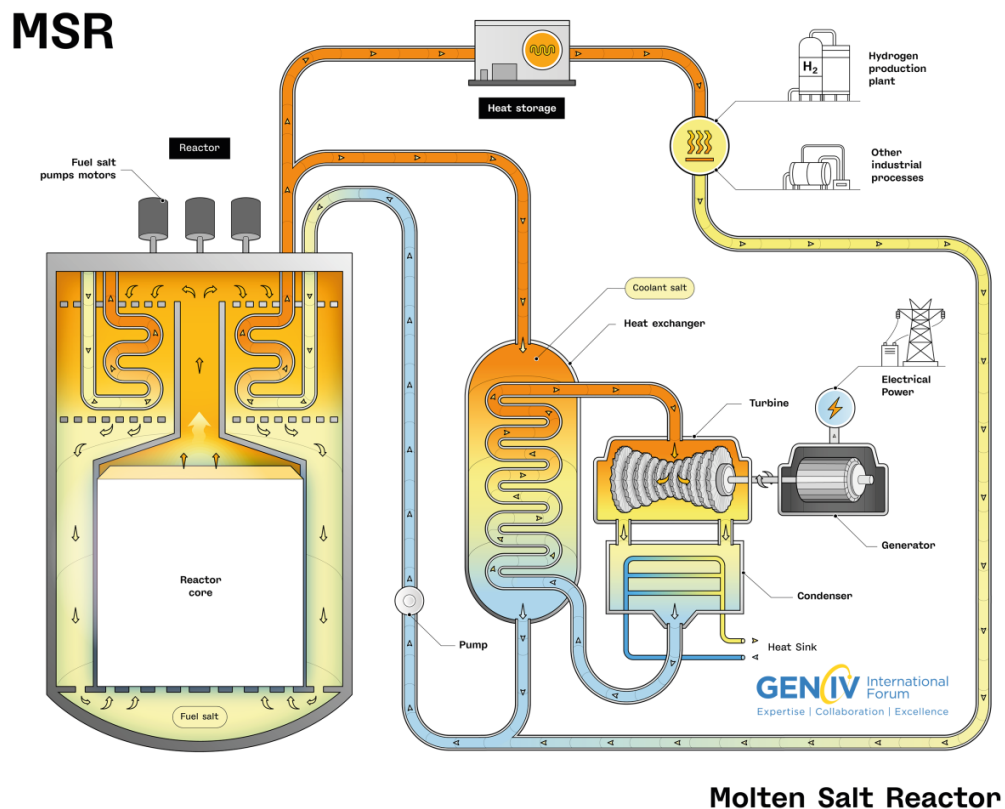


Figure 1.2: MSR in Generation IV International Forum [24]

The MSR is a concept, indeed, the MSR generic name covers thermal and fast reactors, operated with a U/Pu or a Th/²³³U fuel cycle, or as TRans-Uranium (TRU) burners, with a fluoride or a fluoride-carrier salt.

Depending on the fuel cycle, MSRs can reuse fissile and fertile materials from LWRs. They can also use uranium, or burn plutonium or minor actinides. They have an increased power-conversion efficiency, since fission directly occurs in the carrier salt, which transfers its heat to the coolant salt in the heat exchangers. MSRs are operated at low pressure, slightly above atmospheric pressure. They can be deployed as large power reactors or as Small Modular Reactors. Their deployment today is limited by technological challenges, such as high temperatures, structural materials, and corrosion.

Liquid-fueled reactors, possess several potential advantages over their solid-fueled counterparts. These benefits arise from the liquid fuel's unique properties, which allow for a more efficient and flexible system. A primary advantage is the ability to adjust fuel composition and reprocess fuel without needing to shut down the reactor. This continuous process enhances operational efficiency. Furthermore, homogeneous reactors circumvent the complexities associated with the fabrication and refabrication of solid fuel, especially when handling large quantities of transuranic elements. This eliminates a significant hurdle in fuel cycle management. Additionally, these systems offer the potential for superior resource utilization, as transuranic elements can remain in the liquid fuel for extended periods, undergoing fission or transmutation into fissile elements and thus achieving high fuel burnups.

Beyond the inherent properties of liquid fuel, the design in which it also acts as a coolant offers further distinct benefits. This circulating liquid fuel system eliminates the delay in heat transfer inside the core, as heat is produced directly within the substance that also serves as the coolant. The homogeneity of the fuel negates the need for a complex loading plan, simplifying reactor management.

Finally, the design allows for rapid, passive reconfiguration of the fuel geometry through gravitational draining, a key safety feature.

More details about the advantages of employing MSRs are provided below, but first, an overview of the different classes of Molten salt reactors is shown in Table 1.2.

| MSR family | Graphite-based MSRs | | Homogeneous MSRs | | Heterogeneous MSRs | |
|---------------------|---|--|---|--|---|--|
| | Fluoride-salt-cooled reactors | Graphite-moderated MSRs | Homogeneous fluoride MSRs | Homogeneous chloride fast MSRs | Non-graphite-moderated fast MSRs | Heterogeneous chloride fast MSRs |
| Major utilized salt | Fluoride | | Chloride | | Fluoride | Chloride |
| Neutron spectrum | Thermal | | Fast | | Thermal | Fast |
| MSR type | Salt-cooled reactor with pebble-bed fuel or fixed fuel | Single-fluid Th-U breeder Two-fluid Th-Pu breeder Uranium converters, etc. | Fluoride-fast Th-U breeder Pu containing fluoride-fast reactor | Chloride-fast breeder reactor Chloride-fast B&B reactor | Solid or liquid moderator heterogeneous MSR | Heterogeneous salt-cooled or lead-cooled fast MSR |

Table 1.2: Classification of MSRs by the IAEA [18]

1.2.1. Safety Advantages

During recent years, significant research has been carried out on MSR technology in various Member States of the IAEA, thanks to its various set of features that distinguish MSRs from conventional Light-Water reactors. To have a clearer sight when dealing with molten salt systems, the following list is meant to capture its potential safety advantages and highlights some of the key points already discussed [18].

- Near atmospheric operating pressure. This leads to a reduction in mechanical stresses to the structural materials, meaning a lower risk is present with respect to the Light-Water Reactors.
- Radioisotope retention. Because of their feature of being excellent solvents, molten salts have the capability to bond with fission gases, giving rise to an additional barrier to the accidental case of radioisotope release. This quality represents a fundamental distinction between MSRs and Light-Water Reactors, where fission products are retained inside the fuel pins, increasing the plenum pressure.
- Chemically inert and not flammabale. Typically, molten salts have a low reactivity, resulting in no potential for a hydrogen explosion or any kind of chemical reaction with air, water and nearby materials.
- Removal of gaseous fission products. As already underlined, this will lower the risk of an accidental scenario involving the core.
- No irradiation damage or mechanical failure of the fuel. Potential hazard regarding the mechanical failure of the fuel system will not occur anymore, with the fuel being in a liquid phase.
- Strong negative reactivity temperature feedback. Intrinsic stability in MSRs is due

to a combination of Doppler effects, fuel salt expansion and moderator temperature.

- Molten salt as a heat sink. They will absorb some of the decay heat after the reactor shutdown. In addition, when dealing with moderated MSR, an additional region of the core will act as a heat sink.
- Good physical properties. Molten salts are characterized by having a high boiling point and an elevated heat capacity, allowing the fuel to accommodate extreme temperature transients in case of an accidental scenario, without losing its capacity to cool down.
- Excellent neutron economy. The absence of cladding and metallic materials, as well as burnable poisons, enhances neutron economy as fewer neutrons are captured and removed from the fission reaction purpose. This is valid for MSR employing a liquid fuel mixture.

1.2.2. Economic Advantages

Among the advantages of the MSR, several economic statements can be made. This subsection also aims to underline how economic benefits may derive directly from the safety assets [18]. Indications concerning economic gains can be retrieved in Table 1.3.

| Advantages | Detailed Description |
|----------------------------------|---|
| High Temperature | Working with operative temperatures greater than 600°C, allows to exploit high thermodynamic efficiencies, up to 50% [24]. To do so, it is possible to explore both Rankine cycles and Brayton cycles as power conversion loops since we are dealing with highly energetic salts. In further evidence of high temperature benefit, non-electrical applications also may be investigated, such as petrochemical industry, solid oxide electrolyzers, ammonia and liquid fuel production and desalination facilities. |
| Effective Load Following | Among the qualities, some MSR concepts provide great promise in terms of flexibility, with negative temperature reactivity feedback acting instantaneously as fuel temperature increases, enabling the system to reach a new equilibrium condition in a reasonable time. |
| High Resource utilization | Accordingly, even when MSRs are working with an open cycle, waste is minimized with respect to commercial power plants. Because of its excellent features cited above, Molten salt reactors are able to work with a higher burnup and lower initial fissile fuel enrichment. |
| Fuel qualification | With solid fuel reactors, ensuring integrity necessitates years of testing and dedicated irradiation programs where any damage is identified, while with liquid fuel reactors, a simplified fuel qualification process is adopted. [7]. |
| Compact form factor | The reactor core volume results in better utilization when using liquid fuels. In particular, both thermal and fast-spectrum reactors open the possibility of modularity and, coupled with their load-following capabilities, make MSRs very attractive for modern use of power grids. |

Table 1.3: Economic advantages of Molten salt reactors

1.2.3. Technical Challenges

Before mentioning the ongoing projects about MSR in Section 1.2.4, a few declarations about the technological challenges need to be addressed. Although great importance is given to the demonstration of the Molten Salt Reactor Experiment done in the 1960s, being capable of operating continuously without any troubles [25], a few technical and developmental hurdles lie ahead of the modern MSR commercial deployment [18].

For the sake of simplicity, these challenge areas will be treated separately.

- **Reactor Physics:** Even though MSR reactor physics is well known, some Multiphysics simulations are still facing some hurdles, as the lack of acceptability by a regulatory body for MSR multiphysics simulation software represents a significant challenge [18].

As evidence of this, no data about low energy thermal scattering for different kinds of salts is available. Furthermore, information about damage caused by irradiation on structural material, i.e. Displacement per Atom, still has to be found.

A way to overcome this lack is related to performing some significant modeling and experimental validation, which would fill the remaining gaps.

- **Salt Chemistry and Material Science:** Accordingly, material discovery and testing via multiscale simulations and machine learning approaches will lead the way. A key point in salt definition is the determination of both its physical and chemical properties. This objective can be treated in molecular dynamics simulations, giving useful information for nuclear reactor design.

Material science also deals with the degradation of structural materials, as corrosion may induce this phenomenon; this is why strict control over the fuel composition plays a crucial role. Another aspect to keep track of, is the Redox Potential, since its monitoring and control may mitigate corrosion issues.

In addition to that, working with graphite-moderated reactors requires rapid replacement in the core volume, since it might be subjected to fast degradation, due to volume changes and structural deformation, leading to the swelling phenomenon. Consequently, being a technical challenge, the capability to extend graphite lifetime in the reactor core is still under investigation. Even for what concerns instrumentation in MSRs, devices may not be put in contact with the fuel salt mixture due to the harsh environment, which means studies cannot yet guarantee salt compatibility.

- **Engineering Design:** Several challenges under this aspect need to be revised yet. Even though reactor experiments in 1960s, like MSRE, showed good prominent results, further accuracy in thermal hydraulic studies needs to be conducted to gen-

erate data, as issues may arise from high temperature environment in pumps, heat exchangers and piping.

To summarize the previous discussion, an off-gas system has to be present to separate gaseous fission products from the circulating fuel. Studies have demonstrated how degassing may affect positively neutron economy, as neutron poisons are removed (^{135}Xe) [18]. This will lead to a decrease in the potential risk as no pressure buildup would be possible within the reactor core and an increase in fuel efficiency as higher burnups may be achieved.

To finish with, designing and manufacturing mechanical components for which poor data is available are among the key challenges of Molten Salts Reactors. Harsh environments like the one cited may deteriorate those components faster than expected. This is why remote predictive maintenance is likely to be required, complicating things and increasing the overall cost, leading to a new design requirement with the possibility to access the core with low difficulty when changing or repairing selected components.

1.2.4. Ongoing Projects

Within the European Union, several MSR projects are under development. In particular, the ENDURANCE project aims to review thermal and fast-spectrum of several MSR designs, mainly employing chloride salts as fuel carrier. A summary of the current technologies under development can be found in Table 1.4.

| Concept | Fuel carrier | Moderator | Neutron spectrum | Fissile matter / Fuel cycle | Power [MW _{th}] | Use |
|-------------------------------|--------------|-------------|------------------|--|---------------------------|--|
| ARAMIS-A (CEA + ISAC project) | Chloride | None | Fast | Pu + Am | 300 | Electricity production + Waste reduction |
| ARAMIS-P (CEA / Orano) | Chloride | None | Fast | Pu | 300 | Electricity production + Waste reduction |
| CMSR (Seaborg) | Fluoride | Graphite | Thermal | U-based | 250 | Electricity production |
| Copenhagen Atomics MSR | Fluoride | Heavy water | Thermal | Th-based | 100 | Heat production + Waste reduction |
| MSFR-F (CNRS + EU projects) | Fluoride | None | Fast | ^{233}U – enrichU – Pu + MA/Th fuel cycle | 3000 | Electricity production |
| MSFR-CI (CNRS + SAMOSAFER) | Chloride | None | Fast | Pu + MA/U fuel cycle | 3000 | Electricity production + Waste reduction |
| RAPTOR (CNRS/Orano) | Chloride | None | Fast | Pu + MA | 300/500 | Waste reduction + Electricity production |
| Stellarium (Stellaria) | Chloride | None | Fast | U-based or Pu-based | 250 | Energy + Waste reduction |
| Thorizon One (Thorizon) | Chloride | None | Fast | Th and Pu or U based | 250 | Electricity and possibly heat production + Waste reduction |
| XAMR (Naarea) | Chloride | None | Fast | Pu-based | 80 | Electricity and/or heat production + Waste reduction |

Table 1.4: MSRs EU Designs

Among the MSR projects, it is possible to split them into two groups: Fast-spectrum

reactors, which typically use chloride salts and aim at waste reduction or breeding and thermal-spectrum reactors, making use of fluoride salts and requiring a moderator. With reference to Table 1.4, a detailed breakdown by reactor type can be done:

- **Large scale fast reactors:** In the last two decades, the National Centre for Scientific Research (CNRS, France) has focused R&D efforts on the development of a new MSR concept called the Molten Salt Fast Reactor (MSFR) supported by successive Euratom's projects. It is referred to as a fast-spectrum breeder reactor with a large negative power coefficient. The initial version was based on a fluoride LiF salt and could operate with a thorium fuel cycle. A new version was developed in a recent European project [18], which was based on a chloride NaCl salt, operating with a uranium fuel cycle. Other advantages of the MSFR include homogeneous fuel irradiation and the possibility of fuel reload and online processing or in batch mode, without requiring reactor shut-down and involving the transfer of small volumes of fuel. Both versions of MSFR are 3 GWth breeder reactors.
- **Small to medium fast reactors:** This group primarily uses chloride salts in a fast spectrum to optimize the burning of transuranic elements or plutonium. Among this group, the Stellarium reactor can be found, dealing with chloride salts, as a fast breeder reactor. It aims for natural convection, eliminating the need for primary pumps. In addition, it is possible to find the smallest fast concept of a reactor, working at 80 MWth, where its core is a silicon carbide (SiC) plate heat exchanger, aiming to burn the excess plutonium and minor actinides from the existing UOX and MOX cycles. One peculiarity of this concept, is the use of supercritical CO₂ as a working fluid in the power conversion loop. One last example features a modular core composed of multiple individually contained replaceable modules, offering fuel cycle flexibility, with the primary goal of burning LWR-plutonium.
- **Thermal reactors:** These cited reactors make use of fluoride salts and employ a moderator to slow down neutrons. The Copenhagen Atomic Waste Burner is a unique design, using heavy water as the moderator and it is housed in a shipping container-sized vessel [18]. The reactor doesn't require refueling, human intervention, or maintenance for its 5-year design life and operates completely autonomously with passive decay heat removal.

Member States and international organizations have been conducting R&D activities on MSRs under various project schemes. For instance, in Canada, the Canadian Nuclear Safety Commission adopts a risk-informed regulatory framework for licensing advanced reactors. Two small modular MSRs, the IMSR by Terrestrial Energy and the SSR-W300

by Moltex Energy, are among a range of SMR designs under the pre-licensing vendor design review [18]. While in 2011, the Chinese Academy of Sciences restarted a research programme, known as the Thorium Molten Salt Reactor (TMSR) programme, to achieve the safe and economic use of Generation IV MSR and the highly efficient use of the thorium resource [18]. In particular, the TMSR-0 simulator was built and completed in 2019, for testing, verifying and licensing technologies and the training of reactor operators. Furthermore, in recent years, the TMSR-LF1, being a molten salt experimental reactor with liquid fuel and a power design of 2 MWth, has been designed and constructed. The technical goal is to develop a MSR based on thorium and to verify its feasibility [18]. Up to now, the TMSR-LF1 is the only operational molten salt reactor in the world to have loaded thorium-based fuel, confirming the technical feasibility of the thorium-uranium fuel cycle.

1.3. Aim of the Thesis

The first objective of the thesis is to build a model able to replicate, both from a geometrical and operational point of view, the Molten Salt Reactor Experiment (MSRE) primary circuit, utilizing the simulation environment Dymola. The goal of the following work is to provide a validated model of a molten salt reactor, in order to be further exploited for studying its flexibility and so load following capabilities, as well as the coupling with non-electrical applications.

To validate the model, experimental data are taken as a reference from the successful operation of the MSRE developed in the 1960s by the ORNL.

This study is conducted within the scope of the ENDURANCE project, with one of the main objectives being to support the safe development and deployment of MSR technology in Europe by advancing technical knowledge and bridging research and development gaps. The inherent safety, the sustainability, the fuel management and the efficiency, are the key areas of interest in MSR research. In the optics of this work, the goal is to gain knowledge about the dynamic behavior of the MSR, with reference to the MSRE experimental data. This is done to further exploit the safety aspects of the MSR flexibility in terms of operation and cogeneration requirements to safely adopt molten salt reactors in an energy mix with intermittent energy sources.

Due to its highly parameterized nature, the model can be readily adapted to represent various thermal MSR designs, extending its utility well beyond the specific constraints of the MSRE.

This study establishes that foundational molten salt technology reached a significant stage of development decades in the past. Specifically, the MSRE successfully proved the

conceptual integrity of the MSR, with the primary engineering challenges related to its technical realization being largely addressed by the mid-1970s. However, MSRs did not receive the level of funding necessary to proceed into large scale development and deployment. This is why, as of today, a lot of effort is put into the future development of this technology, being one of the most promising advanced nuclear technologies for achieving decarbonization goals in Europe.

The following chapters, will first provide a historical and technical introduction to the application of the MSRE. Subsequently, the focus will shift to the development of the dynamic simulator of the primary circuit, analyzing in detail each model elaborated to represent the various components of the primary loop. Then, the validation of the overall developed model will be presented, along with a further dynamic analysis of the system under specific accidental situations. Therefore, a qualitative and quantitative analysis between the experiments conducted by the ORNL and the present model results will be presented in Chapter 4. Finally, an overview of the limitations of the present model, as well as the future perspective, will be provided. In addition, Appendix A and Appendix B, respectively display further information about the features of the Modelica language employed in this work and the graphite element capabilities to thermalize neutrons.

This thesis work differentiates itself from many other MSR simulation studies primarily through its methodology, rigorous validation approach, and future-oriented application towards system integration. Unlike many simulations that use established codes, this work employs the Modelica language. This allows for the creation of a declarative, non-causal, and modular object-oriented model, which is superior for complex, integrated system analysis. Crucially, this structure makes the model immediately ready for a 'plug-and-play' approach, facilitating seamless connection with other dynamic models of energy conversion systems and/or non-electric applications. In addition, the work moves beyond simple steady state verification by explicitly validating the model's dynamic behavior against historical MSRE experimental transient data. Furthermore, the stability of the model is further tested by simulating specific accident conditions, such as primary pump failure and cold slug insertion.

2 | MSRE Overview

In this chapter, a comprehensive description of the Molten Salt Reactor Experiment has been prepared, showing technical details and its development throughout the years. It describes the origin of the molten salt reactor concept and how the successful results of the aircraft reactor program have established the possibility to deploy molten salt reactors for electricity production. Furthermore, an insight into the fission products' behavior as well as issues related to it, is provided.

2.1. History of MSRE

The Molten Salt Reactor Experiment (MSRE) was conducted by the Oak Ridge National Laboratory to demonstrate if the desirable features of the molten-salt concept could be embodied in a practical reactor that could be constructed and maintained smoothly and one that could be operated safely and reliably [25]. Additional important objectives, were to provide the first large-scale, long-term, high-temperature tests in a reactor environment of the fuel salt, graphite, moderator, and high nickel-base alloy (INOR-8). The operational data gathered from the MSRE was crucial for assessing the feasibility of developing future large-scale molten-salt reactors.

The purpose of the MSRE was to demonstrate key features of a molten salt power reactor, although a steam generator and a turbine/generator were not provided. They achieved many unique features, such as stability of fuel salt, integrity for Hastelloy N and graphite, and the removal capability of gaseous radioactive fission products such as xenon and krypton from fuel salt. One more unique achievement was operation by ^{233}U .

In 1954, the Aircraft Reactor Experiment (ARE) was constructed at Oak Ridge National Laboratory (ORNL) to prove the nuclear viability of operating a molten salt-fueled reactor at high temperatures [25]. Following the successful operation of the ARE, the Aircraft Reactor Test (ART) was started at ORNL as part of the Aircraft Nuclear Propulsion Program (ANP). Although the ART was discontinued in 1957, the high promise of MSRs for achieving low-cost electricity generation in central power stations, prompted ORNL

to continue its foundational research on technology.

Among the many interesting features that characterize the MSR concept, some of them need to be mentioned again, being also valid for MSRE, but a more detailed description may be found in Section 1.2.1.

1. A liquid mixture is representative of the fuel state at the reactor operational temperatures, thus eliminating the extra costs associated with the fabrication, handling, and reprocessing of solid fuel elements. Moreover, burnup in the fuel is not limited by radiation damage or reactivity loss. The fuel can be reprocessed continuously in a side stream for the removal of fission products, and new fissionable material can be added without shutting the reactor down.
2. Molten salt reactors can operate at high temperatures and produce high-pressure superheated steam to achieve thermal efficiencies in the power conversion loop equal to the best fossil fuel-fired plants. The relatively low vapor pressure of the salt permits the use of low-pressure containers and piping.
3. Due to the negative temperature coefficient of the reactor and low excess reactivity, nuclear safety is not primarily dependent upon fast-acting control rods.
4. The fuel salt has a low cross section for the parasitic absorption of neutrons, and when used with bare graphite as the moderator, very good neutron economies can be achieved. Molten salt reactors, are thus attractive as highly efficient converters and breeders on the thorium cycle.
5. The fluoride salts used as the fluid fuel mixture, have good thermal and radiation stability and do not undergo violent chemical reactions with water or air. They are compatible with the graphite moderator and can be contained satisfactorily in a specially developed high nickel alloy, i.e., INOR-8.

Although several studies were conducted, a few fields still needed to be exploited, that is why in 1960, the construction of an experimental facility of a molten salt reactor was proposed to investigate the remaining areas of uncertainty.

In April 1961, ORNL received a directive from the United States Atomic Energy Commission to design, construct and operate the Molten Salt Reactor Experiment.

General view of the building where MSRE construction occurred is shown Figure 2.1.

On a design basis, MSRE had to investigate two main purposes, one was related to its capability to be implemented in a central power station, therefore it was designed in a straightforward installation, without experimental setups that would affect its stability.

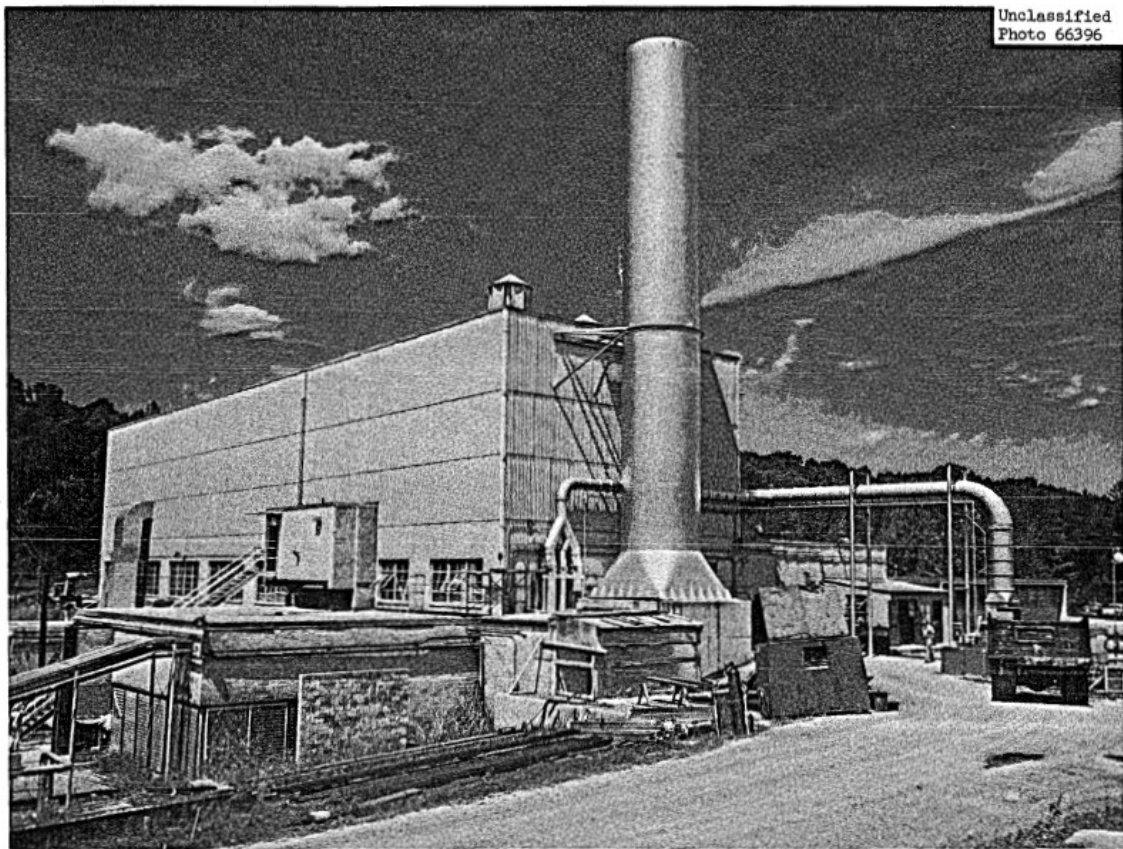


Figure 2.1: Rear View Building 7503 during MSRE construction [25]

Whereas the second goal, was to obtain a large enough capacity for the experimental outcomes to be meaningfully extrapolated for full-scale plants.

As a consequence of this, 10 MW thermal output was chosen, in order to satisfy both requirements. Conversion of the 10 MW of heat to useful electricity was not considered to be necessary to demonstrate the concept, so existing blowers and stack were used to dissipate the heat to the atmosphere. Later that year, its construction officially started.

By the end of 1964, notwithstanding some troubles regarding the graphite moderator installation, the first criticality was reached. A summary of MSRE data activities is shown in Figure 2.2. It operated for 4 years, from 1966 to 1969, without any trouble.

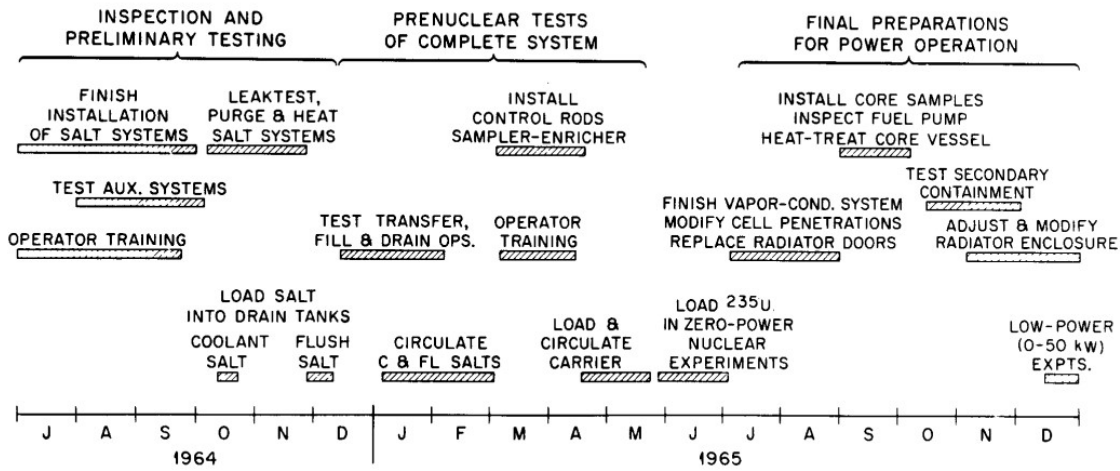


Fig. 4. MSRE activities, July 1964-December 1965.

Figure 2.2: MSRE activities [10]

It demonstrated the possibility of circulating a liquid fluoride mixture without corrosion problems. This was achieved by using a nickel-based alloy and oxidation control of the fuel by use of the U^{3+}/U^{4+} buffer. However, this 10 MWth thermal reactor only tested fissile isotopes (^{233}U , ^{235}U , Pu) and not fertile ones such as ^{238}U or Th due to the capture cross sections which are large with thermal neutrons.

Nevertheless, a continuous physical processing of the fuel was successfully tested, consisting of contacting the fuel with a neutral gas to extract gaseous fission products such as Kr and Xe before they decay into Rb and Cs, which are poisons for thermal neutrons. Unexpectedly, this processing also removed most of the metallic fission products.

Although successful, these tests did not lead to the construction of the Molten Salt Breeder Reactor (MSBR) studied in details by ORNL, partly, because its thermal spectrum requires intensive chemical processing for fission products removal as well as Pa extraction, related to proliferation issues due to the possible ^{233}Pa decay in pure ^{233}U in such conditions, to avoid neutron captures leading to minor actinides. However, these drawbacks are eliminated by using a fast spectrum.

As shown in Figure 2.3, the reactor power was stepped up to 1 MW, 5 MW, and 8 MW over a two-week period in January, with dynamics tests and observations of reactivity and radiation heating at each level.

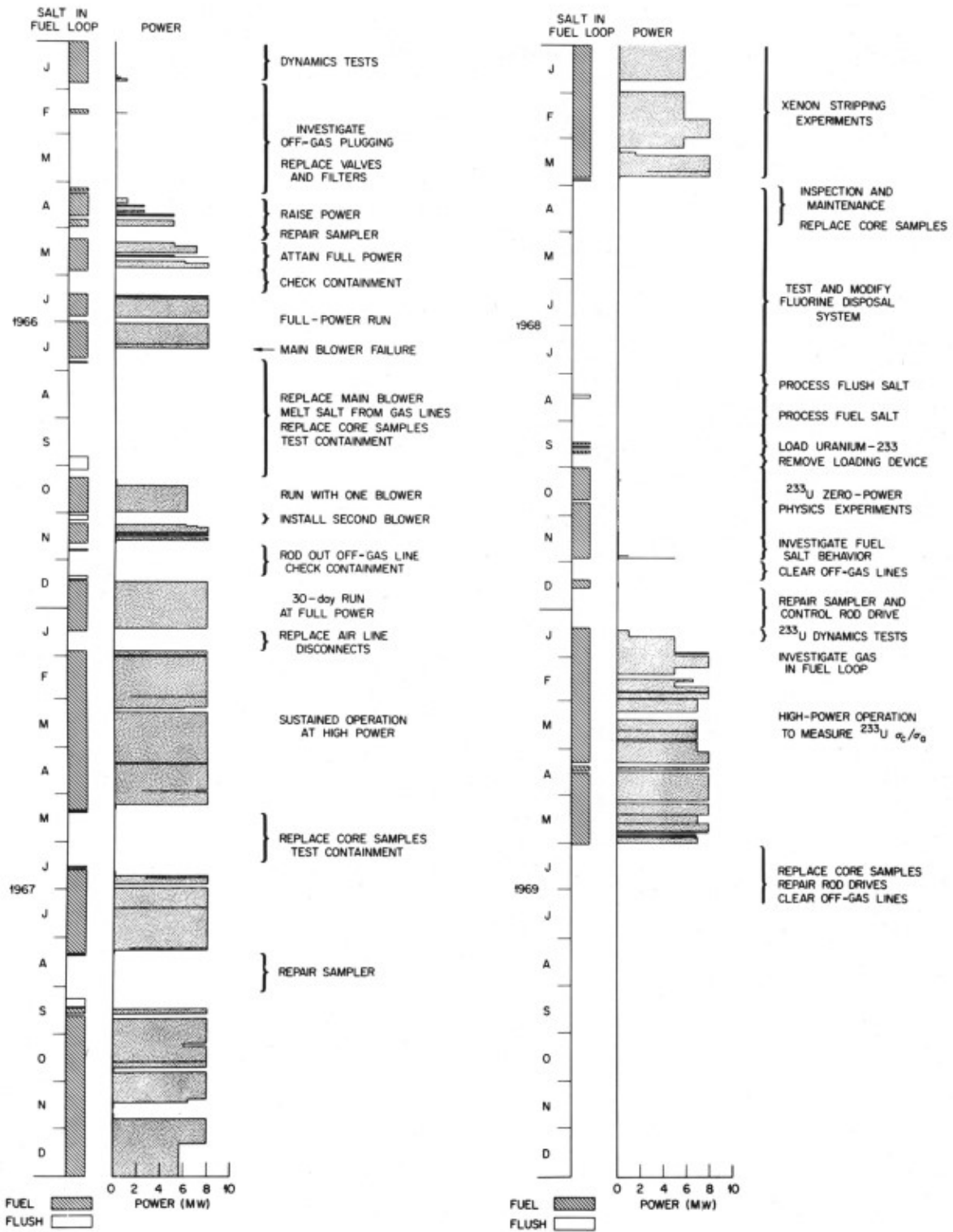


Figure 2.3: Experience of Molten Salt Reactor Experiment [10]

2.1.1. Layout

The Molten Salt Reactor Experiment can be classified among the graphite-moderated MSRs, being a single-region, circulating fluid fuel type of reactor with a nominal power output of 10 MW. The circulating salt is a mixture of lithium, beryllium, and zirconium fluoride salts containing uranium or thorium and uranium fluorides. Heat generation occurs as the fuel flows through cartridges in the graphite core, and the heat is transferred from the fuel salt to a secondary coolant salt in a shell and tube heat exchanger. Finally, the heat is dissipated to the air, in an air blast radiator.

Since power production is not an objective of this experiment, no electric power generation equipment is utilized. This kind of reactor has a prominent position from a historical perspective, and the highest experimental and theoretical efforts so far have been investigated in this technology.

The flowsheet of the MSRE in Figure 2.4, shows the normal operating conditions at 8 MW, that is the maximum heat removal capability of the air-cooled secondary heat exchanger.

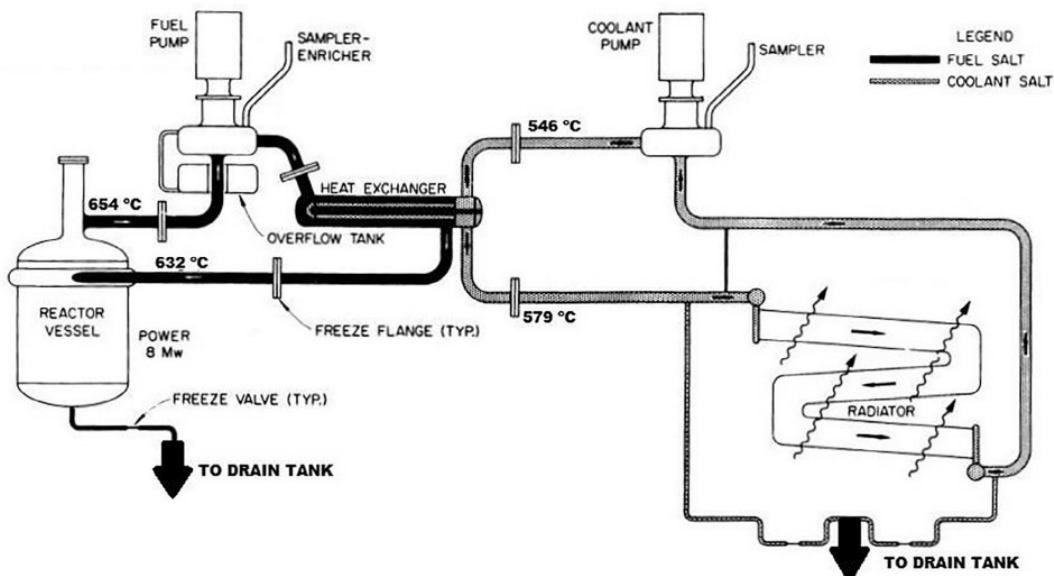


Figure 2.4: Layout of MSRE [25]

The fuel-circulating system is clearly visible, and it is part of the primary circuit system, in which there is the presence of a reactor vessel, where the fission nuclear reaction occurs and the fuel heat exchanger where the heat flows from the fuel to the coolant salt. From

the simplified diagram above, the plant layout can be subdivided into two different loops, a primary circuit and a secondary circuit, both working with different salt mixtures. Information about the main operation parameters of MSRE are shown in table 2.1. Whereas, compositions and physical properties of fuel and coolant salts taken from [25] are shown in Table 2.2.

| Parameter | Value |
|-------------------------------------|---|
| Design Full Power | 10 MWth |
| Actual Full Power | 7.4 MWth |
| Hot Leg Temperature | 632 °C |
| Cold Leg Temperature | 654 °C |
| Core ΔT | 22 °C |
| Primary Fuel Salt | LiF – BeF ₂ – ZrF ₄ – UF ₄ |
| Primary Mass Flow Rate | 0.07571 m ³ /s |
| Primary Pressure | 0.03447 MPa |
| Moderator | Graphite |
| Secondary Salt | LiF – BeF ₂ |
| Secondary Loop Mass Flow Rate | 0.05363 m ³ /s |
| Secondary Loop Hot Leg Temperature | 579 °C |
| Secondary Loop Cold Leg Temperature | 546 °C |

Table 2.1: MSRE Design and Operational Parameters [15]

Three different kinds of fuel salts are reported, as they have all been employed throughout the life of the MSRE. Favorable neutron absorption and chemical and physical properties were important requirements for the composition selected. Beryllium fluoride is used to obtain a low melting point. Lithium fluoride (99.99 % ⁷Li in both fuel and coolant salts) imparts good fluid flow properties to the mixture. Zirconium fluoride protects the fuel salt against precipitation of UO₂ from contamination by air and moisture, because Zr precipitates as an oxide preferably to uranium, thorium and plutonium.

The first experiments in the MSRE have been run with partially enriched uranium since uncertainties were present concerning the chemical behavior of that fuel. Later, the reactor was operated with highly enriched uranium fuel and thorium-uranium fuel.

| | Fuel Salt | | | Coolant Salt |
|---------------------------------------|----------------------|-------------------|----------------------|--------------------|
| | Th-U | Highly Enriched U | Partially Enriched U | |
| Composition, mole % | | | | |
| LiF (99.99% ⁷ Li) | 70 | 66.8 | 65 | 66 |
| BeF ₂ | 23.6 | 29 | 29.1 | 34 |
| ZrF ₄ | 5 | 4 | 5 | – |
| ThF ₄ | 1 | 0 | 0 | – |
| UF ₄ | 0.4 | 0.2 | 0.9 | – |
| Physical Properties, at | 922 K | | | 844 K |
| Density, kg/m ³ , at 922 K | 2242.6 | 2082.4 | 2146.5 | 1922.2 |
| Viscosity, mPa · s | 7.44 | 7.03 | 8.27 | 9.92 |
| Heat Capacity, J/(kg · K) | 1884.1 (at 922 K) | 2010 | 1967.8 | 2219 (at 922 K) |
| Thermal Conductivity, W/(m · K) | 5.56 | 5.54 | 5.54 | 6.06 |
| Liquid Temperature, K | 722 | 722 | 722 | 728 |

Table 2.2: Composition and Physical Properties of Fuel and Coolant Salts [25]

2.2. Primary Circuit

The primary circulating loop consists of the reactor vessel, the fuel pump, the heat exchanger, connecting pipes and auxiliary systems. The major components of this system were located in the reactor hot cell, which provided safety against salt freezing.

2.2.1. Reactor Vessel

The main parts of the MSRE reactor core included an inlet pipe, a flow distributor, an annular downcomer, a lower plenum, a core support structure, a horizontal graphite lattice, a vertical graphite core barrel, an upper plenum, and an outlet nozzle.

The reactor vessel is a 1.52 m diameter, 2.44 m height tank, containing a 1.44 m diameter by 1.63 m high graphite core structure. Under design conditions of 10 MW of reactor heat, the fuel salt enters the flow distributor at the top of the vessel at around 635°C and 2 bar. The fuel is then distributed uniformly around the circumference of the vessel and

then flows turbulently downward in a spiral path through an annulus between the vessel wall and the core can, i.e. downcomer. The fuel salt loses the rotational motion in the straightening vanes in the lower plenum, where it turns and flows upward through the graphite matrix in the core can. More details are shown in Figure 2.5.

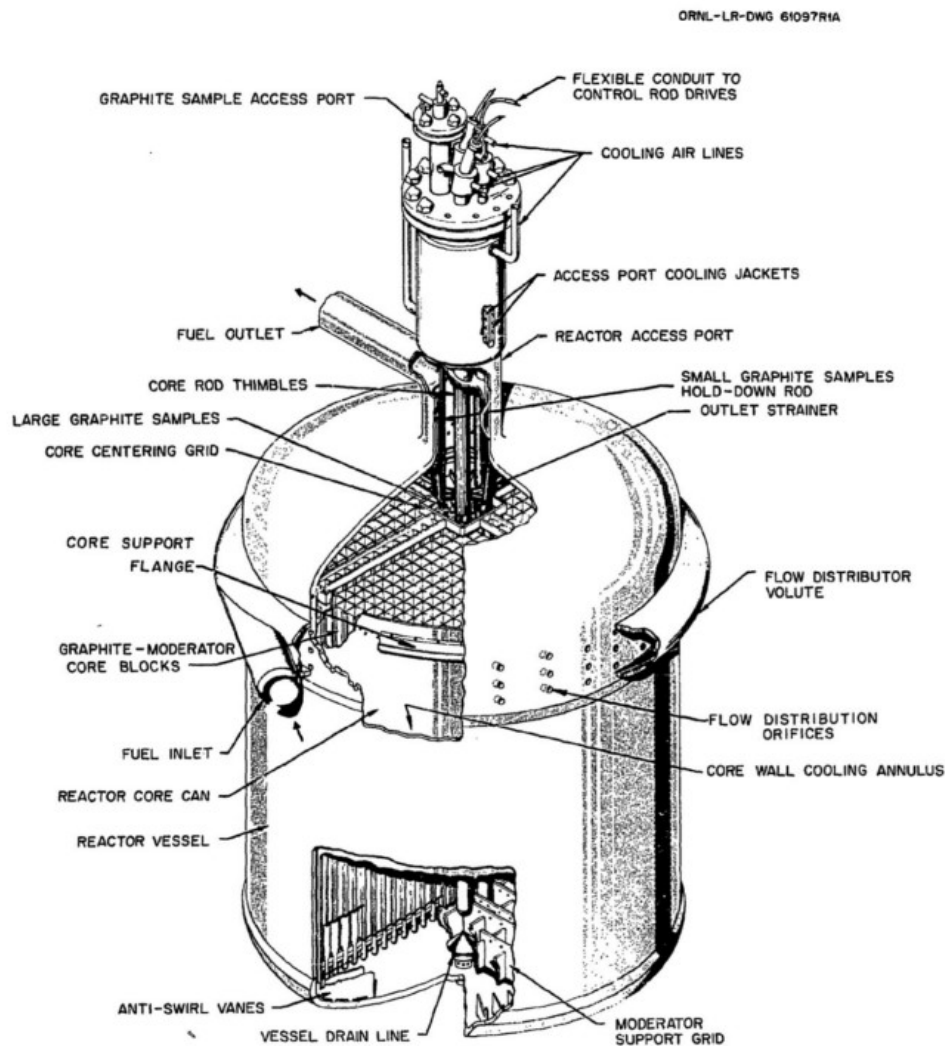


Figure 2.5: MSRE Reactor Core [25]

The graphite matrix is a solid assembly of 1140 vertical bars, named cartridges, 5.08 x 5.08 cm and 170 cm long [25]. The structure of the graphite block, as well as the flow channel for the fuel salt, is illustrated in Figure 2.6. It is particularly desirable, that the moderator should be used without cladding in order to obtain high breeding or conversion ratios. At 10 MW thermal output, and with no fuel absorbed by the graphite, heat was generated in the core through fissions in the fuel salt, as well as internal heating from gamma, beta, and neutron irradiation in core structures.

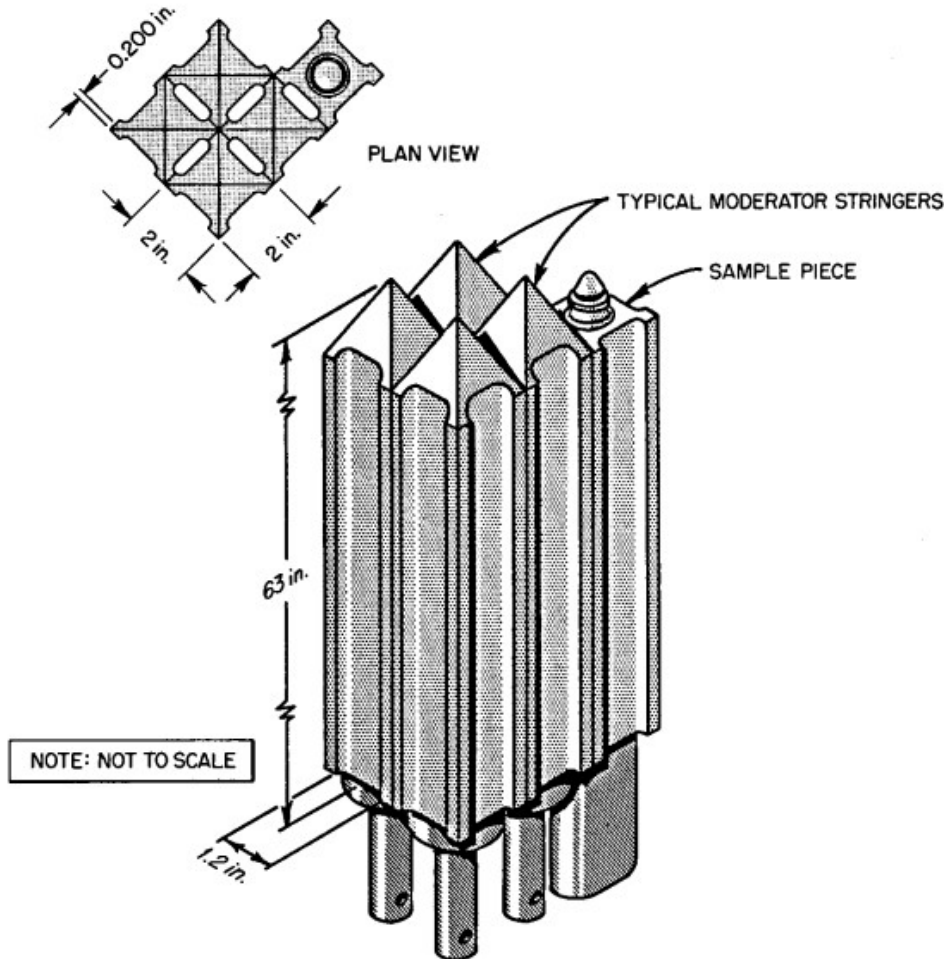
UNCLASSIFIED
ORNL-LR-DWG 56874 R

Figure 2.6: MSRE Graphite block [25]

Around 88% of the fissions occurred in the fuel channels, with 6% in the upper plenum, 3% in the downcomer, and 3% in the lower plenum [15].

Flow in the coolant channels is laminar, nonetheless, both the graphite and the fuel have good thermal conductivities, that is why the maximum temperature of the graphite is only about 15°C above the mixed mean temperature of the adjacent fuel. In addition, with the core being quite small, neutron leakage is quite high, but no blanket of fertile material is present.

As cited before, graphite is compatible with molten salts, therefore use of unclad graphite is employed, making it possible also for the consistency with fission products and INOR-8.

2.2.2. Fuel Pump

The reactor fuel salt is circulated directly to the centrifugal-type pump. The pump has a vertical shaft and overhung impeller and operates at a speed of 1160 rpm to deliver 0.076 m³/s at a discharge head of around 15 m. The pump is equipped with ball bearings that are lubricated and cooled with oil circulated by an external pumping system. Mechanical shaft seals keep the oil contained within the bearing housing [25].

The pump bowl is equipped with devices to measure the liquid level and, once the level reaches the nozzle of the overflow pipe, the fuel salt will be discharged into the overflow tank placed under the pump bowl. In addition, helium gas flows inside the pump bowl to remove gaseous fission products such as ¹³⁵Xe and ⁸⁵Kr to the off-gas disposal system. A schematic view of the fuel pump is displayed in Figure 2.7.

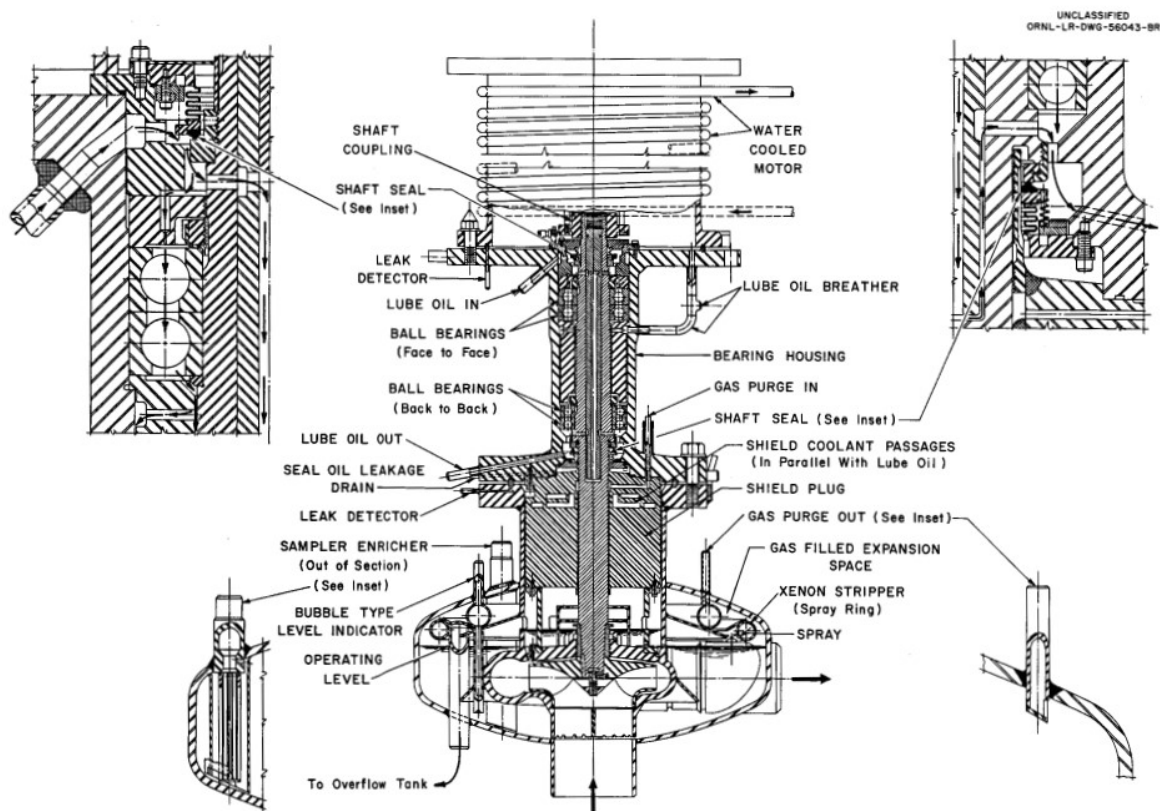


Figure 2.7: Fuel Pump [25]

2.2.3. Heat Exchanger

The heat exchanger is a shell and U-tube type, with the fuel salt circulating in the shell and the coolant salt in the tubes (see Figure 2.8). It is of all-welded construction, and it is fabricated of INOR-8 throughout, except for the back-braze alloy used in the tubesheet joints.

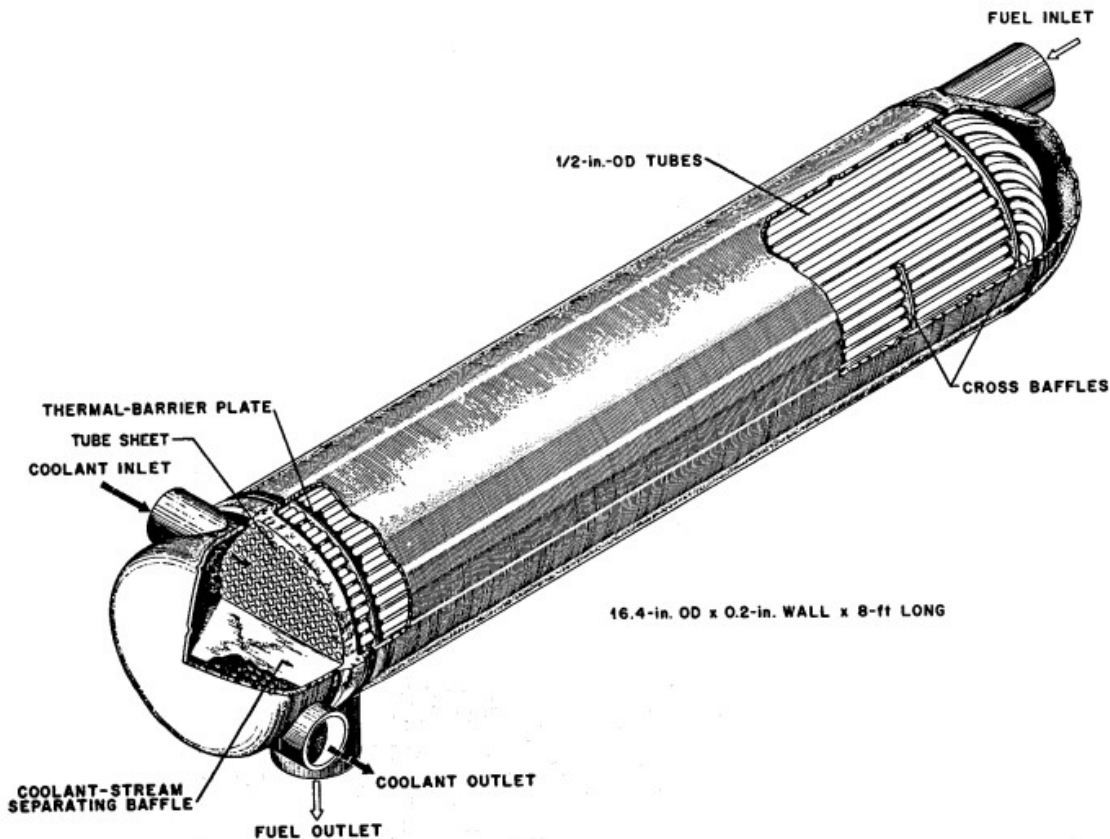


Figure 2.8: Heat Exchanger [25]

The overall dimensions and design data are summarized in table 2.3. Salt discharged by the fuel pump flows through the shell side of the heat exchanger, where it is cooled from 662°C to 635°C . The heat exchanger is about 0.406 m in diameter and 2.44 m long and contains one hundred sixty-three 12.7 mm OD U-tubes with an effective surface of 23.6 m^2 . Whereas, the coolant salt circulates through the tubes at a rate of $0.0536\text{ m}^3/\text{s}$, entering roughly at 552°C and leaving at 593°C .

The heat exchanger was designed for low holdup of salts, simplicity of construction, and moderately high performance. The space limitations within the containment cell, required a fairly compact unit. A U-tube configuration best satisfied this requirement and minimized the thermal expansion problems in the exchanger.

In ORNL models, heat transfer coefficients, were assumed to be constant on both sides of the tube wall. In particular, with a circulating velocity in the tubes of about 3.69 m/s, this gave rise to a turbulent flow regime with a Reynolds number of about 9'060, therefore a heat transfer coefficient was calculated to be around 27'723 W/(m² · K). On the other hand, the heat transfer coefficient on the shell side is estimated to be 18'700 W/(m² · K), for a Reynolds number of 13'000 [25].

MSRE operation has shown that conventional design calculations adequately predict heat transfer in molten-salt heat exchangers and there is no change in heat transfer over an extended period of operation.

2.2.4. Downcomer

Salt flowed from the flow distributor into the annular downcomer of the reactor vessel. The downcomer consisted of the space between the 142 cm outer diameter core barrel and the 147 cm inner diameter of the cylindrical portion of the reactor vessel.

It had a height of approximately 162.6 cm from the flow distributor inlet to the lower plenum [15]. There were small gaps in the support flange at the top of the downcomer annulus that allowed 0.001514 m³/s of bypass flow from the top of the downcomer directly to the upper plenum.

This served to cool the support flange and to prevent localized overheating due to internal heat generation in the metallic structures. Around 3% of the total fission power was produced in the downcomer region [15].

2.2.5. Lower Plenum

After leaving the cooling annulus, the fuel salt enters the lower head of the vessel, which serves as a plenum where the salt is distributed to the reactor core passages.

48 vanes are present, fabricated 3.175 mm thick INOR 8 plate, in the head have a radial length of about 28 cm, or about 30% of the vessel radius. The vanes check the swirl developed in the annulus to reduce the radial fluid pressure gradient in the lower head. This small gradient is judged to have a negligible effect on the distribution of the fuel to the core passages.

Measurements concerning heat transfer were made in the lower plenum of both the small and full scale models. The latter appeared to give the most reliable results, indicating a heat transfer coefficient of about 8517 W/(m² · K) at a point about 43 cm radial distance from the outer circumference [25]. This value is based on both heat meter measurement and on calculations which make use of the measured velocity profiles. The average heat

generation within the wall of the lower head was estimated to be 0.61 W/cm^3 .

If the walls were so insulated, that all internally generated heat must be dissipated to the fuel solution, the inner wall surface temperature would be higher than the bulk fluid temperature. However, for simplicity, in this work we are considering no heat transfer to the internal walls.

All the estimated values mentioned above, assume no deposition of solids on the lower head. If solid particles of ZrO_2 were formed in the MSRE by oxidation of the fuel salt, these particles would probably settle on the lower head. The presence of this sludge would increase the temperature of the wall of the lower head by increasing the heat source at the wall and by reducing the heat transfer coefficient from the wall to the salt.

2.2.6. Upper Plenum

The fuel salt flowed from the fuel channels into the upper plenum of the reactor vessel, where 6 % of the fission power was generated [15]. The upper plenum contained the upper core support structures, control rod thimbles, sampler basket thimbles, and graphite strainer. The fluid volume of the upper plenum was estimated to be approximately 0.321 m^3 .

The upper plenum combined the flows from the core bypass and fuel channels. The salt then flowed out of the reactor vessel through the upper outlet nozzle. During operation, the reactor outlet temperature was measured with a thermocouple on the surface of the pipe at the reactor outlet nozzle.

2.3. Secondary Circuit

2.3.1. Radiator

One of the main considerations in the design of the MSRE radiator, was to be protected against freezing of the coolant salt in the tubes in an accidental event of sudden loss of reactor power. Other important design factors, were that the radiator was to be used in conjunction with air-handling equipment already installed as part of the ART program, that the heat dissipation rate would be adjustable from zero to 10 MW, and that the unit must be capable of operating for long periods of time without direct access for inspection or maintenance. The salt should move downward through the radiator as it is cooled.

The radiator consists of 65.03 m^2 of cooling surface, provided by 120 tubes, approximately 2 cm in diameter and 9 meters long, with cooling air being supplied by two 250 horsepower axial blowers with a volume flowrate of air of about $94.4 \text{ m}^3/\text{s}$. Concerning the coolant salt

temperature, it enters at 593°C and leaves at 552°C, whereas the cooling air temperature is 93°C at design power. Each of the radiator tubes is provided with a thermocouple, to give a warning of restricted coolant salt flow in any of the passages.

A total of 149 thermocouples is installed within the radiator, 120 on the tubes and the remainder on the inlet and outlet headers and tube supports.

The radiator coil configuration used, might be seen in Figure 2.9.

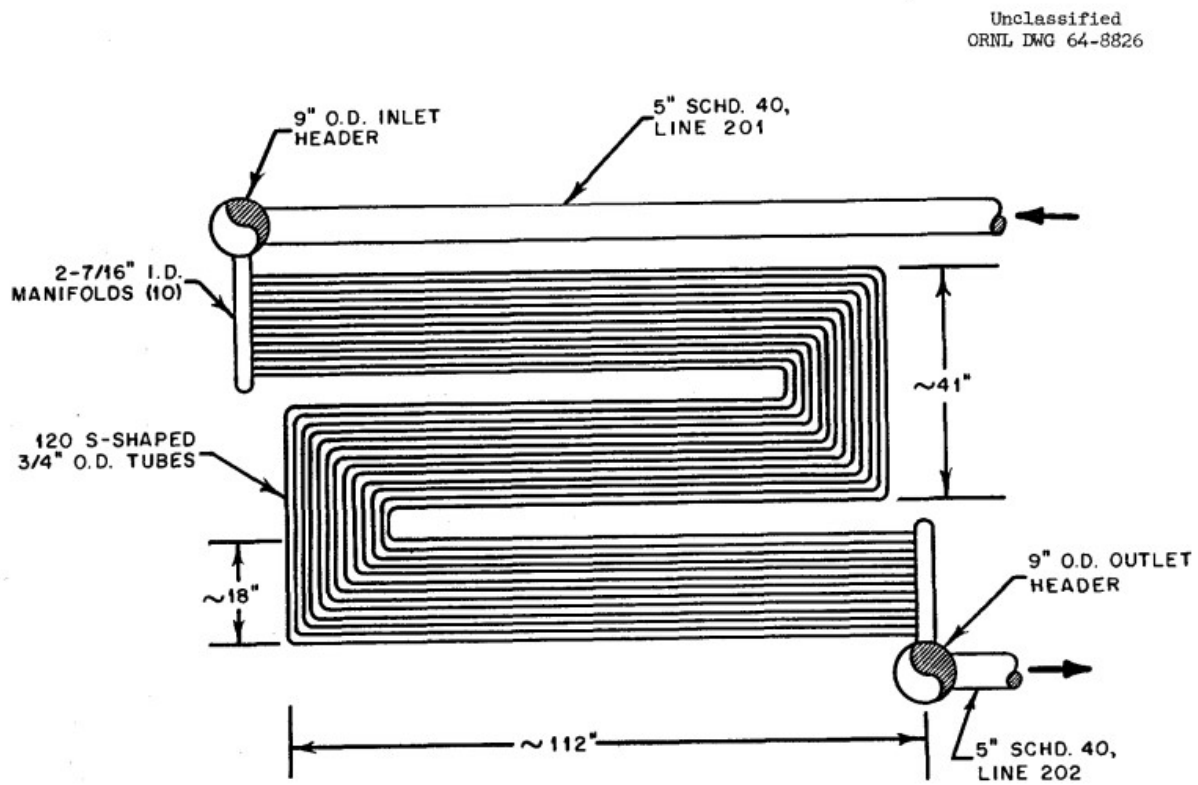


Figure 2.9: Radiator [25]

2.4. Further equipment and processes

2.4.1. Materials Compatibility

The piping system and equipment are made of INOR-8, consisting of a high nickel and molybdenum alloy with good resistance to attack by fuel and coolant salts at temperatures at least as high as 1500°C. The well performing mechanical properties are superior to those of many austenitic stainless steels, with the alloy being weldable by established procedures. The chemical composition and some of the physical properties are given in Table 2.4.

| Chemical Properties | | | |
|----------------------------|-----------|---------|-------|
| Ni | 66–71% | Mn, max | 1.0% |
| Mo | 15–18 | Si, max | 1.0 |
| Cr | 6–8 | Cu, max | 0.35 |
| Fe, max | 5 | B, max | 0.010 |
| C | 0.04–0.08 | W, max | 0.50 |
| Ti + Al, max | 0.50 | P, max | 0.015 |
| S, max | 0.02 | Co, max | 0.20 |

| Physical Properties | |
|---|-----------------------|
| Density, kg/m ³ | 8775.7 |
| Melting point, K | 1627.6–1674.4 |
| Thermal conductivity, W/(m · K) at 1033 K | 22.01 |
| Modulus of elasticity at ~ 1033 K, GPa | 171.0 |
| Specific heat, J/(kg · K) at 1033 K | 577.8 |
| Mean coefficient of thermal expansion, 294–1033 K range, 1/K | 1.44×10^{-5} |

Table 2.4: Chemical and Physical Properties of INOR-8 [25]

Over a three years period, several hundreds of fuel salt mixtures were analyzed and specimens exposed in the core for many thousands of hours were examined, demonstrating the compatibility of the salt, the moderator, and the container material.

Looking at corrosion, it has been demonstrated how chromium, belonging in the fuel salt, is the best indicator of corrosion of the INOR-8, since corrosion selectively attacks the chromium in the alloy and the product, CrF₂, is quite soluble in the salt.

Finally, the physical properties of the INOR-8 were affected by irradiation in the MSRE as expected on the basis of prior irradiation experiments. Results demonstrated little change in ultimate strength, yield strength, and secondary creep rate.

2.4.2. Instrumentation and Control

Nuclear and process control are both important to the operation of the MSRE. The reactor has a negative temperature coefficient of 11.5 to 17.8 pcm/K, depending on the type of fuel that is being used. The excess reactivity requirements are listed in Table 2.5.

Three control rods are present, and they have a combined worth of 5.6 to 7.6 % $\delta k/k$, depending upon the fuel composition. Their major functions are to eliminate the wide temperature variations that would otherwise accompany changes in power and xenon poison level. They consist of hollow cylinder of $Gd_2O_3-Al_2O_3$ ceramic, canned in Inconel and threaded on a stainless steel hose, which also serves as a cooling-air conduit. They also ensure some safety functions, most of which are concerned with the startup of the reactor.

Rapid action is not required of the control rods, since thermal feedback always steps in, as variations of fuel and moderator temperature occur. However, a magnetic clutch is provided in the drive train to permit the rods to drop into the thimbles with an acceleration of 0.5g, as a convenient way of providing insertion rates that are more rapid than the removal rates. Rods are inserted or extracted at a maximum speed of 1.27 cm/s.

Power level is determined by measuring the flow rate and temperature difference in the coolant salt system. The control rods operate to hold the fuel outlet temperature from the reactor constant, and the inlet temperature is permitted to vary with power level. At low power, the control rods operate to hold the neutron flux constant, and the heat withdrawal at the radiator or the input to the heaters on piping and equipment, is adjusted to keep the temperature within a specified range.

Over one thousand thermocouples are installed throughout the fuel and coolant salt systems, and about three-fourths of these serve indication, alarm, or control functions.

| | Reactivity, $\% \delta k/k$ |
|---|---------------------------------------|
| Loss of delayed neutrons by circulating fuel | -0.3 |
| Entrained gas | -0.2 |
| Power coefficient (from rise in graphite temperature) | -0.1 |
| Xenon poisoning (steady state at 10 MW) | -0.7 |
| Samarium-149 transient | -0.1 |
| Burnup (120 g of fuel) | -0.1 |
| Margin for operation of control rods | -0.4 |
| Total | -1.9 |
| Uncertainty in estimates (primarily xenon) | (+1.0 to -)0.4 |
| Total | -2.9 to -1.5 |

Table 2.5: Reactivity balance in MSRE [25]

2.4.3. Fuel Chemistry

Fuel chemistry plays a crucial role in a fluid fuel reactor comparable to fuel structure, cladding integrity, and coolant stability in a solid fuel reactor. When assessing the safety of fluid fuel reactors, perhaps the first question that comes to mind is the possibility of uranium separating from the fluid.

The fuel salt is subject to only two mechanisms for uranium separation: the contamination of the salt with moisture or oxygen to the point that uranium oxide precipitates, and the reduction of so much UF_4 to UF_3 that the UF_3 begins to transform into UF_4 and insoluble uranium. Neither condition is approached during operation. Oxide formation in the MSRE salt is controlled by providing a blanket gas, helium, that has had oxygen and moisture reduced to <10 ppm by passage through a 922 K titanium sponge. When the core access is opened for specimen removal, moist air intrusion is minimized by first filling the system with denser argon and working through a standpipe filled with dry nitrogen. Then, before the fuel salt is put back in the core, the flush salt is first circulated to react with any moisture that may have entered. Evidence of the effectiveness of these measures is the extremely low oxide level in the fuel after four years in the reactor: analyses consistently show only 60 ppm oxide. However, the chemistry of the fuel salt is such that the first oxide to form is ZrO_2 and its solubility is around 700 ppm. The ZrF_4 was put in the fuel as a cushion; without it, the UO_2 that would have been formed, would still have been far below its solubility limit of 1000 ppm [10].

The success of the MSRE in keeping oxide contamination down, argues that ZrF_4 need not be included in the fuel of future molten salt reactors. The second possibility, precipitation of reduced uranium, was the reason for specifying that the uranium to be used in the original power operation be only 33% ^{235}U instead of highly enriched. At that time, they didn't know precisely what the average total valence of the products of one fission would be in the reactor environment. They expected it to be close to four, but if it had been more, it would, in effect, tie up more than the four fluorine atoms, made available by the destruction of the uranium atom. Operation of the MSRE, indeed, has shown that the average total valence of the products of a fission is slightly less than four. This means that the tendency is actually away from the reduction of UF_4 to UF_3 , hence eliminating the possibility of uranium precipitation.

2.4.4. Drain Tank Systems

Safe storage of the salt mixtures was provided by four tanks when they were not in use in the fuel salt and coolant salt circulating systems. Among them, three of the four tanks were connected to the reactor by means of the fill and drain line. Moreover, the fuel drain tanks were provided with a cooling system capable of removing 100 kW of fission product decay heat [25]. The fourth tank was provided for the coolant salt. To conclude, the fuel dump tank was equipped with electrical heaters in order to maintain the clean fuel in a liquid phase, reminding of those provided in the piping system, to avoid freezing of the salt.

3 | MSRE Plant Simulator

The aim of this chapter is to describe the development of the primary circuit of the MSRE using the Modelica language on the Dymola simulation environment, as more information regarding this engineering tool can be retrieved in Appendix A.

Briefly, the high flexibility of the Modelica language and its ability to describe any mathematical model, while making it a very powerful simulation tool for multi-domain systems, also prevents the use of problem-specialized numerical solver. While not being a problem for simple linear systems, this fact, together with the non-linearity of thermal-hydraulics equations, makes it impossible to assure global convergence for the initialization problem. Within the Dymola simulation environment, the primary circuit of the MSRE has been modeled. In particular, the nuclear reactor is represented by four main components, each representing different locations of the fuel salt circulating system, where each stage is properly modeled. The reactor core constitutes the principal element within the reactor vessel, and its modeling was addressed using a multiphysics approach. As the fuel salt carrier approaches the reactor, it first enters the upper region of the core and starts flowing downwards in a region confined between the core can and the vessel wall, known as the downcomer. Once the fuel starts accumulating in the lower head, it begins to flow upwards among the fuel channels available in the graphite block; here, neutrons are thermalized and neutron fission is likely to occur. However, as mentioned before, fission events are also present in the other regions due to a higher leakage probability of neutrons because of the small dimensions of the core. Finally, the fuel salt has reached the upper head and flows out of the reactor through an outlet nozzle.

The two regions representing the downward flow of the fuel salt and the accumulation of it within the lower head, have been treated separately, as well as the outer part of the reactor core when it starts to approach the outlet nozzle. Then, the hot fuel salt travels in the hot leg and is pumped to the primary heat exchanger, where it is cooled with a secondary salt and then flows back to the reactor vessel in the cold leg.

A detailed description of the aforementioned components, here treated as interchangeable models, is provided, as the chapter will show the construction of the models and how they are linked, as visible in the following sections. For our purposes, the secondary loop

was neglected; therefore, much attention was devoted to the primary circuit components, considering the secondary coolant salt loop as a boundary condition for the fuel circuit. This is carried out since a preliminary validation of the model was necessary in order to perform further evaluations.

The overall system is built by connecting the different models with the aid of physical connectors. The final scheme of the MSRE model is shown in Figure 3.1.

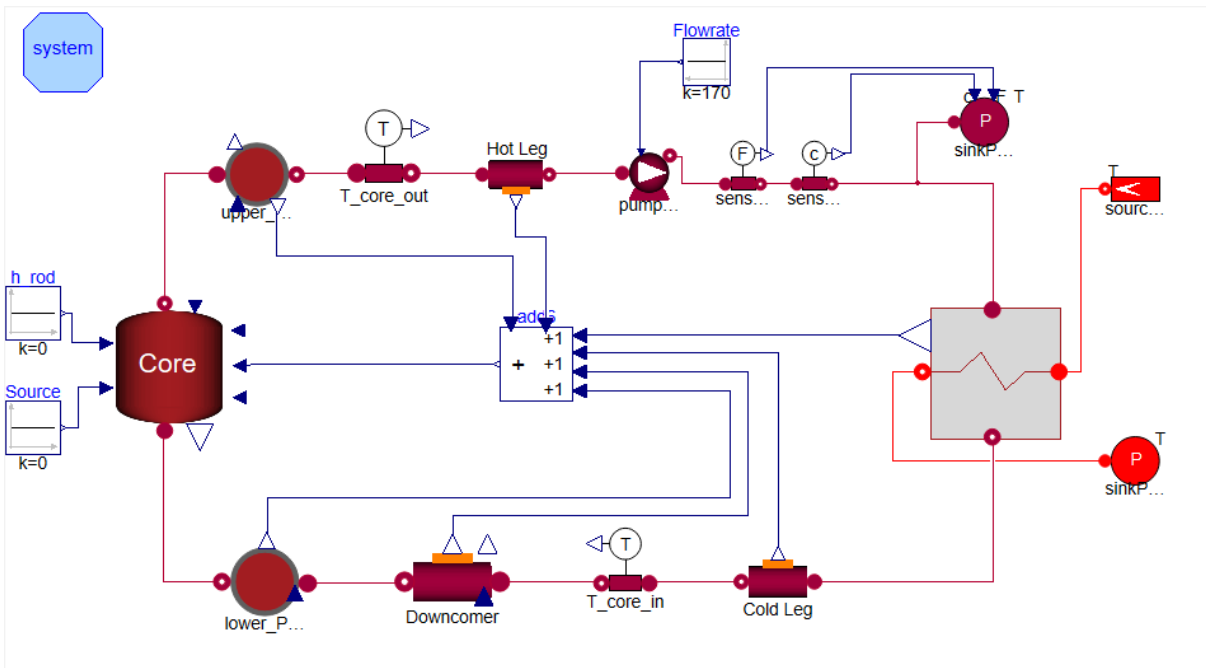


Figure 3.1: Object-oriented modeling of the MSRE

3.1. Reactor Core

The first component to be modeled is the reactor core, where most of the fission occurs. The core model is made of three principal objects: a *NeutronKinetics* model, a *Flow1DFV* model and a *GraphiteBlock* model, where they communicate and exchange variables. In Figure 3.2 a schematic view of the core model is presented.

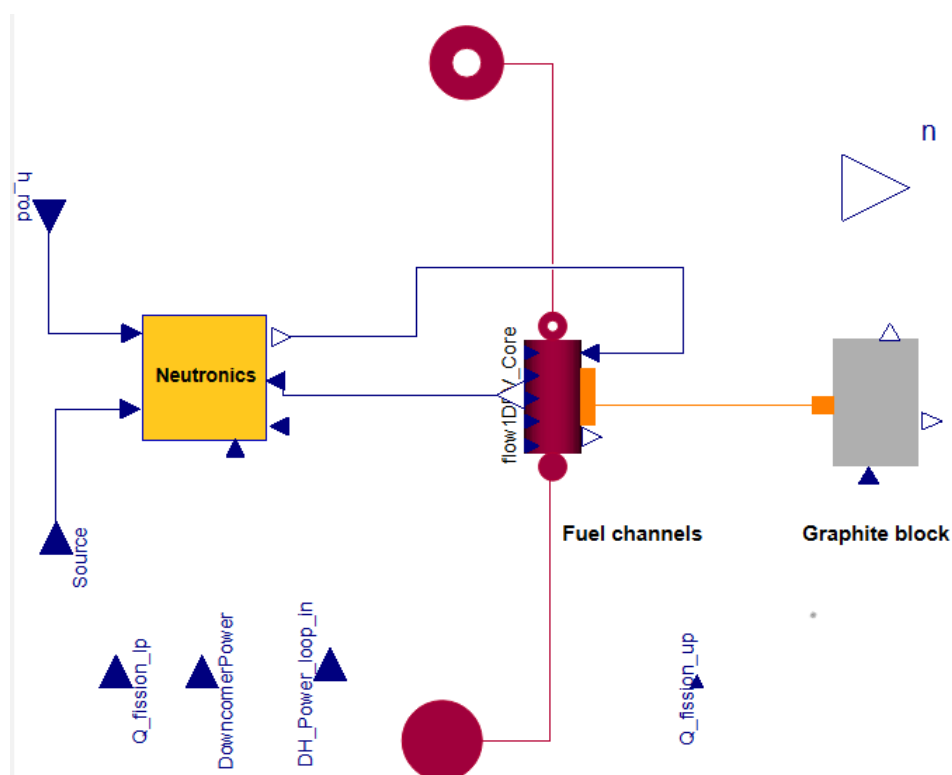


Figure 3.2: Object-oriented modeling of the core

3.1.1. Fuel model

To model the fuel salt flow, a *Flow1DFV* component is employed, representing an axial discretization of a core channel. This system was first developed in the *NRGCollection* library, as part of the [30] work and then modified, taking into account specific features of the Molten Salt Reactor Experiment. For instance, different geometrical and operational parameters, as well as different fuel salt carriers and heat transfer correlations, were considered.

As cited in the chapter before, two types of fuel salt carriers were adopted. Accordingly, the literature review showed similar physical properties developed over the last few years

[9]. Table 3.1 shows the physical properties employed in the Dymola simulation environment when defining the fuel salt media adopted.

| Property | Unit | Fuel salt | Coolant salt | Graphite |
|--------------------------|-------------------|---|---|----------|
| Density ρ | kg/m ³ | 2575 – 0.513T(°C) | 2280 – 0.488T(°C) | 1860 |
| Heat capacity c_p | J/(kg · K) | 1983 | 2415.78 | 1758.5 |
| Thermal conductivity k | W/(m · K) | 1.44 | 1.1 | 58.8 |
| Dynamic viscosity μ | Pa · s | $11.6 \times 10^{-5} e^{\frac{3775}{T(K)}}$ | $11.6 \times 10^{-5} e^{\frac{3775}{T(K)}}$ | – |

Table 3.1: Thermophysical properties of media and graphite [9]

In this work, based on the geometric assumption of the axial coordinate, the neutron flux shape for a critical finite cylindrical reactor core, will be treated as Equation (3.1), being in accordance with [17]. However, a radial discretization is not performed, but it is welcomed for future developments.

$$\varphi(z) \sim \sin\left(\frac{\pi(z + 14.53)}{198.5}\right). \quad (3.1)$$

As the fuel flows, a governing equation concerning the delayed neutron precursors is employed, considering both the variation in time and the convection term of each precursor group. Further details of the kinetic parameters are shown in Section 3.1.3. Therefore, the 1D equation for delayed neutron precursors (DNPs) concentration is:

$$\frac{\partial c_i(z, t)}{\partial t} + \frac{w(z)}{A_{\text{Core}}\rho(z)} \frac{\partial c_i(z, t)}{\partial z} = \frac{\beta_i}{\Lambda} n(t)\varphi(z) - \lambda_i c_i(z, t) \quad (3.2)$$

In this equation $w(z)$ represents the mass flow rate inside the fuel channel and $n(t)$ embodies the normalized fission power provided by the *NeutronKinetics* component. In addition, $\frac{w(z)}{A_{\text{Core}}\rho(z)}$ is a representation of the drifting velocity $v(z)$. Knowing the neutron flux shape for the mono-energetic system we are describing, we assume it to be the weighting function of the calculated variables, therefore the effective DNPs concentration profiles are calculated with Equation (3.3), as visible in [33].

In a similar way, the effective density and the effective temperature of the fuel salt are core averaged, with the latter being transmitted to the *NeutronKinetics* model.

$$c_{i,eff}(t) = \frac{\int \varphi(z)c_i(z,t)dz}{\int [\varphi(z)]^2 dz} \quad (3.3)$$

DNPs equation as well as thermal-hydraulic equation, is a modified version of the *Flow1DFV* component, meaning that the following set of balance equations must be satisfied. To begin with, an energy balance showing different contributions for volumetric power can be seen in Equation (3.4), where the fluid state, hence the fuel temperature, is calculated by means of enthalpy and pressure.

$$\rho \frac{Dh(z,t)}{Dt} = q_{fiss}''' + q_{DH}''' + q_{exc}''' \quad (3.4)$$

To express the energy equation, the use of the total derivative is adopted, which is a compact representation of two different terms: the partial derivative with respect to time and the convective derivative. In our case,

$$\frac{Dh}{Dt} = \frac{\partial h}{\partial t} + \mathbf{v} \frac{\partial h}{\partial z} \quad (3.5)$$

In Equation (3.4), the first term is the representation of the power produced in the reactor core through nuclear fission, weighted by Equation (3.1), considering the fraction of power generated in the core. However, when implemented in the Modelica language, a finite-volume method for nodal discretization is adopted.

$$q_{fiss}''' = \frac{n(t)P_0 f_{core}}{AlN_t \sum \varphi(z)} = q_{fiss,max}''' \varphi(z) \quad (3.6)$$

Equation (3.6) displays the power generated in each volume due to fission. The decay heat power term refers to the contribution of the decay of the precursors within the core can. It can be determined as the sum of each decay heat group.

$$q_{DH}''' = \sum F_k(z,t) \quad (3.7)$$

This helps us to introduce a further balance equation for the decay heat density, Equation (3.8), where the 'k' index depicts the three precursor groups adopted to describe the decay power function. A summary of the decay heat parameters employed is shown

in Table 3.2, as they are taken as a reference from previous works in the SAMOFAR framework [12].

$$\frac{\partial F_k(z, t)}{\partial t} + \frac{w(z)}{A_{\text{Core}}\rho(z)} \frac{\partial F_k(z, t)}{\partial z} = f_k \lambda_k q_{fiss}''' - \lambda_k F_k(z, t) \quad (3.8)$$

| Parameter | Symbol | Value |
|-----------------------------|-------------------------|--------------------------------------|
| DH fraction – group 1 | f_1 | 0.0117 |
| DH fraction – group 2 | f_2 | 0.0129 |
| DH fraction – group 3 | f_3 | 0.0186 |
| DH decay constant – group 1 | $\lambda_{\text{DH},1}$ | 0.01973 s^{-1} |
| DH decay constant – group 2 | $\lambda_{\text{DH},2}$ | 0.0168 s^{-1} |
| DH decay constant – group 3 | $\lambda_{\text{DH},3}$ | $3.58 \times 10^{-4} \text{ s}^{-1}$ |

Table 3.2: Decay Heat parameters

To conclude, within the *Flow1DFV* model, the overall analysis based on the power produced in the circuit is employed, underlining how it is generated throughout the circulating fuel system. It is clearly visible how the actual thermal power output is made of contributions also coming out of the core, indeed, decay heat terms as well as fission terms are taken into consideration when a steady state is sought, as shown in Equation (3.9).

$$P_{tot} = \sum_{\text{Core}} (Q_{\text{DH}} + Q_{\text{fiss}}) + \sum_{\text{UP}} (Q_{\text{DH}} + Q_{\text{fiss}}) + \sum_{\text{LP}} (Q_{\text{DH}} + Q_{\text{fiss}}) + \sum_{\text{DC}} (Q_{\text{DH}} + Q_{\text{fiss}}) \quad (3.9)$$

Note that when considering the reactor core, a heat contribution from graphite must be considered, as 7 % of power is generated within graphite, mainly due to neutron and gamma irradiation.

The *NeutronKinetics* block and the *Flow1DFV* component exchange several crucial variables: fuel temperature, effective delayed neutron fraction, and effective precursor concentration. In return, the *NeutronKinetics* block supplies the normalized fission power to the thermal-hydraulic component. Table 3.3 summarizes the main core equations needed

to describe this system.

| Equation | Description |
|---|---|
| $\frac{L}{A} \frac{dm}{dt} + P_{\text{out}} - P_{\text{in}} + \Delta P_{\text{stat}} + \Delta P_{\text{fric}} = 0$ | <p>Momentum balance equation.</p> <p>It describes the rate of change of momentum for a fluid flow being equal to the sum of the forces acting on it.</p> |
| $\rho \frac{Dh}{Dt} = q_{\text{fiss}}''' + q_{\text{DH}}''' + q_{\text{exc}}'''$ | <p>Energy balance equation.</p> <p>It represents how the specific fluid enthalpy changes over time, considering a thermal spectrum reactor system. It is portrayed on a volumetric basis.</p> |
| $\frac{\partial c_i}{\partial t} + \frac{\dot{m}}{\rho A} \frac{\partial c_i}{\partial z} = \frac{\beta_i}{\Lambda} n \varphi(z) - \lambda_i C_i$ | <p>DNP balance equation.</p> <p>It is a method for modeling the concentration and transport of neutron precursors. However, when dealing with a laminar flow in a channel, the diffusion contribution will be far lower than the convective one.</p> |
| $\frac{\partial F_k}{\partial t} + \frac{\dot{m}}{\rho A} \frac{\partial F_k}{\partial z} = q_{\text{fiss}}''' \lambda_k f_k - \lambda_k F_k$ | <p>Decay Heat Density balance equation.</p> <p>It describes the conservation of decay heat into the fluid volume from the decay of radioactive isotopes, as they are transported within the fuel circulating system [34].</p> |
| $\frac{dm}{dt} = \dot{m}_{\text{in}} - \dot{m}_{\text{out}}$ | <p>Mass balance equation.</p> <p>It indicates how mass can neither be created nor destroyed in an isolated system.</p> |

Table 3.3: Main core equations

3.1.2. Graphite model

As part of the reactor core, graphite plays a fundamental role. Graphite has been chosen as the moderator medium to favor scattering events with emitted neutrons. The key features of this element can be found in Appendix B.

As previously cited in Equation (3.1), the power resulting from fission events in graphite has been modeled considering a sine approximation, representing the neutron flux shape; hence, an axial discretization is also applied in the graphite model. Focusing on the thermal analysis, the energy balance considered is the following:

$$\rho c_p \frac{dT(z, t)}{dt} = q'''_{fiss, g} + q'''_{exc} \quad (3.10)$$

As visible from Equation (3.10), no decay heat is present in the graphite matrix. Moreover, a heat exchange term is present as the fuel salt and graphite exchange heat.

With reference to the previous paragraph, the fission power term in graphite can be described as follows.

$$q'''_{fiss, g} = \frac{n(t) P_0 f_{graphite}}{Al \sum \varphi(z)} = q'''_{fiss, max, g} \varphi(z) \quad (3.11)$$

To focus now on the heat exchanged between fuel and graphite, data showed how fuel salt flow may be classified as a laminar flow with $Re \approx 1500$; therefore, a forced laminar heat transfer correlation must be applied.

Among several, Equation (3.12) shows a Nusselt correlation that has been chosen from [23].

$$Nu \approx 4.36 \quad (3.12)$$

However, further extended versions of heat transfer correlations may be found in [22] and can be taken as an example the Martinelli and Boelter correlation, expressed in Equation (3.13) for forced laminar flow in the absence of natural circulation. Further details about the heat transfer in the core can be found in Section 4.1.

$$Nu = 1.62 \left(Re Pr \frac{D}{L} \right)^{1/3} \quad (3.13)$$

3.1.3. Neutron Kinetics

As far as it concerns the *NeutronKinetics* block, the goal is to elaborate the effective DNPs concentrations and to communicate the normalized power towards models where fission events are present, thus including *Lower Plenum*, *Upper Plenum* and *Downcomer*. In this work, neutronics is modeled with the time-dependent neutron population equation, ignoring spatial effects, thus leading to the Point Kinetic equation, expressed in Equation (3.14).

$$\frac{dn}{dt} = \frac{\rho_{tot}(t) - \beta}{\Lambda} n(t) + \lambda_i c_i(t) + S \quad (3.14)$$

Where the total reactivity considered in the model, gathers several contributions. Among them, fuel and graphite feedback coefficients play a crucial role, as they kick in once respective temperatures are out of their set point. A detailed view is presented in Table 3.4. The feedback coming from the variation in temperature in the fuel salt is due to Doppler effects, as Doppler broadening is occurring in ^{238}U . While the feedback coming from the graphite sample is mainly due to variation in density.

As of now, let's define the total reactivity in the core as:

$$\rho_{tot}(t) = \rho_{circ,0} + \rho_{fuel} + \rho_g + \rho_{ext} + \rho_{Xe} \quad (3.15)$$

A specific feature of circulating fluid reactors is the loss of reactivity as a result of fuel circulation within the primary circuit, meaning that after the loss has been quantified, the reactor will have to reach a steady state, also based on this negative contribution. Therefore, the term $\rho_{circ,0}$ is the reactivity compensation needed to counterbalance the reactivity loss due to DNP decay out of the core. An analytical calculation of the reactivity change due to fuel circulation is immediate, since it is determined by evaluating Equation (3.14) in steady state.

$$0 = \frac{\rho_{circ,0} - \beta}{\Lambda} n + \lambda_i c_i + S \quad (3.16)$$

$$\rho_{circ,0} = \beta - \frac{\Lambda}{n} \sum_i \lambda_i c_i - \frac{\Lambda}{n} S \quad (3.17)$$

External reactivity ρ_{ext} , represents an insertion of reactivity into the system due to mov-

able control rods, as the operator changes the height of the control rods into the core.

| Reactivity Feedbacks | Description |
|--|---|
| $\rho_{\text{fuel}} = \alpha_{\text{fuel}}(T_f - T_f^0)$ | It is related to the fuel temperature changes, as it flows into the core, considering a weighted temperature for each fuel node |
| $\rho_g = \alpha_g(T_g - T_g^0)$ | As the graphite temperature changes, it will undergo a change in volume, causing a variation in the effective volume of fuel channels, meaning a negative feedback will be added in the system dynamics |

Table 3.4: Thermal reactivity feedbacks

Although Xenon contribution is not considered in the following chapter, the Bateman equations have been introduced to account for neutron poisons, Equation (3.18). The most important fission product poison is ^{135}Xe , whose thermal absorption cross section is $2.65 \times 10^6 b$ [20]. It is formed as the result of the decay of ^{135}I and is also produced directly in fission.

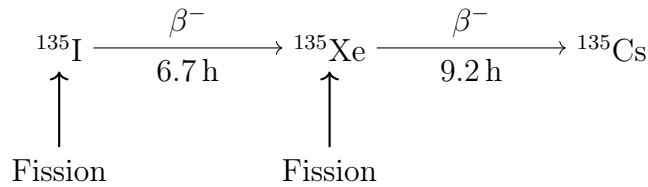


Figure 3.3: Decay chain

$$\begin{cases} \frac{dI}{dt} = \Sigma_f \phi \gamma_I - \lambda_I I \\ \frac{dXe}{dt} = \Sigma_f \phi \gamma_{Xe} + \lambda_I I - \lambda_{Xe} Xe - \sigma_{Xe} \phi Xe \end{cases} \quad (3.18)$$

As an approximation, for a homogeneous reactor modeled with one energy group, with uniform poison concentration, it is possible to quantify the added reactivity as

$$\rho_{Xe} = -\frac{\sigma_{Xe}}{\nu \Sigma_f} (Xe - Xe^0) \quad (3.19)$$

In conclusion, the kinetic parameters employed in the Dymola simulation environment are listed in Table 3.5.

| Group | ²³³ U Fuel | | ²³⁵ U Fuel | |
|--|---|--|---|--|
| | λ_i , Decay Constant (sec ⁻¹) | β_i , Delayed- Neutron Fraction (Static) (pcm) | λ_i , Decay Constant (sec ⁻¹) | β_i , Delayed- Neutron Fraction (Static) (pcm) |
| 1 | 0.0126 | 22.80 | 0.0124 | 22.30 |
| 2 | 0.0337 | 78.80 | 0.0305 | 145.70 |
| 3 | 0.139 | 66.40 | 0.111 | 130.70 |
| 4 | 0.325 | 73.60 | 0.301 | 262.80 |
| 5 | 1.13 | 13.60 | 1.14 | 76.60 |
| 6 | 2.50 | 8.80 | 3.01 | 28.00 |
| Total β | | 264 | | 666.1 |
| Prompt neutron generation time, sec | | 4×10^{-4} | | 2.4×10^{-4} |
| Temperature coefficients of reactivity, pcm/K | | | | |
| Fuel salt, α_{fuel} | | -11.034 | | -8.71 |
| Graphite, α_g | | -5.814 | | -6.66 |

Table 3.5: Comparison of Nuclear Parameters Used in Dynamic Analysis of MSRE with ²³³U Fuel and with ²³⁵U Fuel [29]

3.2. Plenums

With respect to the reactor core, the *Upper Plenum* and the *Lower Plenum* are simulated by using a 0D model; therefore, a lumped approach is employed, always ensuring the heat generated through fission. Equations to describe the dynamical behavior of the model are shown below, considering the same mass balance shown in Table 3.3.

- **Energy Balance:**

$$\frac{dE}{dt} = \dot{m}_{in}h_{in} - \dot{m}_{out}h_{out} + Q_{fiss} + Q_{DH} \quad (3.20)$$

Where fission power is calculated analogously to Equation (3.6) and Equation (3.21), but without considering any shape factor for the flux.

Therefore,

$$Q_{fiss} = n(t)P_0f_{Plenum} \quad (3.21)$$

- **Neutronic balance:**

Similarly, balances concerning delayed neutron precursors are modeled.

$$\frac{dc_i(t)}{dt} = \frac{\dot{m}_{in}}{M_{tot}} (C_i^{in} - C_i) + \frac{\beta_i}{\Lambda} (n(t)f_{Plenum}) - \lambda_i C_i \quad (3.22)$$

$$\frac{dF_k(t)}{dt} = \frac{\dot{m}_{in}}{M_{tot}} (F_k^{in} - F_k) + f_k \lambda_k q_{fiss,Plenum}''' - \lambda_k C_k \quad (3.23)$$

3.3. Downcomer

The fuel salt, once it enters through the flow distributor, flows downward in the cooling annulus, i.e. *Downcomer*. It has been modeled with a similar approach to the tube channel in the core, therefore the *Flow1DFV* model has been employed. Although the fluid flow models employed, remark the ones present in the reactor core in Section 3.1.1, here, a small percentage of heat from fission has to be considered.

The hydraulic diameter, flow area, wetted perimeter, and heat transfer area were calculated based on the annular geometry. The fundamental difference, hence the assumption, lies in not considering any kind of heat exchange as the fuel flows through the downcomer. As cited in Section 2.2.4, the reduced overall flow through the core was not modeled in this work.

3.4. Fuel Salt Legs

Designing a nuclear power plant, also means taking into account the piping system. Therefore, with reference to [25], all the pipe components are Scheduled 40 type, with a hydraulic diameter of 0.127 m and a cross sectional area of 0.0127 m². The exact lengths of the pipes seem hardly available in the ORNL's reports, thus, the lengths of the pipelines were estimated through the mass flow rate of the working fluid and the transporting time between the components.

The overall data are exposed in Table 3.6.

| | Length (m) |
|----------|------------|
| Hot Leg | 4.91 |
| Cold Leg | 4.65 |

Table 3.6: Tubes lengths

3.5. Fuel Circulating Pump

A centrifugal-type pump, based on the *ThermoPower* library with ideally controlled mass flow rate, is employed. Nonetheless, several changes have been made, since DNPs concentrations C_i and decay heat groups F_k needed to be transmitted from the inlet to the outlet.

Moreover, a *SinkPressure* model was used to fix the pressure at the pump outlet and analogously to the pressurizer in a PWR, it may also act as an accommodation for changes in volume of the fuel with temperature.

3.6. Primary Heat Exchanger

Based on previous considerations, a Shell and Tube type heat exchanger may be modeled considering two different *Flow1DFV* components, each one referring to the shell side and the tube side, as displayed in the figure below.

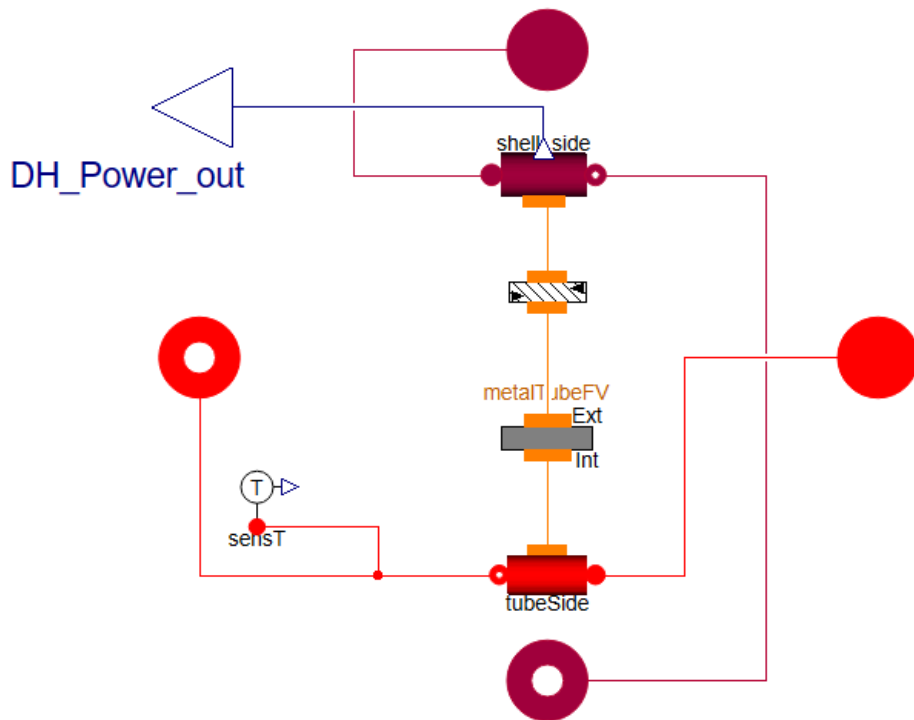


Figure 3.4: Object-oriented modeling of the primary heat exchanger

The cylindrical metal tube (INOR-8) is simulated throughout a *MetalTubeFV* component, with finite volumes and accounts for the heat coming from the shell side. As the fuel salt flows, some precursors will decay, hence generating some decay heat. Such decay heat is evaluated and connected directly to the MSRE core, where it is taken into account when finding steady state conditions.

Data concerning heat transfer evaluation of INOR-8 can be found in Table 3.7. In addition, heat transfer and pressure drop correlations can be included in the *Flow1DFV* component. By default, frictional losses are calculated using specified friction factors or the Colebrook equation [3] .

The set of operational parameters employed in the object-oriented model is shown in Table 3.7.

| | Value | Units |
|----------------------------|-----------------|------------------------------------|
| Heat Load | 8 | MW |
| Number of tubes | 159 | |
| Number of shell passages | 2 | |
| Fuel Salt Flowrate | 170 | kg s ⁻¹ |
| Coolant Salt Flowrate | 103.7 | kg s ⁻¹ |
| Active shell length | 1.83 | m |
| Outer Diameter | 1.27 | cm |
| Thickness | 1.07 | mm |
| Tube pitch | 1.97 | cm |
| Baffle Fraction | 0.25 | |
| CL | 0.87 | |
| CTP | 0.9 | |
| Fouling Factor | 9×10^5 | m ² K W ⁻¹ |
| Nominal Shell Pressure | 4.8 | bar |
| Nominal Tube Pressure | 7.2 | bar |
| Metal Density | 8775 | kg m ⁻³ |
| Metal Specific Heat | 577.8 | J kg ⁻¹ K ⁻¹ |
| Metal Thermal Conductivity | 22 | W m ⁻¹ K ⁻¹ |

Table 3.7: Primary heat exchanger data [25]

In heat exchanger design, CL refers to the tube layout constant, and CTP is the tube count calculation constant that accounts for incomplete tube coverage due to clearances and tube pass lanes. In this case, a value of CL equal to 0.87 is adopted since a triangular pitch is present and a value of CTP corresponding to 0.9 is employed since two-tube passes are adopted [21]. Whereas, the fouling factor represents a further thermal resistance to the heat transfer.

3.6.1. Shell side

Focusing on the shell, the fuel salt mixture is flowing on this side as it tends to heat the secondary coolant salt. From [25], a few considerations about pressure drops can be made, in particular, 1.66 bar of nominal pressure drop on the shell side are expected. Regarding heat transfer aspects, the well-known Dittus-Boelter correlation can be used for molten salts [8].

Therefore, the Nusselt correlation for a cooling fluid is expected to be:

$$Nu = 0.023 Re^{0.8} Pr^{0.3} \quad (3.24)$$

Which is valid for $Re > 10'000$ and $0.7 < Pr < 120$, as in our case. Considering $Re = \frac{\dot{m} D_h}{\mu A}$, $Pr = \frac{\mu c_p}{k}$, as the dimensionless groups employed to characterize heat transfer due to convection.

With the previous consideration, the thermal analysis conducted showed different results with respect to the MSRE report design [25], resulting in an underestimation of the heat transfer coefficient. In particular, when the MSRE was first operated at significant power levels, the heat exchanger performance was observed to be below the design value. The conclusions reached, were that the heat exchanger had been properly designed using the salt's physical property data available at that time, but some of the physical properties, the thermal conductivity in particular, were in fact substantially different from the values used in the design. In recent years, a re-evaluation of the physical properties showed that the thermal conductivity of both the fuel and the coolant salt was sufficiently below the value used in design to account for the heat transfer coefficient [9].

| | Present model | ORNL Report [25] | Units |
|-----|---------------|------------------|-------------------|
| h | 12328 | 18700 | $W m^{-2} K^{-1}$ |

Table 3.8: Heat transfer coefficient on the shell side

3.6.2. Tube side

As mentioned above, a mixture of *FLiBe* was used to cool down the fuel salt. To model it, a decision was made not to create a secondary circuit but just to develop some boundary conditions to mimic the behavior and the operational parameters of the coolant salt.

To do so, a *SourceMassFlow* component was adopted, with the following constraints.

| | Value | Units |
|-------------------|-------|--------------------|
| Coolant Flowrate | 53.6 | l s^{-1} |
| Coolant Density | 1922 | kg m^{-3} |
| Coolant Flowrate | 103.7 | kg s^{-1} |
| Inlet Temperature | 819 | K |
| Inlet Pressure | 7.2 | bar |

Table 3.9: Secondary circuit operational parameters

Moreover, as previously done for the shell side, the tube side itself should be denoted by a heat transfer correlation. The Gnielinski correlation Equation (3.26), was adopted as it fits better for transitional flow regimes, as it is on the tube side.

To define it, first, a brief disclaimer should be provided about the friction factor. Typically, the friction factor is calculated with the Pethukov correlation, a formula used for friction factor evaluation in a smooth pipe, Equation (3.25).

$$f = [0.79 \log(Re) - 1.64]^{-2} \quad (3.25)$$

To be added into Equation (3.26).

$$Nu = \frac{f}{8} \frac{(Re - 1000)Pr}{1 + 12.7 \left(\frac{f}{8}\right)^{0.5} (Pr^{2/3} - 1)} \quad (3.26)$$

The results obtained after employing the Gnielinski correlation are shown in Table 3.10. As noted earlier, the same considerations hold for the tube side, emphasizing the noticeable differences in the outcomes. A Temperature sensor is found at the tube's outlet, as it provides the outlet temperature of the coolant salt. In conclusion, MSRE Report [25] states that the nominal pressure drop on the tube side is estimated to be around 2 bar.

| | Present model | ORNL Report [25] | Units |
|-----|---------------|------------------|---------------------------------|
| h | 7813 | 27723 | $\text{W m}^{-2} \text{K}^{-1}$ |

Table 3.10: Heat transfer coefficient on the tube side

4 | Results and discussion

In this chapter, a dynamic analysis of the Molten Salt Reactor Experiment is carried out via an object-oriented simulation environment, i.e. Dymola. The response of the model is first exploited through the steady state condition, then validated and lastly, two accidental scenarios are simulated. To validate the present Modelica model, three experimental cases were selected, corresponding to three different reactivity insertion scenarios at different power levels. For the validation of the model, both qualitative and quantitative approaches were employed. Graphical comparisons between simulation results and experimental data were used to visually assess the accuracy of the model. In addition, the Root Mean Square Error (RMSE) was calculated to provide a quantitative measure of the discrepancy between the simulation prediction and the experimental data. It is estimated as follows:

$$RMSE = \sqrt{\frac{1}{N} \sum_{i=1}^N (y_i^{exp} - y_i^{sim})^2} \quad (4.1)$$

where 'N' is the number of points on the common temporal grid upon which both curves were interpolated. As a recap from the previous chapter, let's focus on the key operational parameters needed to perform the thermal-hydraulic evaluation, considering 1140 fuel channels and 10 axial nodes. As indicated in Table 4.1, fuel channel lengths are comparable to the graphite stringer. In addition, as the fuel enters and flows into the downcomer region, it is estimated to be as long as the graphite block. The conducted transients may be summarized as follows:

- Reactivity Insertion: Several step reactivity insertions are done, as the dynamic behavior is compared both with experimental data and literature models, to validate the Modelica model.
- Primary Pump Failure: This kind of scenario is widely carried out when looking at operational anomalies. It is conducted in this work and it is compared with the literature.
- Cold Slug Insertion into the Core: A colder mass is flowing for a certain period of

time in the reactor, inserting an amount of reactivity, such that power will surge significantly. Modeling of both the power and reactivity has been carried out.

All the results are analyzed and discussed in the light of the prefixed goal, which is to validate the present model and describe the dynamic behavior of the MSRE upon accidental situations. Merits and defects of the models will be pointed out. But first, to implement a steady state simulation is a very crucial step to check the present model, before doing the transient simulation.

| | Value | Units |
|--|-----------------------|------------------------------------|
| Power | 8 | MW |
| Fuel channel length | 1.70 | m |
| Cross-Section Area | 2.89×10^{-4} | m ² |
| Hydraulic Diameter of the Core | 0.01585 | m |
| Fuel Salt Flowrate | 170 | kg s ⁻¹ |
| Graphite Density | 1870 | kg m ⁻³ |
| Graphite Volume in the Core | 1.95 | m ³ |
| Graphite Specific Heat | 1758.5 | J kg ⁻¹ K ⁻¹ |
| Core fractional Power | 0.8184 | - |
| Graphite fractional Power | 0.07 | - |
| Downcomer fractional Power | 0.0279 | - |
| Lower Plenum fractional Power | 0.0279 | - |
| Upper Plenum fractional Power | 0.0558 | - |
| Lower Plenum Volume | 0.2832 | m ³ |
| Upper Plenum Volume | 0.2973 | m ³ |
| Hydraulic Diameter of the Downcomer | 0.0254 | m |
| Downcomer Area | 0.11548 | m ² |

Table 4.1: Geometrical and operational parameters at nominal conditions

4.1. Steady-state results

When considering a steady state condition, we are looking at the comparison between the reference data, widely known in literature, and the data obtained with an object-oriented simulator. This simulation also allowed us to evaluate the reactivity losses as the fuel

leaves the reactor core, comparing the behavior for the ^{233}U and the ^{235}U case. One of the main differences between operation with ^{233}U and ^{235}U is the smaller fraction of delayed neutrons with the ^{233}U , as can be seen by comparing values of delayed neutron fractions in Table 4.5.

The simulation results for a nominal power of 8 MW and the comparison with experimental data are summarized in Table 4.2 and Table 4.3. Just to mention, no data comparison was made concerning power production in different regions of the core and decay heat, due to the unavailability of experimental data.

| Variable | Value | ORNL [26] | Units | Relative error (%) |
|--------------------------------------|--------|-----------|-------|--------------------|
| Inlet Core Temperature | 904.82 | 905 | K | 0.02 |
| Outlet Core Temperature | 928.78 | 930 | K | 0.13 |
| Average Fuel Temperature | 916.82 | 918 | K | 0.13 |
| Average Graphite Temperature | 931.47 | 936 | K | 0.48 |
| Inlet HE Temperature (Coolant Salt) | 819 | 819 | K | 0.00 |
| Outlet HE Temperature (Coolant Salt) | 852.62 | 852 | K | 0.07 |

Table 4.2: Steady state results at 8 MW

| Variable | Value | Units |
|----------------------------|---------------------|-------|
| Core Fission Power | 6.418×10^6 | W |
| Core Decay Power | 1.294×10^5 | W |
| Graphite Power | 5.6×10^5 | W |
| Lower Plenum Fission Power | 2.232×10^5 | W |
| Upper Plenum Fission Power | 4.464×10^5 | W |
| Downcomer Fission Power | 2.232×10^5 | W |
| Loop Decay Power | 1.864×10^5 | W |

Table 4.3: Power results at 8 MW

It is important to point out that the mean graphite temperature is referred to the design power level, since no information during the experimental operation was provided. However, the results obtained are quite in accordance with the experimental data, provided by the ORNL. In addition, it is fair to notice the good consistency in the core temperature difference, visible in Table 4.2. In particular, when looking at the actual working temperatures of the MSRE, the corresponding power level was measured to be around 7.4 MWth, resulting in an astonishing agreement with the ORNL experimental data [15].

These conclusions can be seen in Table 4.4 where the respective temperature differences across the core at different power levels are shown.

| | 7.4 MW | 8 MW | 10 MW [2] | Units |
|-----------------------------------|--------|-------|-----------|-------|
| ΔT_{core} (Present model) | 22.15 | 23.96 | 29.94 | K |
| ΔT_{core} (ORNL) | 22.2 | 25 | 27.78 | K |
| Relative error | 0.225 | 4.16 | 7.78 | % |

Table 4.4: Core temperature difference at different power levels

As cited before, the effective delayed neutron fraction, calculated as Equation (3.3), is a variable of enormous importance, since it highlights the capability to control a nuclear reactor. In this sense, a relevant point is highlighted in the following lines, as the effective delayed neutron fraction is determined with respect to the static fuel case.

| | U-233 | U-235 | Units |
|------------------|-------|-------|-------|
| β_{static} | 264 | 666 | pcm |
| β_{eff} | 134 | 381 | pcm |

Table 4.5: Effective delayed neutron fraction

Furthermore, as previously cited in Section 3.1.2, the heat transfer correlation in the core region, chosen as part of this model, is given by Equation (3.12). The outcome is then compared with [25] in Table 4.6, showing good agreement. The value of the present model was calculated based on the fuel properties, which can be found in Table 4.1 and Table 3.1.

| | Present model | ORNL Report [25] | Units |
|-----|---------------|------------------|--------------------|
| U | 0.038 | 0.036 | MW K ⁻¹ |

Table 4.6: Global heat transfer coefficient between primary salt and graphite

4.2. Transient behavior during normal operation

In this part, several types of transients are simulated in order to investigate the dynamic behavior of the MSRE system. For each of the three power levels, reactivity insertion tests are performed. To compare them, [28] provides several experimental data working with ^{233}U fuel. Therefore, the goal of this section is to validate the Modelica simulation against the results obtained from ORNL.

In addition, as clearly visible from the figures below, experimental results show oscillations throughout the transient, since during the ^{233}U phase of operation, the neutron flux signal was contaminated by a large noise component. The noise was the result of the increased amount of fission gases entrained in the fuel salt mixture. The model is initialized in steady-state nominal conditions and simulations are performed with Dymola 2025x. Computational times required are typically below 2 seconds. Before showing the results, let's define the change of power evaluated as Equation (4.2).

$$\Delta P = P(t) - P_0 \quad (4.2)$$

The comparison was carried out among the ORNL, the Modelica model and the paper [34], when feasible.

4.2.1. Dynamic response to a step reactivity insertion

The first transient to be simulated refers to a step insertion of 13.9 pcm in a 8 MW power operation with ^{233}U . Figure 4.1 presented the power response with the step reactivity addition, where a power peak appeared at the beginning as predicted and then the power decreased and finally converged to a new equilibrium due to the negative reactivity feedback caused by the temperature increase.

It is worth noting that in [28], the authors suggest a wrong reactivity insertion data with respect to 8 MW. This was widely discussed in recent years, with an inversion of reactivity inserted for the 1 MW and the 8 MW cases [9]. Table 4.7 shows the transients simulated. In addition, the shape function and the weighting function are assumed to be fixed during the transient.

| | 1 MW | 5 MW | 8 MW | Units |
|----------------------------|------|------|------|-------|
| Reactivity Inserted | 24.8 | 19 | 13.9 | pcm |

Table 4.7: Reactivity inserted at different power levels

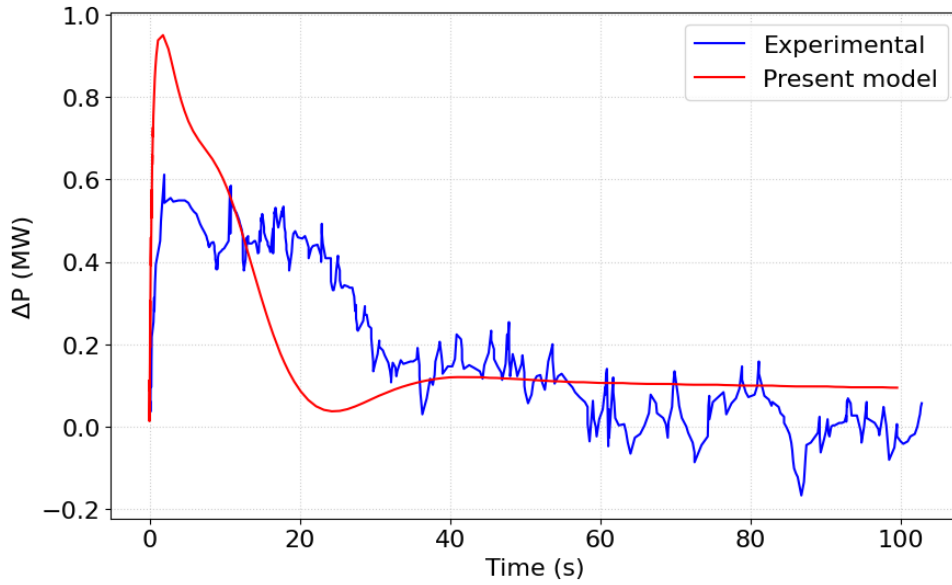


Figure 4.1: Power response to a 13.9 pcm insertion at 8 MW

Up to now, control rod insertion has been considered to be a step change mechanism, but to have a more realistic representation, a finite insertion rate has to be considered. To do so, [25] states a maximum speed of the regulating control rod of 1.27 cm/s, meaning a constant rate of 5.3 pcm/s, as for [34].

For the 8 MW case scenario, Figure 4.2 shows significant differences when evaluating power during a transient response, therefore, from now on, only ramp reactivity insertions will be treated. It is also worth noting that no void considerations have been made in this work, as well as any fuel burnup models been implemented.

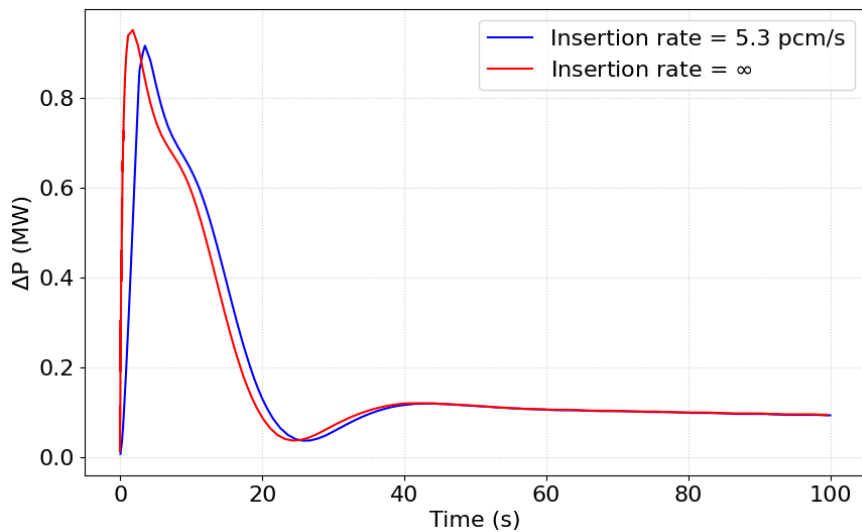


Figure 4.2: Step and ramp comparison

When there is a variation of reactivity, the salt temperature changes immediately, leading to a fast injection of negative reactivity due to the large negative prompt feedback coefficient. The adopted values are shown in Table 3.5.

Referring to Figure 4.3, after the first peak, a plateau is present within a few seconds. A series of plateaus should figure as the system evolves, however, the present model only hints at a tiny plateau and then directly evolves to reach a new steady state condition. Although the model utilizes ten axial nodes for core thermal-hydraulics, as detailed in Chapter 3, it currently neglects radial considerations. This is a potential source of inaccuracy, as the thermal variations between inner and outer fuel rings significantly impact local fuel temperature and, consequently, the transient response [34]. Furthermore, the re-entry of cooled fuel containing delayed neutron precursors can subtly influence the shape and magnitude of subsequent power plateaus.

Nevertheless, the variation in temperature response, shown in Figure 4.4 and Figure 4.5, is quite consistent with the ORNL data in terms of overall trend. The graphs reveal a notable difference in the system speed: the faster dynamics inherent in the present model, which is a direct result of its current parameterization, is also clearly evident in the temperature plots, contrasting with the slower dynamics observed in the ORNL model.

Both elements in the system, fuel and graphite, will face a temperature increase such that negative reactivity will counteract the increasing power level. Accordingly, once we account for the fuel temperature variation and the graphite temperature to obtain a slower dynamics, the present model will be in accordance with experimental data.

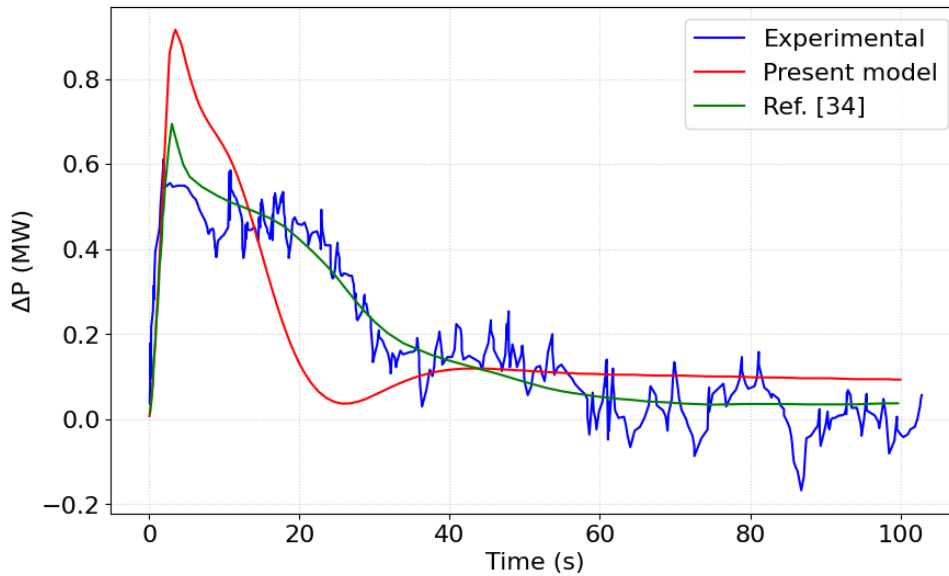


Figure 4.3: Power response to a 13.9 pcm insertion at 8 MW, with insertion rate

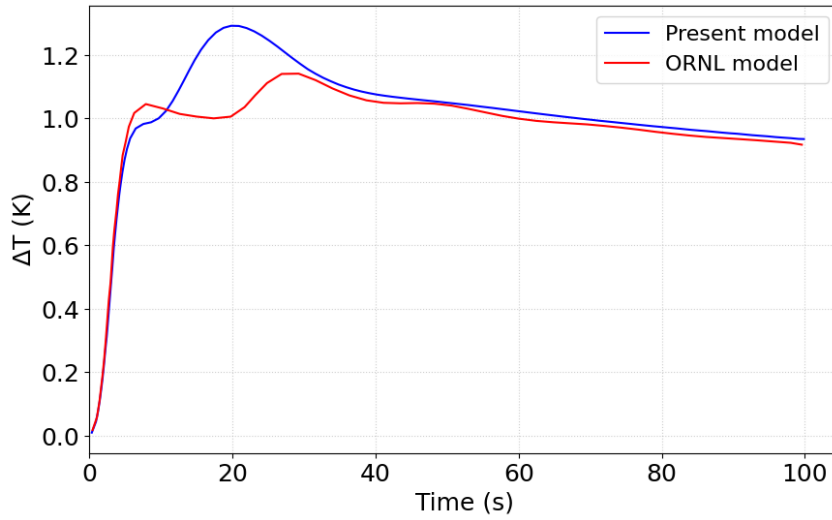


Figure 4.4: Mean fuel temperature variation in the core

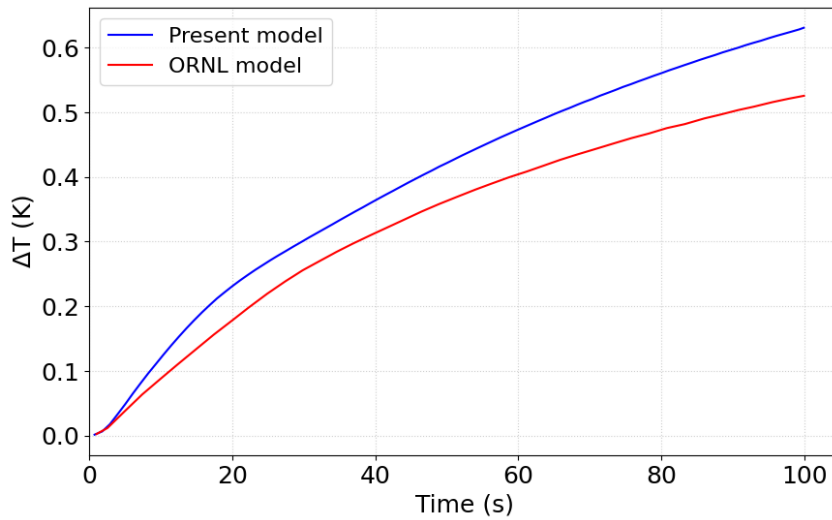


Figure 4.5: Mean graphite temperature variation in the core

To predict the robustness of the model, a quantitative analysis was performed too. In particular, the Modelica model yields a power difference RMSE of about 0.1533 MW. Although, the two sets of data show a similar trend, an overestimation of the peak is clearly visible; however, once the system reestablishes a new critical condition, the present model tends to stabilize near the power experimental results region. For the 8 MW test, other variables require specific consideration, as an example, Figure 4.6 and Figure 4.7 display the intrinsic role of the feedback coefficients, when coupling neutronics with thermal-hydraulics.

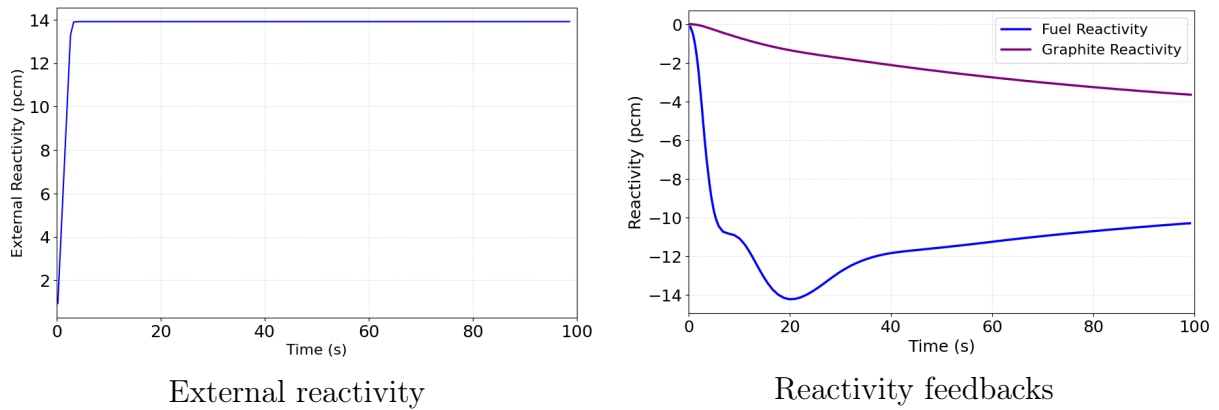


Figure 4.6: Plant response to a 13.9 pcm insertion of reactivity

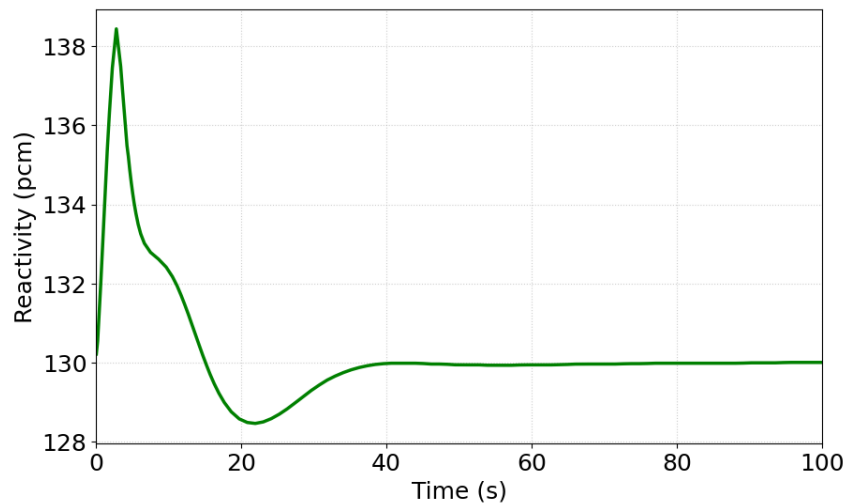


Figure 4.7: Circulation reactivity

Much experimental data from ORNL, also deals with power levels well below the nominal ones. As mentioned before, other two cases were under discussion. One of which is the 19.6 pcm reactivity insertion for a 5 MW power reactor.

As cited, a comparison between different models and experimental data, is shown. The simulation of the transient is presented in the following figures.

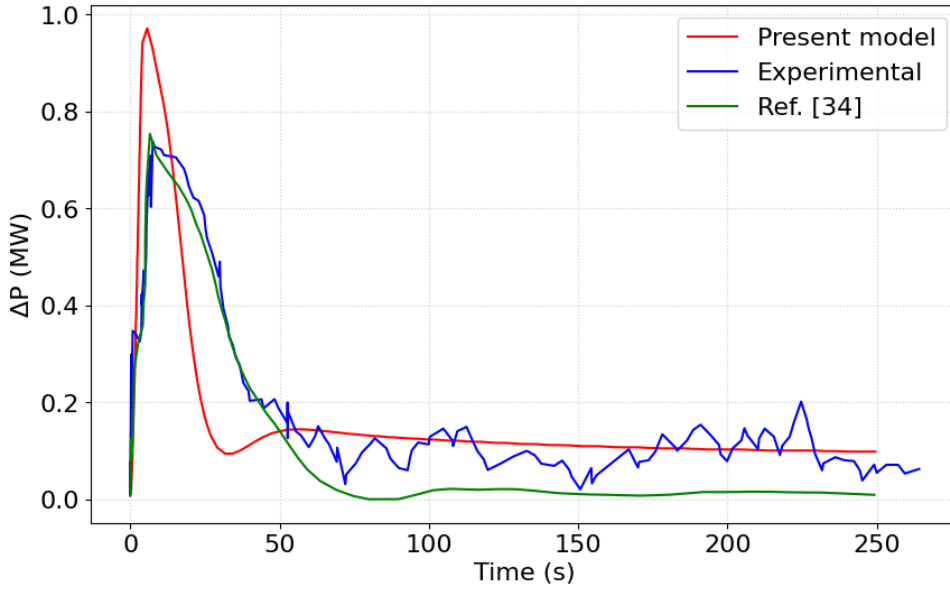


Figure 4.8: Power response to a 19 pcm insertion at 5 MW

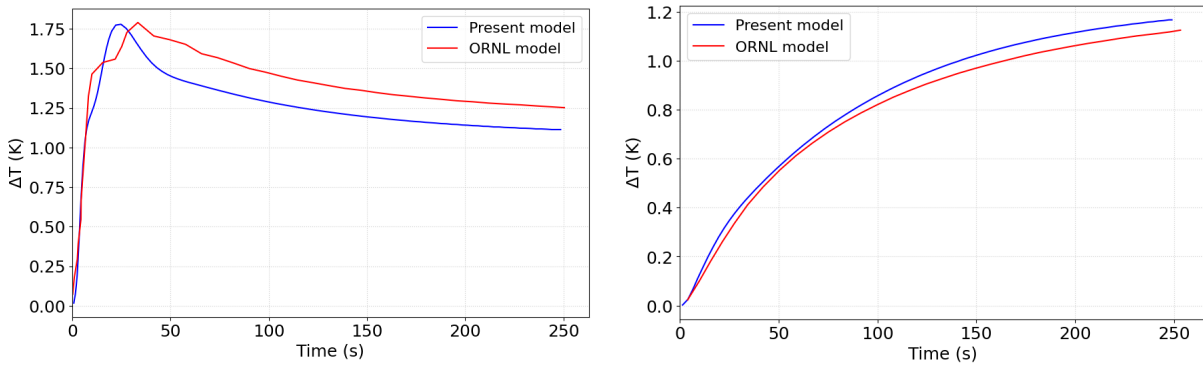


Figure 4.9: Average Fuel (left) and Graphite (right) temperature variation in the core during a 19 pcm insertion transient at 5 MW

Similarly to the previous case, the power presents a sharp increase within a few seconds and then, as the fuel temperature increases, meaning that the feedback effects are present, criticality is established once again. With reference to Figure 4.8, the first power plateau, typically observed in these transients, is no longer present due to the mitigating effects of the thermal behavior of the graphite moderator. Under stationary conditions, the graphite is typically cooled by the circulating fuel salt. However, when reactivity is inserted and the power level rapidly increases, the fuel salt temperature quickly rises. This increase causes an inversion of the heat flux, resulting in the salt now heating the cooler graphite, as explained in [6]. This rapid reversal of heat transfer quickly engages the negative temperature reactivity feedback from the graphite, adding a swift and strong stabilizing

effect, thus eliminating the first plateau.

The average power RMSE resulting from the described procedure was evaluated to be around 0.1156 MW, meaning lower RMSEs are obtained when considering a lower power level transient response. As a further representation of the model's developed capabilities, the following figures are shown.

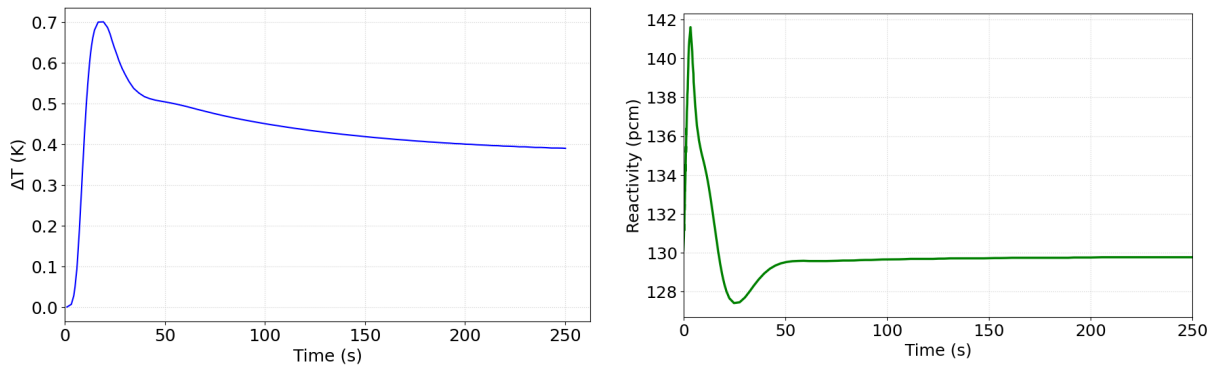


Figure 4.10: Circulation reactivity (right) and variation in coolant outlet temperature (left)

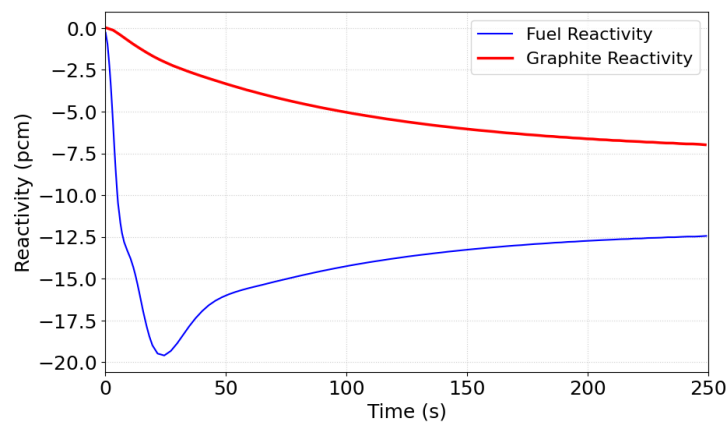


Figure 4.11: Reactivity feedbacks at 5 MW

From Figure 4.10, it can be seen how the increasing heat in the reactor, is being removed at the primary heat exchanger level, with an increment in the coolant temperature outlet. No changes as depicted in the inlet temperature of the coolant as being fixed throughout the transient.

The final case scenario in a validation optics, is a huge insertion of reactivity, such that $\rho_{ext} \simeq \beta$ in the 1 MW power level case, see Table 4.7. The results shown are in good agreement with the experimental data provided by ORNL. This is mainly due to the lower contribution of the feedback reactivities, based on a low power value. Different from before, no plateaus are expected to be present.

To avoid any kind of computational issues regarding heat exchange at the primary heat exchanger level, constant heat transfer coefficients are implemented, with values being consistent with previous evaluation, as per [27].

The adopted values are shown in Table 4.8.

| | Shell side | Tube side | Units |
|-----|------------|-----------|---------------------------------|
| h | 8500 | 11300 | $\text{W m}^{-2} \text{K}^{-1}$ |

Table 4.8: Heat transfer coefficients employed at 1 MW

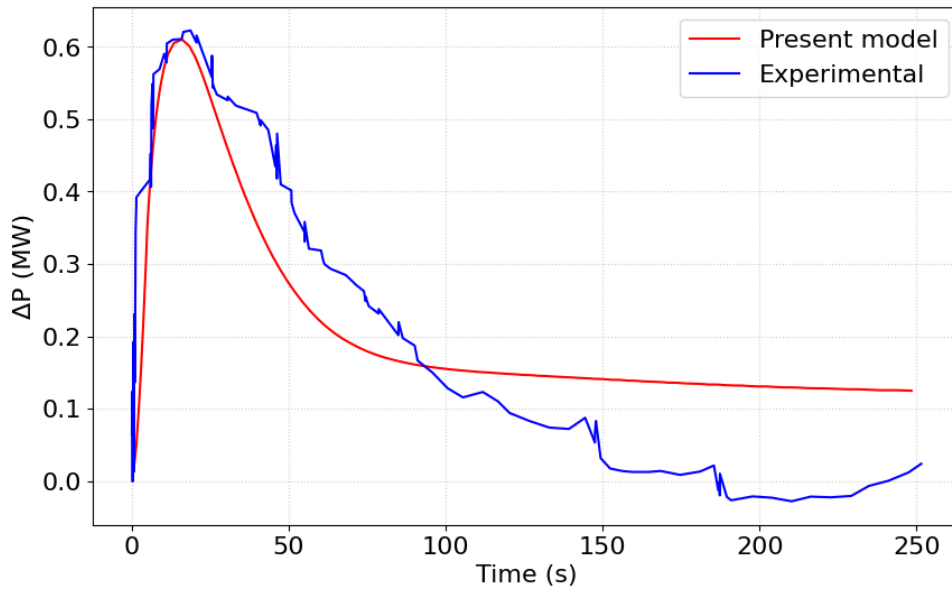


Figure 4.12: Power response to a 24.8 pcm insertion at 1 MW

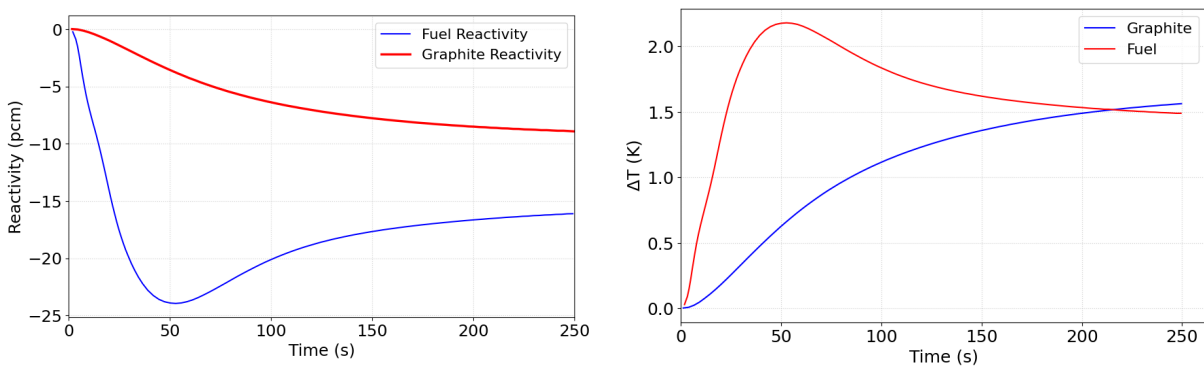


Figure 4.13: Reactivity feedbacks (left) and variation in fuel and graphite temperature (right) at 1 MW

From Figure 4.12 and Figure 4.13, it can be seen that due to the slower rate of temperature increase in the fuel at low power, the prompt negative temperature feedback is delayed. This prevents the reactor power from completing its initial peak and decaying to its asymptotic value before the warmer fuel salt completes its circulation through the external loop and flows back into the core. While the Modelica model provides a smooth, predictable long-term response, the experimental data are characterized by significant noise and instability, leading to discrepancies in the post-peak regime.

Overall, the average power RMSE for the 1 MW scenario is expected to be around 0.1235 MW. From the qualitative analysis performed, shown in Figure 4.12, it may seem to have a good fit between the present model and the experimental data, however, after 150 seconds, the two power levels tend to stabilize to different values. As a consequence of this, most of the errors in the power evaluation are depicted in the final part of the transient.

4.3. Operational anomalies

Results from the simulation of accidental situations using the Modelica model are reported in this section. Loss of flow simulations in the primary system and cold slug insertions inside the core with associated reactivity excursion are presented below.

4.3.1. Primary Pump Failure Accident

The simulation of the primary pump failure accident during critical operation is a crucial safety scenario for this system. The most likely cause of a loss of flow in the primary system is a pump trip, in which case the flow rate reduces exponentially over a coast-down period. In MSRs, this kind of accident is usually caused either because of a blackout from the grid or an accident that disconnects the power plant from the grid. In this work, the obtained outcomes are compared with ORNL results and those of [27]. No corrective actions by the control rods were considered.

To exploit the results coming from this simulation, we first have to identify a common definition for the pump coast-down. The idea is to consider an exponential decrease in the fuel mass flow rate, as indicated by Equation (4.3).

$$\dot{m}(t) = \begin{cases} \dot{m}_{\text{nominal}}; & t < t_0 \\ \dot{m}_{\text{nominal}} \cdot \exp\left(-\frac{t-t_0}{\tau_p}\right); & t \geq t_0 \end{cases} \quad (4.3)$$

where the characteristic time of the pump τ_p is equal to 2.5 s and the initial time of the transient t_0 is set at 20 s.

From Figure 4.14, it can be seen that after 20 seconds the pump completely stops. Similarly, the power response remarks the usual trend, as depicted in Figure 4.15, where the power instantaneously decreases due to the highly negative fuel salt temperature coefficient.

Overall, the change in the primary flow, causes a decrease in the transport rate of the delayed neutron precursors and reduces the heat removed from the core. As a result, this behavior immediately affects the power and temperature. Therefore, the two effects can be summarized in a first loss of delayed neutrons, causing the power to decrease, and subsequently, the temperature rise due to inadequate cooling triggers the negative temperature feedback, which further drives the power down rapidly.

It is also worth mentioning that simulations were conducted by a different algorithm, i.e. Esdirk45a (Explicit Singly Diagonally Implicit Runge-Kutta, Order 4/5), having excellent stability properties, as the Dassl solver could not converge at very low mass flow rates.

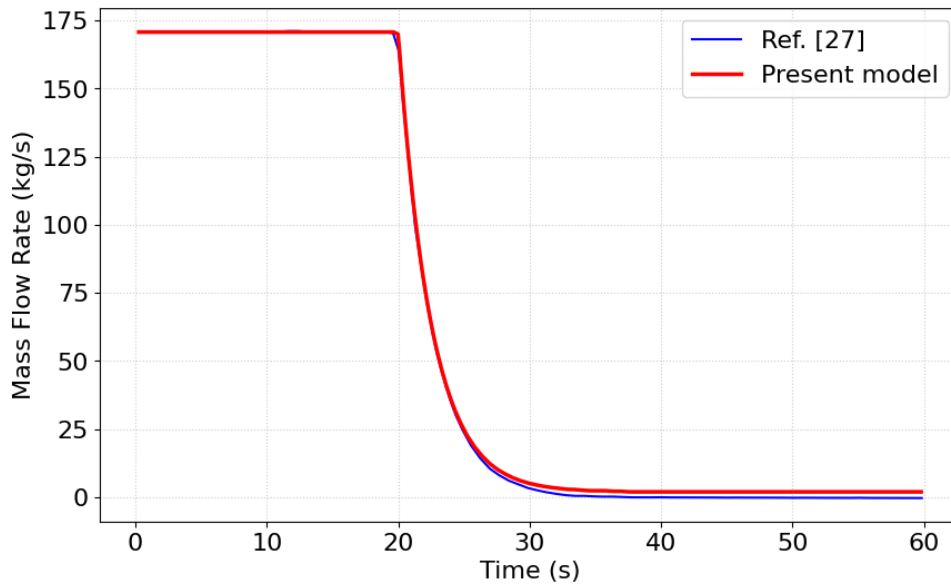


Figure 4.14: Mass flow rate response to a pump coast down

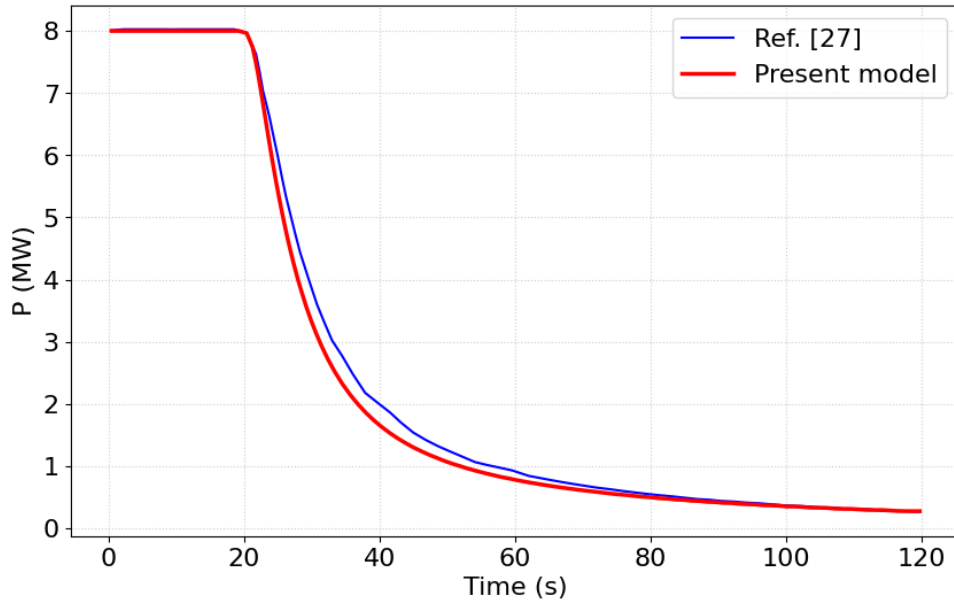


Figure 4.15: Power response to a pump coast down

The discrepancies observed in the pictures above might refer to a different final condition, since in the present model the final mass flow rate is expected to be 1% of the nominal one, whereas the simulation performed in [27] is made throughout a MATLAB/Simulink model, therefore a better representation of this dynamic system is provided.

When dealing with a circulating fluid reactor, special attention must be paid to the reactivity losses due to the DNPs decay out of the core. In particular, as hinted in Table 4.5, the real amount of delayed neutrons within the core is way lower with respect to the static fuel case, hence some compensation reactivity must be considered when designing a molten salt reactor. Special attention is indeed devoted to it, as displayed in Figure 4.16 as the pump coast down occurs.

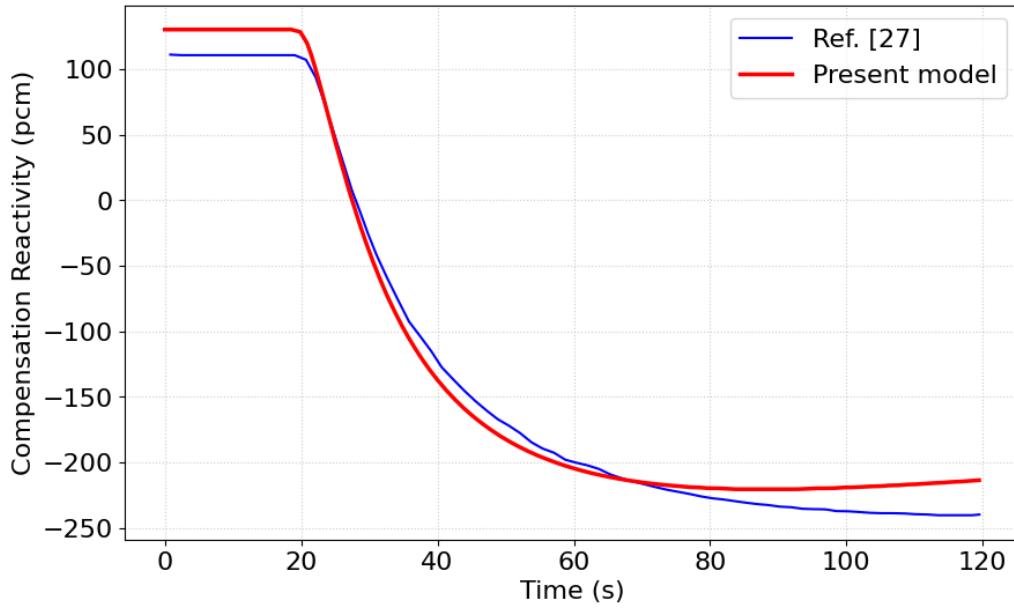


Figure 4.16: Reactivity during a pump coast down

With quite evidence, once total reactivity decreases, thus power too, compensation reactivity becomes negative as fewer delayed neutron precursors flow in the primary circuit. The average compensation reactivity RMSE is around 14.64 pcm, resulting in a good agreement with reference data.

As noted earlier, the temperature behavior would be worth investigating, however, no available data were found for the ^{233}U -fueled case. On the other hand, [16] provides interesting calculations with ^{235}U -fueled 10 MW reactor power. Therefore, considering a further verification of the present model, the ^{235}U case scenario has been modeled to compare the results. The highlighted variable tracked in this scenario is the mean temperature variation in the core during the pump transient.

The reduced heat removal in the heat exchanger, results in a jump in the fuel temperature, as visible in Figure 4.17.

These temperature transients lead to a negative additional reactivity within the system as the temperature feedback step in, causing a rapid loss in power.

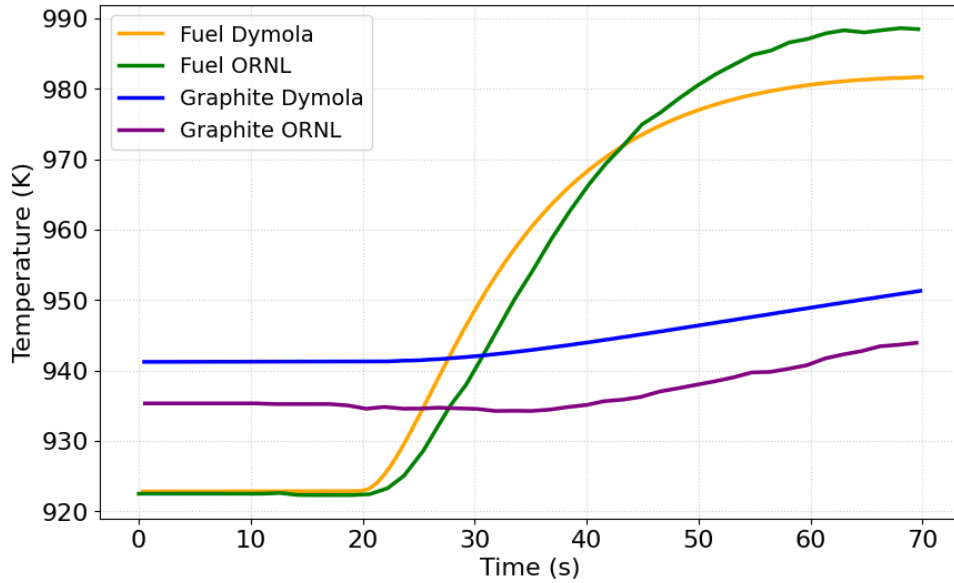


Figure 4.17: Average temperature variation at 10 MW

Although it is not shown here, it would be quite interesting to investigate fuel temperature behavior over hours of operation following a pump trip, as we expect to re-establish criticality because of the low fission present in the core, thus leading to a decrease in fuel temperature, hence a positive reactivity insertion. However, as of now, the behavior of the temperatures shown is in good accordance with the ORNL data. The small contrasts can be referred to different considerations of heat transfer between fuel and graphite in the core.

4.3.2. Cold slug insertion into the core

A cold slug insertion refers to a situation in which a colder than normal mass of fuel salt is introduced into the reactor core. The accidents analyzed consisted of pumping 0.57 m^3 and 0.85 m^3 of fuel into the core at a rate of 170 kg/s .

The adopted procedure resembles the ORNL's approach, as explained in [16], where instead of modeling the cold mass inside the core, the equivalent reactivity resulting from the temperature change was calculated and introduced. The expected outcomes are of inducing a noticeable increase in reactivity, such that power will quickly erupt.

Initial conditions are set to be critical at 922 K , while working at 10 kW . Therefore, to simulate the dynamic responses, the initial temperature of the fuel entering the core is set at time $t=0$, to be 922 K .

Depending on the duration for which the switch is active, a certain volume of colder salt

is introduced into the core. Results from simulations for slug volumes of 0.57 m^3 and 0.85 m^3 are reported here.

Considerations were made concerning the tantamount reactivity insertion following the temperature excursion, leading to a reactivity behavior as depicted in Figure 4.18.

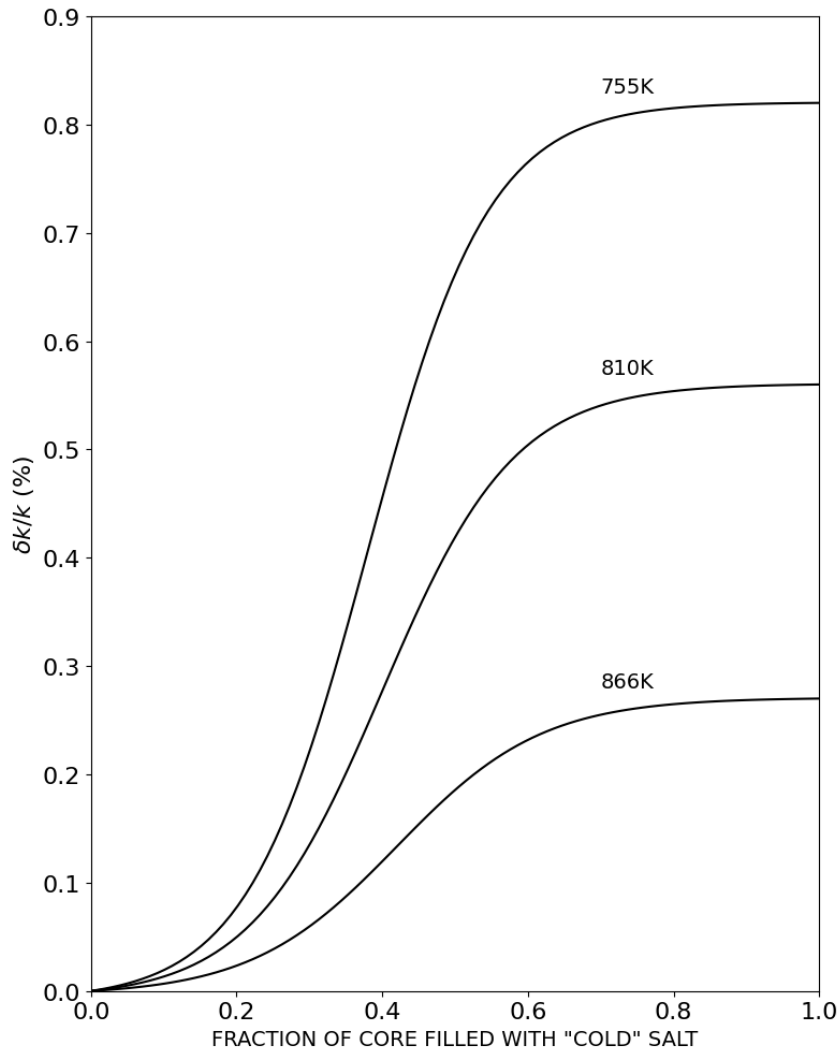


Figure 4.18: Excess reactivity due to replacing part of the core with a colder slug [16]

Based on the cold slug temperature, a different amount of reactivity will be taken into account as the cold slug travels. In this work, our attention will be devoted to the worst case scenario, where the cold slug temperature is equal to 755 K, leading to a maximum insertion of $0.820 \delta k/k$. To be consistent with [16], a reactivity model was developed to resemble the reactivity transient as the cold mass flows within the core.

At 170 kg/s , fuel passes from the bottom of the core to the top in about 7.3 seconds.

Providing this information, it was possible to obtain the following reactivity model, as the slug passes out in 18.2 seconds.

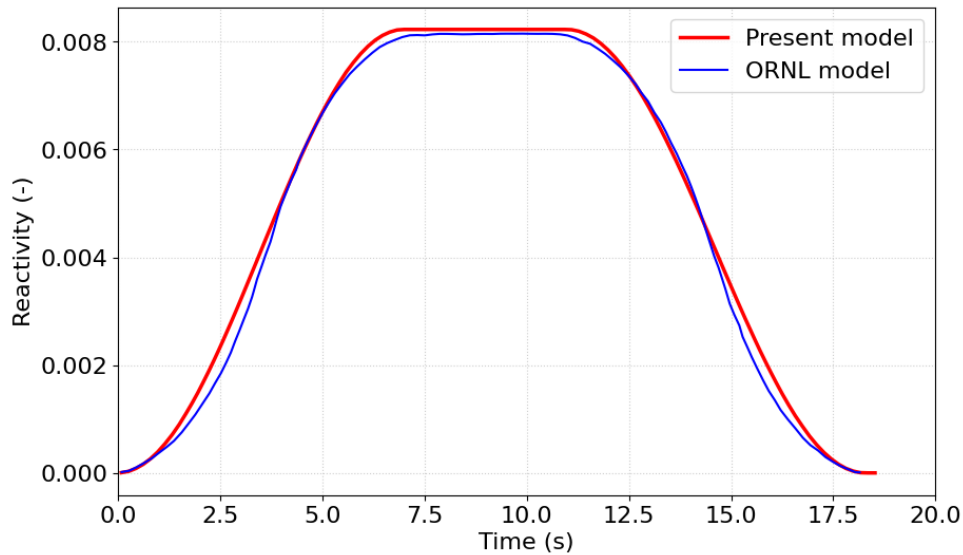


Figure 4.19: Reactivity transient due to 0.85 m³ cold slug passage

The simulation setup is performed by employing at zero time, a negative contribution of $0.300 \delta k/k$ to represent the loss of delayed neutron precursors when fuel circulation is present. Although this feature is already within the framework of the present work, to have consistency with work [16], we decided to couple the negative step of reactivity due to fuel circulation with Figure 4.19. The simplified scheme adopted is shown in Figure 4.20. The dynamic response within the core is shown in Figure 4.21. No considerations were made about the presence of the void fraction within the fuel salt mixture; moreover, no control action was provided.

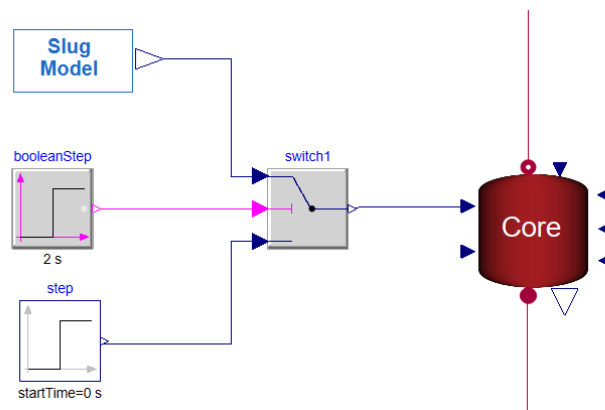


Figure 4.20: Simulation of a cold slug accident

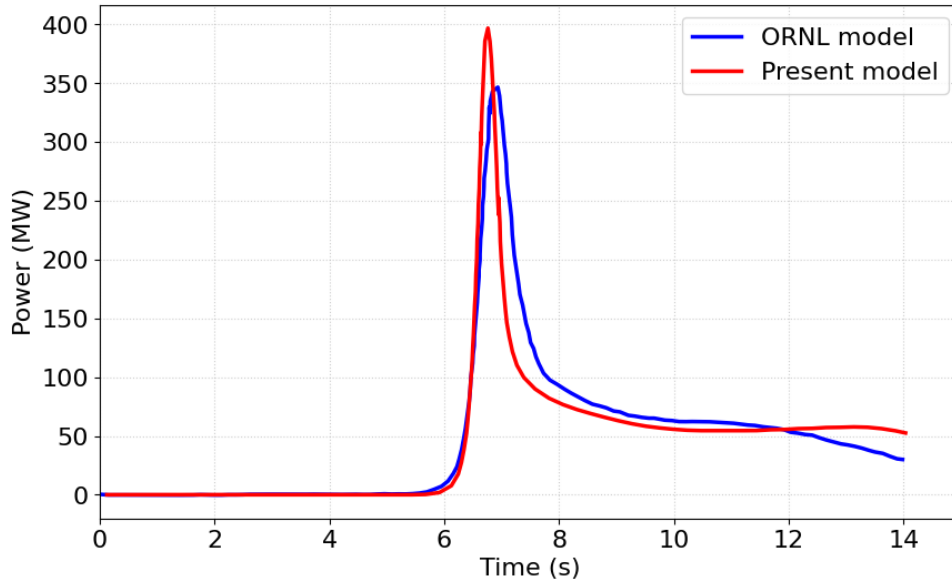


Figure 4.21: Power induced by a 0.85 m^3 cold slug at 755 K

The visible trend in the figure above, generally reflects the ORNL results; however a difference in the power peak height can be noticed. This can be related to a different value of circulating delayed neutron precursors obtained in both simulations. Indeed, the resulting β_{eff} in the present work is expected to 381 pcm , while ORNL states it at 340 pcm . These further 40 pcm provides additional reactivity to the core, as more fissions are likely to occur, resulting in a higher power production.

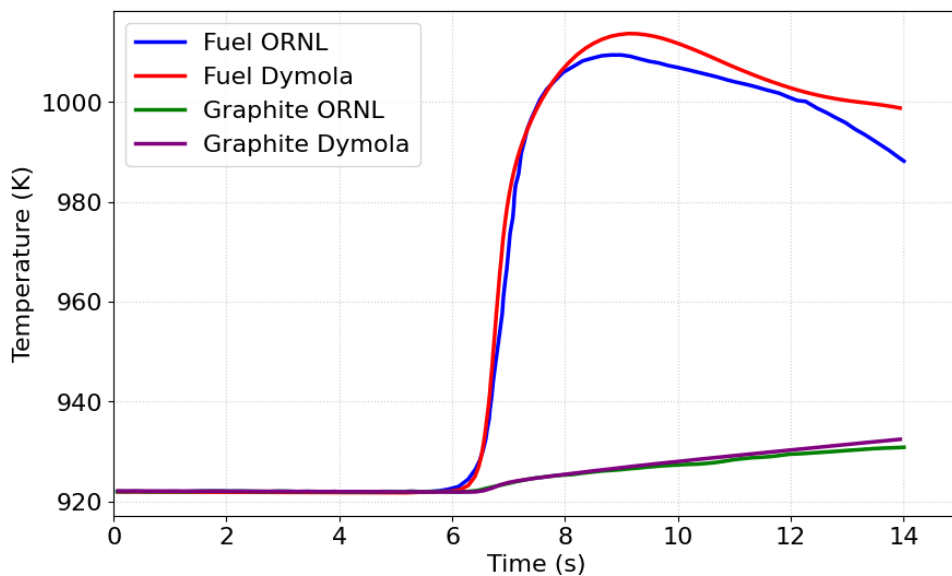


Figure 4.22: Temperature comparison induced by a 0.85 m^3 cold slug at 755 K

Fuel temperature, as well, will tend to increase a bit more, as reactivity feedbacks step in, thus counteracting more deviation from criticality.

Similarly, the 0.57 m³ cold slug transient is simulated, as reactivity figures a different behavior, without the presence of any plateau at the maximum reactivity of 0.820 $\delta k/k$. In this case, the slug passes out in 14.6 seconds.

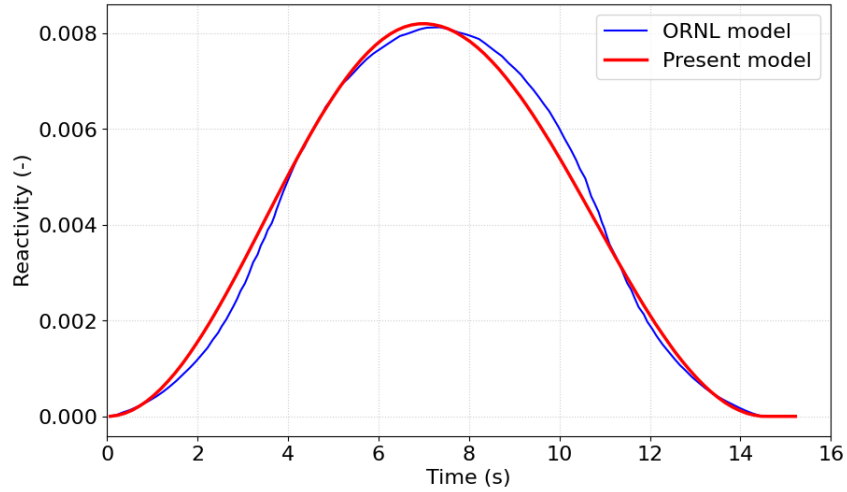


Figure 4.23: Reactivity transient due to 0.57 m³ cold slug passage

The power response and average fuel salt and graphite temperatures are shown in Figure 4.24 and Figure 4.25.

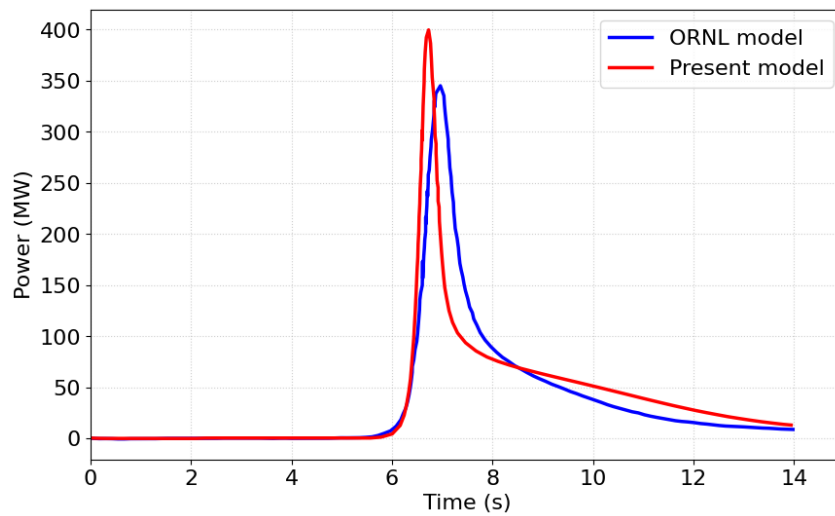


Figure 4.24: Power induced by a 0.57 m³ cold slug at 755 K

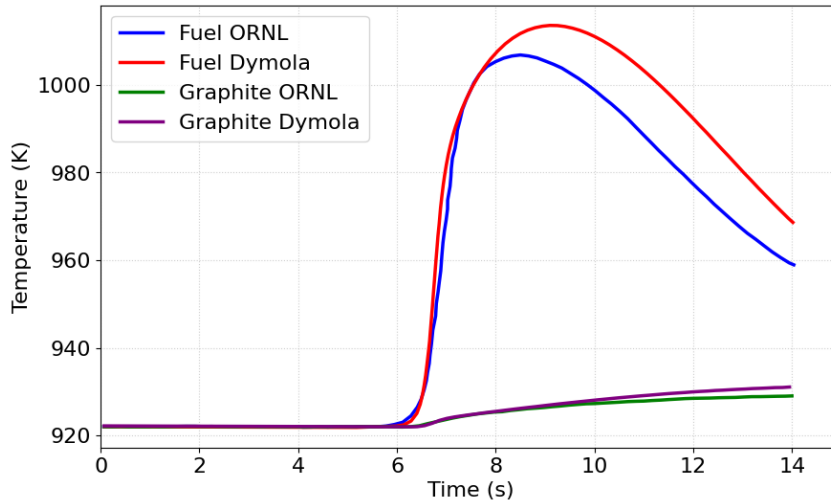


Figure 4.25: Temperature comparison induced by a 0.57 m^3 cold slug at 755 K

Similar considerations hold for this different volume of cold slug. Moreover, the error evaluation presented in Table 4.9, highlights that the model's deviation from the ORNL data is mainly driven by the magnitude error observed at the peak of the transient.

In summary, a comparison of the results of the present model, after a cold slug insertion for a ^{235}U fuel type, is depicted in Figure 4.26, as the power profiles show analogous behavior.

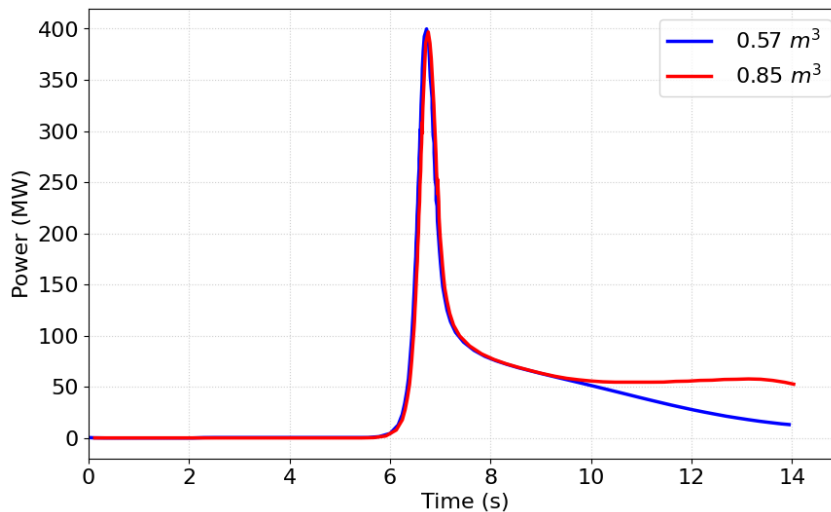


Figure 4.26: Power comparison induced by a cold slug at 755 K

The different trend visible after 10 seconds, might be related to the presence of a plateau at the maximum reactivity insertion, as shown in Figure 4.19.

| | 0.85 m ³ | 0.57 m ³ | Units |
|------|---------------------|---------------------|-------|
| RMSE | 50.10 | 73.27 | MW |

Table 4.9: Average power RMSE in a cold slug accident

5 | Conclusions and future developments

The work presented in this thesis aims at investigating the dynamic behavior of a molten salt reactor system, based on a reference MSR design, that is MSRE. In this context, a validation of the model was primarily conducted, in order to see if consistency with previous models and experimental data was present. Subsequently, the numerical model was submitted to different accidental scenarios, as widely mentioned in Section 4.3. The outcomes align well with literature models, establishing a reliable foundation for the analysis of the primary circuit.

As cited in Chapter 3, the present model consists of several approximations. To make it easier to read, some of them are listed below.

1. Although 10 axial nodes were considered in core thermal-hydraulics, no attention was given to the radial part of the reactor core. This would have let us obtain a better representation for each part of the core, thus improving system dynamics with respect to the experimental data analyzed. It is possible to state, that this represents a possible source of inaccuracy due to the lack of a radial description of the core power, hence of a local evaluation of the feedback aspects. These variations seem to be responsible for significant differences in the power peak caused by reactivity variations.
2. As the fuel salt flows, some gaseous fission products may be entrained in the circulating mixture, thereby perturbing the system reactivity, with negative additional reactivity added to the core. Paper [34] shows a void coefficient evaluation with Serpent, JEFF 3.1 cross section library, considering homogeneous distribution of voids. In this way, reactivity effects due to void presence would be accounted.
3. The presence of the control rods in the reactor core was not considered, implying that no corrective action via external reactivity insertion was simulated. However, as previously cited, when considering the radial contribution in the reactor core, this feature would be appropriate to add.

4. No CFD evaluation was done in this work. This would allow us to have a more detailed description of the fuel salt flow within the fuel channels, considering it as a typical laminar flow.
5. Another approximation was not to develop models for the secondary circuit. This would also enable us to simulate transients on the secondary side.

It is pertinent to mention that thanks to the Modelica language, several benefits were useful, as the interchangeability of the models allowed to design them independently of one another. However, the results obtained in this work, even when discrepancies are present, showed good stability when a perturbation in the system occurs, providing a solid base for further exploitation. In particular, at low power levels, the model displays a sluggish response, whereas at higher power, the system response is damped due to the strong negative reactivity feedback. In Chapter 4, a plateau is seen in the power response for the ^{233}U fueled case as a consequence of the higher negative reactivity coefficient and lower delayed neutron fraction. In particular, the plateau presence is due to the temporary balance between the residual negative reactivity from the temperature balances and the slowing rate of reactivity loss due to DNP decay. This dynamic balance temporarily slows the power's overall decay, creating the plateau. Therefore, much attention should be paid to the effective delayed neutron fraction, as it plays a crucial role when developing a control strategy for the nuclear system.

A fundamental difference is achievable by using a multi-dimensional approach, in which the system of coupled partial differential equations is solved simultaneously within a multi-dimensional domain. In particular, the modeling of the single-channel radial dimension allows taking into account local effects, such as the temperature increase close to the channel wall, which can affect the overall transient behavior by notably reducing the time required to reach the asymptotic value.

Therefore, with a more accurate description of the system, it would be possible to further extend the analysis towards other safety analyses and non-electrical applications, exploiting the high temperatures that characterize the primary circuit.

The methodology employed in this thesis leverages the intrinsic advantages of the Modelica language to deliver a highly flexible and adaptable simulation platform. The object-oriented nature of the model ensures that the physical components, such as the core, heat exchanger, and plenums are developed independently from their final application. This allows the primary circuit model to be easily modified and adapted to various Generation IV designs, beyond the MSRE geometry. Furthermore, the acausal and equation-based structure of Modelica inherently simplifies the connection to diverse energy conversion systems and non-electric applications. This facilitates future research into comprehensive

Nuclear Hybrid Energy Systems (NHES), where the reactor can seamlessly optimize its output to simultaneously supply electricity, industry, and flexible non-electric demands, such as hydrogen production or industrial heat.

Therefore, future developments should focus both on the improvement of the dynamic models presented in this work and on their integration into a comprehensive framework for the analysis of hybrid energy systems.

Bibliography

- [1] Net zero act, 2024. URL <http://data.europa.eu/eli/reg/2024/1735/oj/eng>.
- [2] S. J. Ball and T. W. Kerlin. Stability analysis of the molten-salt reactor experiment. Technical Report ORNL-TM-1070, Oak Ridge National Laboratory (ORNL), 1965.
- [3] R. B. Bird, W. E. Stewart, and E. N. Lightfoot. *Transport Phenomena*. John Wiley & Sons, New York, 2 edition, 2007.
- [4] BloombergNEF and The BNEF Team. New energy outlook, 2024.
- [5] K. E. Brenan, S. L. Campbell, and L. R. Petzold. *Numerical Solution of Initial-Value Problems in Differential-Algebraic Equations*. 1989.
- [6] A. Cammi, C. Fiorina, C. Guerrieri, and L. Luzzi. Dimensional effects in the modelling of msr dynamics: Moving on from simplified schemes of analysis to a multi-physics modelling approach. *Nuclear Engineering and Design*, 246:12–26, 2012.
- [7] U. N. R. Commission and O. R. N. Laboratory. Fuel qualification for molten salt reactors. Technical Report NUREG/CR-7299 / ORNL/TM-2022/2754, U.S. Nuclear Regulatory Commission (NRC) and Oak Ridge National Laboratory (ORNL), 2022.
- [8] M. M. El-Wakil. *Nuclear Heat Transport*. International Textbook Company, illustrated edition, 1971.
- [9] M. Elhareef and Z. Wu. Benchmarking a point reactor kinetics method with delayed neutron precursors transport using data from molten salt reactor experiment. *Annals of Nuclear Energy*, 217, 2025.
- [10] P. N. H. . J. R. Engel. *Experience with the Molten-Salt Reactor Experiment, Nuclear Applications and Technology*, 8:2, 118-136, <https://doi.org/10.13182/NT8-2-118>. 1970.
- [11] European Commission. Fit for 55: delivering the eu’s 2030 climate target on the way to climate neutrality, 2021. URL <https://eur-lex.europa.eu/legal-content/EN/TXT/?uri=celex:52021DC0550>.

- [12] C. Fiorina, D. Lathouwers, M. Aufiero, A. Cammi, C. Guerrieri, J. L. Kloosterman, L. Luzzi, and M. E. Ricotti. Modelling and analysis of the msfr transient behaviour. 2013.
- [13] P. Fritzson. *Principles of Object-Oriented Modeling and Simulation with Modelica 2.1*. Wiley-IEEE Press, first edition, 2003.
- [14] Grand View Research, Inc. Pink hydrogen market size, share & trends analysis report, 2023. URL <https://www.grandviewresearch.com/industry-analysis/pink-hydrogen-market-report>. Data analysis period 2023–2033.
- [15] M. S. Greenwood and D. De Wet. Status report on the msre transform model for thermal-hydraulic benchmarking. Technical report, Oak Ridge National Laboratory (ORNL), Oak Ridge, TN (United States), 2019. URL <https://www.osti.gov/biblio/1615806>.
- [16] P. N. Haubenreich and J. R. Engel. Safety calculations for msre. Technical Report ORNL-TM-251, Oak Ridge National Laboratory (ORNL), Oak Ridge, TN, 1962.
- [17] P. N. Haubenreich, J. R. Engel, B. E. Prince, and H. C. Claiborne. Msre design and operations report, part iii. nuclear analysis. Technical Report ORNL-TM-730, Oak Ridge National Laboratory (ORNL), Oak Ridge, TN, 1964.
- [18] International Atomic Energy Agency (IAEA). Status of molten salt reactor technology. Technical Report 489, IAEA, Vienna, Austria, 2023. URL https://www-pub.iaea.org/MTCD/Publications/PDF/STI-DOC-010-489_web.pdf.
- [19] International Energy Agency (IEA). Net zero by 2050: A roadmap for the global energy sector, 2021. URL <https://www.iea.org/reports/net-zero-by-2050>.
- [20] J. R. Lamarsh and A. J. Baratta. *Introduction to Nuclear Engineering*. 3 edition, 2001.
- [21] N. Manfred and R. O. G. *Heat Exchanger Design Guide: A Practical Guide for Planning, Selecting and Designing of Shell and Tube Exchangers*. 2015.
- [22] R. C. Martinelli and L. M. K. Boelter. The analytical prediction of superposed free and forced viscous convection in a vertical pipe. *University of California Publications in Engineering*, 1942.
- [23] J. P. Meyer, M. Everts, N. Coetzee, K. Grote, and M. Steyn. Heat transfer coefficients of laminar, transitional, quasi-turbulent and turbulent flow in circular tubes. *International Communications in Heat and Mass Transfer*, 105, 2019.

- [24] I. L. Pioro, editor. *Handbook of Generation IV Nuclear Reactors: A Guidebook*. Woodhead Publishing (Elsevier), second edition, 2022.
- [25] R. C. Robertson. *MSRE Design and Operations Report, Part I, Technical Report ORNL-TM-0728*. ORNL, 1965.
- [26] V. Singh, A. M. Wheeler, M. R. Lish, O. Chvála, and B. R. Upadhyaya. Nonlinear dynamic model of molten-salt reactor experiment: Validation and operational analysis. *Annals of Nuclear Energy*, 113:177–193, 2018.
- [27] B. Spinelli. Preliminary analysis of the msre dynamic behaviour. Tesi di laurea specialistica in ingegneria nucleare, Politecnico di Milano, 2010.
- [28] J. Steffy, R. C. Experimental dynamic analysis of the msre with ^{233}U fuel. Technical Report ORNL-TM-2997, Oak Ridge National Laboratory (ORNL), Oak Ridge, TN, 1970.
- [29] R. C. Steffy and P. J. Wood. Theoretical dynamic analysis of the msre with U-233 fuel. Technical Report ORNL-TM-2571, Oak Ridge National Laboratory (ORNL), Oak Ridge, TN, 1969.
- [30] C. Tripodo. Development of control-oriented simulation tools and control strategies for the gen-iv molten salt fast reactor. Master’s thesis, Politecnico di Milano, 2018.
- [31] United Nations, Department of Economic and Social Affairs, Population Division. World population prospects 2017: The 2017 revision, key findings and advance tables, 2017.
- [32] United Nations Economic Commission for Europe (UNECE). Life cycle assessment of electricity generation options, oct 2021. URL https://unece.org/sites/default/files/2021-11/LCA_final.pdf.
- [33] M. Zanetti. *Development of new tools for the analysis and simulation of circulating-fuel reactor power plants*. Ph.d. thesis, Politecnico di Milano, 2016.
- [34] M. Zanetti, L. Luzzi, A. Cammi, and C. Fiorina. An innovative approach to dynamics modeling and simulation of the molten salt reactor experiment. In A. E. S. of Japan (AESJ), editor, *PHYSOR 2014: The Role of Reactor Physics Toward a Sustainable Future*, 2014.

A | Modelica language

Modelica is an object-oriented, declarative, equation-based language for physical modeling and simulation, whose development began in 1996 with the primary goal of creating easily exchangeable models. Introduced as an international standard in 1997, Modelica is particularly well-suited for simulating complex, multi-domain, cyber-physical systems (e.g., mechanical, hydraulic, thermal, and electrical).

Its features make it a powerful tool for engineering simulations. Some of them are listed below [13].

- Object-oriented: It is based on the creation of individual model components that represent actual physical elements. This ensures encapsulation of the models and abstraction of the models.
- Hierarchical modularity: Complex models can be decomposed into submodels.
- Inheritance Modeling: It allows for the creation of specialized models, such as subclasses from generic models, inheriting their basic properties and adding specific equations.
- Acausal: The programmer simply writes the set of model equations, and the compiler establishes the proper causality direction for the specific simulation.
- Physical-Based Modeling: The equations employed are often simply the basic physical conservation equations like mass, momentum and energy balances, making the language intuitive and easy to read.
- Large Libraries Substances: The increasing popularity of Modelica has led to the availability of numerous validated pre-existing component libraries, such as the *NRGCollection* library and the *ThermoPower* library, also adopted in this work.

Modelica can be implemented in both open-source environments, like OpenModelica and licensed environments, such as Dymola (Dynamic Modeling Laboratory). Dymola, which was used for the models described in the thesis, incorporates sophisticated algorithms, including symbolic manipulation of equations and linkage to state-of-the-art numerical integration codes like DASSL [5], ensuring fast and efficient simulations.

B | Graphite

In this section, a brief overview of the graphite properties is shown. To start with, let's first recall the key features of this element.

When considering a scattering event, where E depicts the energy of a neutron before a scattering event and E' represents the energy loss after having collision with a target nucleus of mass number A , it is fair to consider that the neutron will suffer the largest possible loss in energy when scattered backward, thus happening when the scattering angle is equal to 180° . This leads to a simplified equation, i.e. Equation (B.1), representing the minimum energy of a scattered neutron after it collides.

$$E' = \left(\frac{A-1}{A+1} \right)^2 E = \alpha E \quad (\text{B.1})$$

With α being the *collision parameter*, some values are shown in Table B.1.

| Nucleus | Mass No. | α |
|------------------|----------|----------|
| Hydrogen | 1 | 0 |
| H ₂ O | | / |
| Deuterium | 2 | 0.111 |
| D ₂ O | | / |
| Beryllium | 9 | 0.640 |
| Carbon | 12 | 0.716 |
| Oxygen | 16 | 0.779 |
| Sodium | 23 | 0.840 |
| Iron | 56 | 0.931 |
| Uranium | 238 | 0.983 |

Table B.1: Collision parameters for different nuclei

In the table above, it is quite visible how the collision parameter increases monotonically to unity with increasing A . In addition, it is easy to understand why graphite has been chosen as a moderator material for several nuclear reactor concepts throughout the years, since on average a neutron loses 14% of its initial energy when colliding with carbon, hence graphite.

List of Figures

| | | |
|-----|---|----|
| 1 | Economic Transition Scenario [4] | 2 |
| 2 | CO ₂ captured [4] | 3 |
| 3 | H ₂ in NZS and in ETS [4] | 3 |
| 4 | Low emission sources of electricity [19] | 4 |
| 1.1 | Pink Hydrogen Market [14] | 8 |
| 1.2 | MSR in Generation IV International Forum [24] | 9 |
| 2.1 | Rear View Building 7503 during MSRE construction [25] | 21 |
| 2.2 | MSRE activities [10] | 22 |
| 2.3 | Experience of Molten Salt Reactor Experiment [10] | 23 |
| 2.4 | Layout of MSRE [25] | 24 |
| 2.5 | MSRE Reactor Core [25] | 27 |
| 2.6 | MSRE Graphite block [25] | 28 |
| 2.7 | Fuel Pump [25] | 29 |
| 2.8 | Heat Exchanger [25] | 30 |
| 2.9 | Radiator [25] | 34 |
| 3.1 | Object-oriented modeling of the MSRE | 40 |
| 3.2 | Object-oriented modeling of the core | 41 |
| 3.3 | Decay chain | 48 |
| 3.4 | Object-oriented modeling of the primary heat exchanger | 52 |
| 4.1 | Power response to a 13.9 pcm insertion at 8 MW | 62 |
| 4.2 | Step and ramp comparison | 62 |
| 4.3 | Power response to a 13.9 pcm insertion at 8 MW, with insertion rate | 63 |
| 4.4 | Mean fuel temperature variation in the core | 64 |
| 4.5 | Mean graphite temperature variation in the core | 64 |
| 4.6 | Plant response to a 13.9 pcm insertion of reactivity | 65 |
| 4.7 | Circulation reactivity | 65 |
| 4.8 | Power response to a 19 pcm insertion at 5 MW | 66 |

| | | |
|------|--|----|
| 4.9 | Average Fuel (left) and Graphite (right) temperature variation in the core during a 19 pcm insertion transient at 5 MW | 66 |
| 4.10 | Circulation reactivity (right) and variation in coolant outlet temperature (left) | 67 |
| 4.11 | Reactivity feedbacks at 5 MW | 67 |
| 4.12 | Power response to a 24.8 pcm insertion at 1 MW | 68 |
| 4.13 | Reactivity feedbacks (left) and variation in fuel and graphite temperature (right) at 1 MW | 68 |
| 4.14 | Mass flow rate response to a pump coast down | 70 |
| 4.15 | Power response to a pump coast down | 71 |
| 4.16 | Reactivity during a pump coast down | 72 |
| 4.17 | Average temperature variation at 10 MW | 73 |
| 4.18 | Excess reactivity due to replacing part of the core with a colder slug [16] | 74 |
| 4.19 | Reactivity transient due to 0.85 m ³ cold slug passage | 75 |
| 4.20 | Simulation of a cold slug accident | 75 |
| 4.21 | Power induced by a 0.85 m ³ cold slug at 755 K | 76 |
| 4.22 | Temperature comparison induced by a 0.85 m ³ cold slug at 755 K | 76 |
| 4.23 | Reactivity transient due to 0.57 m ³ cold slug passage | 77 |
| 4.24 | Power induced by a 0.57 m ³ cold slug at 755 K | 77 |
| 4.25 | Temperature comparison induced by a 0.57 m ³ cold slug at 755 K | 78 |
| 4.26 | Power comparison induced by a cold slug at 755 K | 78 |

List of Tables

| | | |
|------|---|----|
| 1 | Energy source emissions [32] | 5 |
| 1.1 | Overview of Gen-IV systems [24] | 8 |
| 1.2 | Classification of MSRs by the IAEA [18] | 11 |
| 1.3 | Economic advantages of Molten salt reactors | 13 |
| 1.4 | MSRs EU Designs | 15 |
| 2.1 | MSRE Design and Operational Parameters [15] | 25 |
| 2.2 | Composition and Physical Properties of Fuel and Coolant Salts [25] | 26 |
| 2.3 | Design Data for Primary Heat Exchanger [25] | 31 |
| 2.4 | Chemical and Physical Properties of INOR-8 [25] | 35 |
| 2.5 | Reactivity balance in MSRE [25] | 37 |
| 3.1 | Thermophysical properties of media and graphite [9] | 42 |
| 3.2 | Decay Heat parameters | 44 |
| 3.3 | Main core equations | 45 |
| 3.4 | Thermal reactivity feedbacks | 48 |
| 3.5 | Comparison of Nuclear Parameters Used in Dynamic Analysis of MSRE with ^{233}U Fuel and with ^{235}U Fuel [29] | 49 |
| 3.6 | Tubes lengths | 51 |
| 3.7 | Primary heat exchanger data [25] | 53 |
| 3.8 | Heat transfer coefficient on the shell side | 54 |
| 3.9 | Secondary circuit operational parameters | 55 |
| 3.10 | Heat transfer coefficient on the tube side | 55 |
| 4.1 | Geometrical and operational parameters at nominal conditions | 58 |
| 4.2 | Steady state results at 8 MW | 59 |
| 4.3 | Power results at 8 MW | 59 |
| 4.4 | Core temperature difference at different power levels | 60 |
| 4.5 | Effective delayed neutron fraction | 60 |
| 4.6 | Global heat transfer coefficient between primary salt and graphite | 60 |

| | | |
|-----|---|----|
| 4.7 | Reactivity inserted at different power levels | 61 |
| 4.8 | Heat transfer coefficients employed at 1 MW | 68 |
| 4.9 | Average power RMSE in a cold slug accident | 79 |
| B.1 | Collision parameters for different nuclei | 91 |

List of Symbols

| Variable | Description | SI unit |
|--------------|-------------------------------------|------------------------------------|
| t | Time | s |
| P | Power | W |
| Q | Heat | W |
| m | Mass | kg |
| \dot{m}, w | Mass flowrate | kg s ⁻¹ |
| E | Energy | J (or eV) |
| A | Mass number | - |
| g | Gravity acceleration | m s ⁻² |
| T | Temperature | K |
| ΔT | Temperature difference | K |
| ρ | Density | kg m ⁻³ |
| c_p | Specific heat capacity | J kg ⁻¹ K ⁻¹ |
| k | Thermal conductivity | W m ⁻¹ K ⁻¹ |
| μ | Dynamic viscosity | Pa s |
| ϕ | Neutron flux | cm ⁻² s ⁻¹ |
| π | Pi | - |
| z | Axial coordinate | m |
| n | Normalized power | - |
| c_i | Normalized precursors concentration | - |
| A_{core} | Core area | m ² |
| OD | Outer diameter | m |
| N_t | Number of fuel channels | - |

| Variable | Description | SI unit |
|---------------------------|-----------------------------------|--------------|
| φ | Neutron flux shape | - |
| β_i | Delayed neutron fraction | pcm |
| Λ | Prompt neutron lifetime | s |
| λ_i | Decay constant | s^{-1} |
| v | Drifting velocity | $m s^{-1}$ |
| h | Specific enthalpy | $J kg^{-1}$ |
| q''' | Volumetric power | $W m^{-3}$ |
| P_0 | Nominal power | W |
| l | Single volume length | m |
| f | Fractional power | - |
| F | Decay heat density groups | $W m^{-3}$ |
| f_k | Decay heat fraction | - |
| λ_k | Decay heat constant | s^{-1} |
| P | Pressure | Pa |
| ΔP | Pressure drops | Pa |
| α_{fuel}, α_g | Reactivity coefficient | pcm K^{-1} |
| Nu | Nusselt number | - |
| Re | Reynolds number | - |
| Pr | Prandtl number | - |
| D | Diameter | m |
| S | Neutron source | s^{-1} |
| ρ_{fuel}, ρ_g | Feedback reactivity | pcm |
| Σ_f | Macroscopic fission cross section | cm^{-1} |
| γ | Fission yield | - |
| σ | Microscopic cross section | cm^2 |
| D_h | Hydraulic diameter | m |
| f | Friction factor | - |
| L | Tube length | m |
| Xe | Xenon concentration | cm^{-3} |
| I | Iodine concentration | cm^{-3} |

| Variable | Description | SI unit |
|----------|--|---------------------------------|
| ν | Average number of neutrons emitted per fission | - |
| h | Heat transfer coefficient | $\text{W m}^{-2} \text{K}^{-1}$ |
| U | Global heat transfer coefficient | MW K^{-1} |
| τ | Time constant | s |
| $RMSE$ | Root Mean Square Error | - |
| α | Collision parameter | - |

Acknowledgements

My deepest gratitude goes to my Advisor, Prof. Stefano Lorenzi. His vision, unwavering trust in my abilities, and illuminating guidance were crucial in overcoming every technical and conceptual challenge. It has been an honor to learn from his rigorous scientific approach.

A special and heartfelt thank you is reserved for my co-supervisors, Ing. Sophie Deanesi and Ing. Guido Carlo Masotti. Their constant availability, patience in clarifying complex modeling issues, and enthusiasm in sharing their knowledge was an invaluable resource. Finally, I dedicate this achievement to those who supported me throughout this journey. To my Family, thank you for your unconditional love, and for the moral and financial support that never faltered. Without your solid foundation, this challenging journey would not have been possible. I also wish to give a special and warm acknowledgment to Luca. As a fellow engineer, he has been a profound inspiration and role model for me throughout my life.

To my dearest Friends, you were the necessary refuge and distraction during moments of high pressure. A particular thank you to Diego and Marco, for the shared laughter and the lighthearted moments that allowed me to recharge my energy and face the bigger academic challenges with serenity.

To Martina, a fellow engineer, thank you for your patience, technical insight, and unwavering belief in me throughout the intensive period of this thesis. Your support made all the difference.

I also wish to thank the companions with whom I shared countless hours of study and collaboration over the last few years, particularly Riccardo, Alberto, Davide and Emma. Your companionship not only made the long hours at Politecnico manageable and rewarding, but also filled these years with truly great memories.

